Bilge Keel Roll Damping

Combining CFD and local velocities

Mark Jan van Kampen

Delft University of Technology
SBM Offshore

BILGE KEEL ROLL DAMPING

COMBINING CFD AND LOCAL VELOCITIES

by

Mark Jan van Kampen

in partial fulfillment of the requirements for the degree of

Master of Science
in Offshore & Dredging Engineering

at the Delft University of Technology,
to be defended publicly on Friday May 22, 2015 at 14:00.

Student number:	1319043	
Project duration:	July 7, 2014 – May 22, 2015	
Supervisor:	Prof. Dr. Ir. R.H.M. Huijsmans	
Thesis committee:	Dr. Ir. I. Akkerman,	TU Delft
	Dr. A. Romeijn,	TU Delft
	Dr. Ir. R. van 't Veer.	SBM Offshore

An electronic version of this thesis is available at http://repository.tudelft.nl/.

TU Delft Delft University of Technology

ACKNOWLEDGEMENTS

I would like to thank my supervisor Dr. Ir. R. van 't Veen for his support and his guidance during this project. Furthermore I would like to thank my colleagues and fellow students for providing with the necessary breaks between reading the papers and for allowing me to spar with them on certain subjects on which my knowledge was not yet solidified. I would like to thank my predecessor Ir. X. Schut as well for his hard work during the making of his graduation thesis, as well as his continued, enthusiastic support during my thesis. Another heartfelt thank you goes out to J.L. Pelerin for his extensive support and patience during the work on the CFD part of the thesis. Furthermore I would like to thank the Delft University of Technology and Prof. Dr. Ir. R.H.M. Huijsmans for making my education possible and the support given. I would like to thank my other committee members Dr. Ir. I. Akkerman and Dr. A. Romeijn for their input and for their time spent evaluating my work. I would also like to thank P. Dahlin of CD-Adapco for providing me with a license for STAR-CCM+ to use during my graduation.

My education was not only made possible by the Delft University of Technology, but even more by my parents. I am relieved that I have not proven their unrelenting faith in me wrong. I am thankful for their continued support and love. I would also like to thank my girlfriend Frédérique. I believe that without her I would not be who I am and where I am now. Her dedication and support the past six years have been incredible and she helped me celebrate each peak and got me through every valley.

Last but not least I would like to thank you, the reader, for showing interest in this thesis. I hope you can apply this knowledge in projects to come or at least gain some new insights. This is the ultimate goal of this report and this thesis and would thus give me great pleasure. As Stephen Hawking once said:

> "As scientists, we step on the shoulders of science, building on the work that has come before us - aiming to inspire a new generation of young scientists to continue once we are gone."

Mark Jan van Kampen
Schiedam, 8th May, 2015

PREFACE

This thesis contains contents of published works in Chapter 2 as part of a literature review. The proposed methodology is original. The experimental data is obtained from two data sets, one from X. Schut, the other by MARIN in commission by the Roll JIP. This thesis is the original, unpublished work by the author.

After proposing a different subject to SBM Offshore interest was caught and dr.ir. R. van 't Veer approached me to conduct my thesis on variety of other subjects. The subject of FPSO roll damping piqued my interest as it seemed a very relevant and with a possibility to not end up on a shelf somewhere never to be looked at again. For me it seemed to provide sufficient depth and scientific value while keeping in touch with the needs and interests of the industry. Furthermore both prof.dr.ir. R.H.M. Huijsmans and dr.ir. R. van 't Veer seemed very engaged with the subject which continued to be an asset and motivator for me.

The thesis has built upon the work done by dr.ir. R. van 't Veer who has an extensive history in the area of roll motions. His ideas served as a basis for the methodology that is proposed.

Mark Jan van Kampen
Schiedam, 8th May, 2015

“Science may be described as the art of systematic over-simplification — the art of discerning what we may with advantage omit”

— *Karl Popper*

Contents

List of Figures

List of Tables

ABBREVIATIONS

2D Two-Dimensional xiv, xxi, 14, 16, 20, 30, 31, 41, 55, 56, 63, 67, 83, 85, 87, 93

3D Three-Dimensional xiv, 14, 16, 20, 30, 32, 41, 48, 49, 55, 57, 63, 64, 67, 85, 86, 91

BV Bureau Veritas 10, 11, 29, 43, 87

CAD Computer-assisted Design 67

CDF Cumulative Density Function 23

CFD Computational Fluid Dynamics iii, xiii–xv, xxi, 4, 5, 7, 8, 16–20, 23, 29, 31–33, 35–43, 45–47, 49, 50, 53, 55–58, 61, 64, 66, 67, 83, 85–87, 89–94

CoG Center of Gravity 1, 7, 15, 31, 32, 43, 44, 57, 59, 68

Cu Courant number 41

DES Detached Eddy Simulation 85

DNS Direct Navier-Stokes 17

DoF Degree of Freedom 1, 3, 4, 7, 10, 15, 20, 27, 31, 32, 41, 44, 48, 49, 55–57, 59, 63, 85, 87, 91

DVM Direct Vortex Method 11, 16–19, 55, 57, 86

EoM Equation of Motion 13

FFT Fast Fourier Transformation 25, 45, 88

FMM Fast Multipole Method 86

FPSO Floating Production Storage and Offloading v, xiii–xv, xxi, 2–5, 7, 8, 14, 16, 17, 31–34, 46, 50, 55, 56, 59, 63, 64, 83, 93

FSRVM Free-Surface Random-Vortex Method 16

FVM Finite Volume Method 16, 17

HRIC High Resolution Interface Capturing 34, 41, 57, 86

ITH method Ikeda-Tanaka-Himeno Method xiii–xv, xxi, 3, 5–8, 19, 20, 37, 39, 40, 42, 43, 49, 50, 55–57, 69, 83–85, 89, 91–93

ITTC International Towing Tank Conference 4, 31, 55

JIP Joint Industry Project v, xiii, xxiii, 32–34, 41, 43, 44, 48, 50, 59, 61, 72, 89, 93

KC Keulegan-Carpenter xiv, 6, 9, 16, 21, 25, 27, 29, 44, 45, 50, 57, 88, 92, 93

LED Light Emitting Diode 63

LES Large Eddy Simulation 85

LMI Linearize, Match and Iterate 13, 65, 89

MARIN Maritime Research Institute Netherlands v, 59, 67–69, 89

MPM Most Probable Maximum 11, 13, 89

NRMSE Normalized Root Mean Squared Error 41, 43, 56

ODE Ordinary Differential Equation 26, 27, 87, 88

OOP Out-Of-Phase xxi, 83

PDF Probability Density Function 27

PIV Particle Image Velocimetry 14, 15, 17

PUS Pseudo-Unsteady Systems 16

RANS Reynolds-Averaged Navier Stokes 8, 15–19, 38, 57, 86

RAO Response Amplitude Operator xiii, 7, 10–12, 17, 27, 43, 49, 58, 67, 75, 86

RMS Root Mean Squared 65

SBM Offshore Single Buoy Moorings Offshore v, 2, 4, 31, 34, 69, 86, 87, 94

SPAR Single Point Anchor Reservoir 2

SST Shear Stress Transport xxi, 16, 34, 83, 86

TLP Tension Leg Platform 2

TU Delft Technical University of Delft 94

TVD Total Variation Diminishing 17

UD Upwind Difference 34

URANS Unsteady Reynolds-Averaged Navier-Stokes xxi, 16, 34, 55, 56, 83, 85, 86

ViC Vortex-in-Cell 17

VLCC Very Large Crude Carrier 2

VoF Volume of Fluid 16, 34, 86

NOMENCLATURE

A_{bk} Representative bilge keel area [m^2] 84

A_h Hull pressure out-of-phase coefficient [N/s^2] 23, 25, 45, 46, 72, 87

B_h Hull pressure in-phase coefficient [N/s] 23, 25, 45, 46, 72, 87

C_D Drag coefficients [-] xiii, xiv, 6, 9, 17, 19, 23, 25, 32, 38, 45, 46, 64, 84, 86, 90

C_M Intertia or mass coefficient [-] xiii, xiv, 17, 21, 23, 25, 32, 38, 45, 46, 57, 86, 89, 90

C_P Pressure coefficient [-] xiv, 6, 19, 50, 84, 92, 93

F_s A safety factor for the uncertainty in the error estimation [-] 36

M_{bk} Moment generated by the bilge keels [Nm] 87

M_{hp} Moment generated by the hull pressures [Nm] 87

R_n Rotational matrix around axis n [-] 24, 94

U_ϕ The estimated uncertainty of flow quantity ϕ [-] 36

X_n Amplitude of the motion in the n direction [rad or m] 6, 84

Δ_ϕ The data range parameter for use in the evaluation of the uncertainty of U_ϕ [-] 36

Ω A specific frequency in an irregular wave or response spectrum [rad/s] 21, 89

ϵ_ϕ The estimated error of flow quantity ϕ [-] 36

$\left|\frac{X}{Y}\right|$ Response amplitude operator of the amplitude X over amplitude Y [[X]/[Y]] 86

ω Frequency of motion or wave [rad/s] 6, 31, 68, 84, 89

ϕ Phase or phase difference with a subscript denoting which component [rad] 21, 86

ρ Density of water [kg/m^3] 68, 84

σ The standard deviation [-] 36

l_m Moment arm of a point of the hull surface S to the CoG corrected for angle [rad/s] 6, 84

r_{xx} Structural radius of gyration around the x-axis [m] 68

r_{yy} Structural radius of gyration around the y-axis [m] 68

r_{zz} Structural radius of gyration around the z-axis [m] 68

A Added mass matrix or out-of-phase radiated velocity matrix [kg or kgm^2 or m] 24, 87, 94

B Damping or in-phase radiated velocity matrix [kg/s or kgm^2/s or m] 24, 87, 94

C Hydrostatic matrix [kg/s^2 or kgm^2/s^2] 87

F A force or moment with a subscript denoting which component [N or Nm] 87

f Velocity correction factor [-] 6, 7, 9, 69, 84

g Gravitational acceleration [m/s^2] 68

l Moment arm from the CoG to the bilge keel corrected for angle [m] 84

M Mass matrix [kg or kgm^2] 87

P Power [W] 89

p Pressure [Pa] 87

Re Reynolds number [-] 25, 44, 45, 92

S The hull surface [m] 6, 84, 87

T Time or oscillation period [s] 87

U Local water velocity [m/s] 23, 32, 84

x Rigid body motion optionally with subscript n to denote direction [m or rad] 21, 87

ABSTRACT

This thesis aims to provide a practical method to evaluate the roll damping and motions of an FPSO with aberrant bilge keels and/or riser balconies in waves. For this goal a literature review was performed after which it was concluded that the widely used ITH method could be modified to achieve this goal. The coefficients used in the ITH method are obtained from a forced roll oscillation 2D URANS SST CFD model, including the additional Out-Of-Phase (OOP) terms and using radiated wave velocities from linear potential theory instead of an empirical correction factor. The obtained coefficients are then used in conjunction with flow velocities obtained from linear potential flow theory, including radiated, diffracted and incoming wave velocities, to construct a time domain model. This model was compared to forced oscillation and regular wave experiments of the model scale Glas Dowr FPSO. Forced oscillations were reproduced satisfactory after a correction for additional heave and sway motions was applied. Regular wave results were compared to (a) measured roll angels, (b) simulations using damping coefficients obtained from experiments, (c) ITH method coefficients, (d) local velocity-based ITH method coefficients and (e) using the proposed methodology. Results were good when compared to simulations based on measured damping coefficients but inconclusive when compared directly to measured roll amplitudes. Reasonable agreement compared to simulations with damping coefficients obtained from experiments was obtained at low to medium wave amplitudes and an underestimation was obtained at high wave amplitudes. The underestimation at high amplitudes is faulted to the linear increasing hull pressure coefficient while it is more likely to become saturated at higher local velocities. It is concluded that the combination of CFD and local velocities yield promising results and is more flexible than the traditional ITH method. A more thorough validation should be performed against data at various frequencies, hulls, keels and wave amplitudes before application becomes feasible.

For an extended abstract reference is made to **Appendix G** located at the end of the report.

EXECUTIVE SUMMARY

As hydrocarbon supplies dwindle, technology develops and long-term hydrocarbon prices rise it is becoming more and more economical to develop hydrocarbon fields offshore. An FPSO vessel can be favored as it is flexible, quickly commissioned and cost-effective, can be used at all water depths and does not require additional pipelines to shore.

Roll motions of an FPSO can be dominating in many areas of design such as:

- cracks in riser bending restrictors,
- strength and fatigue criteria, for example in a flare tower,
- effective operation of separators,
- crew comfort, and
- helicopter take-off and landing.

To limit roll motions to a maximum of ten degrees bilge keels are installed. Predictions of the roll motion of an FPSO with bilge keels using traditional techniques such as the Ikeda-Tanaka-Himeno (ITH) method are no longer sufficient due to aberrant dimensions and shapes of bilge keels and riser balconies compared to more traditional vessels. The alternative at this time is to use old data of similar vessels or perform new experiments, which are costly and take quite some time scheduling and performing. Furthermore flexibility during the tender/design stage is limited when performing experiments, making it increasingly difficult to optimize bilge keel effectiveness. The goal of this report was thus to provide a practical method to evaluate the roll damping and motions of an FPSO with aberrant bilge keels and/or riser balconies in (ir)regular waves within a time-span available during a tender/design stage (2-4 weeks). For this the traditional ITH method was modified in three ways:

1. by extending current formulations for loads on bilge keels and pressures created by bilge keels with out-of-phase terms;
2. by obtaining relevant coefficients from 2D CFD simulations in forced roll oscillations, serving as a replacement for the empirical basis of the ITH method and thus allowing all shapes and sizes; and
3. by using linear potential theory to obtain local velocities consisting not only of rigid body velocities, but also radiated wave velocities, incoming wave velocities and diffracted wave velocities, thus taking into account the effect of waves in a physical representative manner.

This new methodology was compared to forced oscillation and regular wave experiments performed by MARIN as part of the Roll JIP of a 1/40 model of the Bluewater Glas Dowr FPSO. Motions in calm water in which the model was excited with a moment generated by the inertia of an electric drive were reproduced satisfactory after a correction for additional heave and sway motions was applied. Regular wave results were compared to (a) measurements, (b) simulations using experimentally derived damping coefficients, (c) ITH method damping coefficients, (d) local velocity-based ITH method coefficients and (e) using the proposed methodology. Results were good when compared to simulations based on measured damping coefficients but inconclusive when compared directly to measured roll amplitudes. Reasonable agreement at low to medium wave amplitudes and an underestimation at high wave amplitudes were obtained.

It is concluded that the combination of CFD and local velocities yield promising results and is more flexible than the traditional ITH method. Further more the ITH method based on local water velocities already shows a drastic improvement over the ITH method based on ridid body roll. Including local velocities results in a physical more correct model with different loads on the bilge keels on the windward and leeward side in waves. A more thorough validation should be performed against data at various frequencies, hulls, keels and wave amplitudes before application becomes feasible as there is a discrepancy between measurements and simulations that is not yet explained. Furthermore no simulations and validation was performed in irregular waves where a different behavior is expected than in regular waves.

1

INTRODUCTION

1.1. DOCUMENT STRUCTURE

This document is structured in a conventional format where a short introduction to the subject and the problem is given after which current and past literature is discussed. The literature combined with the problem solution give a possible solution vector which is used to construct a methodology. Afterwards the various parts of this methodology are discussed, verified and validated if possible. In the final Chapter concluding remarks and recommendations are made. It is stressed that more background information is available in the literature review document when the readers feels that there is a lack of more basic information [1].

1.2. DOCUMENT PURPOSE AND SCOPE

The purpose of this document is to cover the work done during the nine-month graduation period as comprehensively and concise as possible.

The scope of this document is limited to work performed that the author perceives as of interest to the reader as well as the scientific community in general. As such not all work done is discussed in detail as to present the reader with a manageable document. The literature review and background information are furthermore kept to a minimum in this report, while reference is made to the literature review for further readings [1].

1.3. CONVENTIONS

From Journée [2] the axis are defined as in Figure 1.1 below. In Figure 1.1 three translations and three rotations all originating from the CoG are depicted. With the translation in x, y and z being respectively the surge in the longitudinal direction positive towards the bow, the sway in the lateral direction positive towards port and heave in the vertical direction positive upwards. The rotations ϕ, θ and ψ being respectively the roll around the longitudinal axis positive right turning, the pitch around the lateral axis positive right turning and yaw around the vertical axis positive right turning. To simplify reading equations the following convention is used:

$$\vec{x} = \begin{bmatrix} x_1 \\ x_2 \\ x_3 \\ x_4 \\ x_5 \\ x_6 \end{bmatrix} = \begin{bmatrix} x \\ y \\ z \\ \phi \\ \theta \\ \psi \end{bmatrix}. \tag{1.1}$$

A capital X_n is used to denote that amplitude of a harmonic motions in the n^{th} DoF.

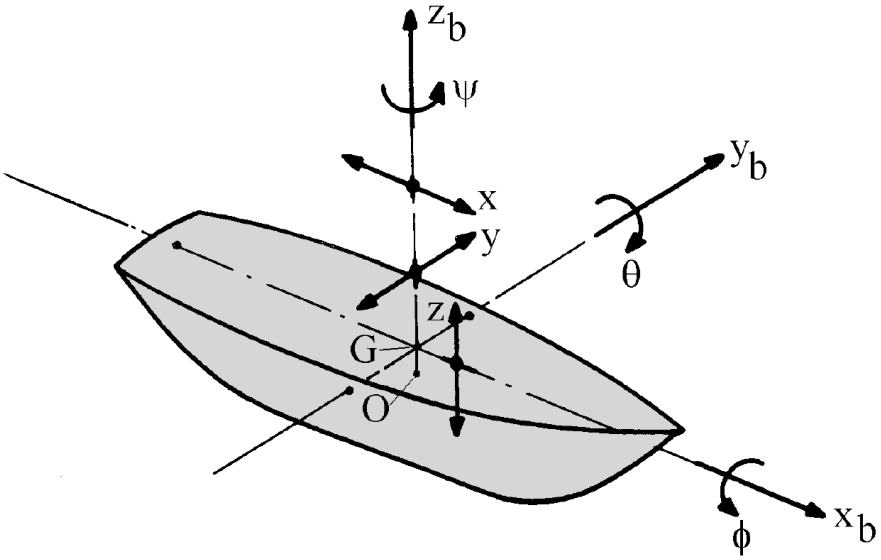

Figure 1.1: Axis conventions according to Journée [2].

1.4. HISTORY AND BACKGROUND

As hydrocarbon supplies dwindle, technology develops and long-term hydrocarbon prices rise it is becoming more and more economical to develop hydrocarbon fields not just simply offshore but in ultra-deep waters as well. Traditional production platforms, such as a jack-up, a gravity based structure and others are not usable in these water depths. Furthermore a complication arises due to the distances from shore, resulting in long and expensive pipelines which are economically unattractive. Various concepts such as a SPAR and a TLP have been developed, but an Floating Production Storage and Offloading (FPSO) vessel can be favored as an FPSO is flexible, quickly commissioned and cost-effective.

An FPSO is a ship-shaped production platform that is usually connected to a sub-sea template from which a mix of water, gas and oil is produced. This mix is processed by the FPSO, after which the processed oil is stored on-board until a tanker is available for offloading. There are a few types of FPSOs which are identified by the presence and type of turret and the type of hull, either new-built or converted. The vessels most of interest are the vessels that are spread-moored and thus do not have an internal or external turret through which risers are fed, but rather a riser balcony on one of the sides and which are converted from a VLCC. These vessels are most suspicable to roll which is relevant for this research. A spread-moored FPSO uses a number of mooring lines at various locations to keep its position. This means it does not weather-vane and can encounter beam waves which can cause large roll motions. A converted FPSO is more suspicable to roll motions as for its original purpose as a VLCC it is designed as a ship with forward speed which are less sensitive to roll.

Roll motions can be dominating in many areas of design such as:

- cracks in riser bending restrictors,
- strength and fatigue criteria, for example in a flare tower,
- effective operation of separators,
- crew comfort, and
- helicopter take-off and landing.

To counter these large roll motions, for which a maximum is maintained of 10° within SBM Offshore, bilge keels are employed. Figure 1.2 shows a hull with bilge keels attached in green. Bilge keels on FPSOs are large in comparison to normal vessels as normal vessels move at a forward speed. As bilge keel sizes increase the drag caused by them increases. This makes it important for regular vessels that have a forward speed to minimize the bilge keel size to maximize fuel economy. Furthermore having a forward speed reduces roll motions as lift is created, limiting the need for a large bilge keel. Another advantage regular vessels have is the ability to

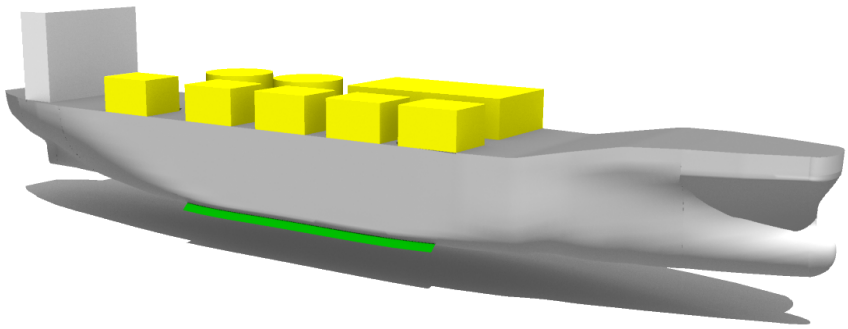

Figure 1.2: A representation of the Glas Dowr FPSO including its exaggerated bilge keel in green

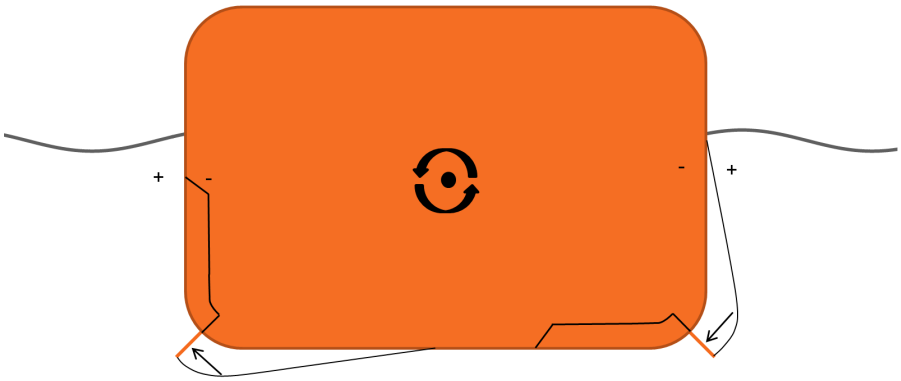

Figure 1.3: Schematic overview of the various components influencing bilge keel generated moments.

put their bow into the dominating wave direction, reducing roll motions. As FPSOs are generally stationary and do not always weather-vane bilge keel size is not limited and thus FPSOs are fitted with larger bilge keels which usually have a deviating geometry, mostly due to the use of bracings to maintain sufficient structural integrity when loaded in multi-axial fatigue, leading to complex shapes. Riser balconies are another example of such complex shapes.

1.4.1. HYDRODYNAMICS AND ROLL DAMPING

Hydrodynamics is the science of moving water and objects in moving water. Contributors include well known names such as Blaise Pascal, Isaac Newton, Daniel Bernoulli, Jean le Rond d'Alembert, Leonhard Euler, William Froude, George Gabriel Stokes, Osborne Reynolds and many others. This thesis focuses on the roll motion of a vessel, which is one of the hardest motions to predict, especially after bilge keels have been added. In general linear potential theory is used to predict ship motions, herein it is assumed that there are no viscous effects present. For most DoF this is a practical and valid approach as the viscous effects only have a small influence on the motion. For roll this is not true, especially when bilge keels are added, as strong viscous effects arise, resulting in a great deal of additional damping, greatly reducing the motions at the resonance frequency. Thus a different approach is required.

A great deal of work has been done on bilge keel induced roll damping by Y. Ikeda, N. Tanaka and Y. Himeno in 1970-1980, summarized by Himeno [3]. In Himeno's work it is assumed that roll damping is composed of seven components of which three are relevant for bilge keel damping. The components are the waves made due to bilge keel, due to the moment generated by the forces acting on the bilge keel and the moment due to pressures created by the disturbances (vortices) in the wake of the bilge keel and pressure build up in front of the bilge keel, reference is made to Figure 1.3 for a graphical overview. These three components are measured from experiments after which a semi-emperical formulation is derived for all components. Reference is made to Chapter 2 for more details on the Ikeda-Tanaka-Himeno Method (ITH method)

1.5. PROBLEM STATEMENT AND RESEARCH QUESTION

While the current methods by Ikeda, Himeno and Tanaka and as stated by the International Towing Tank Conference (ITTC) can be quite accurate they lack flexibility as the empirical foundations are limited to certain bilge keel sizes and geometry. Furthermore they do not allow proper physical representative implementation in waves and other DoF, resulting in under and over predicted loads on the bilge keels and a less then ideal representation of reality. SBM Offshore and the industry in general require a new, more accurate and especially flexible formulation of the hull-pressure and hull-pressure damping based on actual occurring phenomena and which would preferably be applicable in irregular waves as well. This would allow a reduction or elimination of experiments and optimization of bilge keel geometry and size during the tender and design stages. The research question is thus as follows:

"How can the roll damping and roll motion of an FPSO with aberrant bilge and/or riser balconies keel geometry in waves be determined within a timeframe reasonable for a design stage (2-4 weeks)?"

The goal of the next Chapter is to provide a theoretical background on the moments induced by bilge keels. As the questions posed in the literature review are directly linked to the goals of the thesis the questions are stated below:

1. What is an appropriate CFD method that balances accuracy and computation time with the capability to accurately compute vortex shedding and pressures on the hull?
2. What is the current state-of-the-art in the field of roll damping?
3. Which approaches have been taken to estimate the roll damping of an FPSO and what angles seem promising?
4. What are the physical workings of vortices, dependency on velocity and their influence on hull pressure, focusing on the effects of the free-surface and wave orbital velocities?

1.6. METHODOLOGY

The methodology adhered in this thesis is quite straightforward. First the problem is identified and a goal and research question are posed. A theoretical foundation and current situation, as well as possible solution paths are then formulated from the discussion with relevant personae and a comprehensive literature review. After this a solution path is chosen and a proposed methodology is formulated. This methodology is then verified and validated against experiments and possible improvements and identified flaws are discussed.

2

Literature Review

The literature review will be summarized in this Chapter, for further reading reference is made to the original document [1]. Furthermore a more detailed background on the ITH method is provided in the first Section.

The questions the literature review aimed to answer are restated:

1. What is an appropriate CFD method that balances accuracy and computation time with the capability to accurately compute hull-pressures and vortex shedding?
2. What is the current state-of-the-art in the field of roll damping?
3. Which approaches have been taken to solve the roll damping of an FPSO and what angles seem promising?
4. What are the physical workings of vortices, dependency on velocity and their influence on hull pressure, focusing on the effects of the free-surface and wave orbital velocities?

An attempt was made to answer these questions to the fullest using the methodology for a literature review as described by the TU Delft Library [4] and the Delft Design Guide [5]. For this purpose the review was split up into Sections 2.2, 2.3 and 2.4: roll damping, vortices and CFD respectively. It should be noted that nomenclature in this Chapter might differ from the other parts of the report, as the nomenclature as used in the sources is maintained.

2.1. ITH method of roll damping prediction

The ITH method is founded around the relatively easy to understand principle that the roll damping of a vessel can be divided in seven components:

- hull friction damping,
- radiated wave damping,
- eddy damping,
- lift damping,
- bilge keel normal force damping,
- bilge keel hull pressure damping, and
- bilge keel wave damping.

The focus of this thesis are the last three components. There are a few basic assumptions underlying the ITH method. The normal force model is based on the assumption that the relevant damping force can be described by a part of the Morison equation:

$$F(t) = \frac{1}{2}\rho A C_D U(t)|U(t)| \tag{2.1}$$

As it is assumed that the velocity around the bilge is proportional with a factor f with the roll velocity, and roll damping is a force in phase with the roll velocity only the drag part is relevant, as it is in phase with the roll velocity. Furthermore it is assumed that C_D can be defined as:

$$C_D = \frac{22.5}{KC} + 2.4 \tag{2.2}$$

with KC being the dimensionless Keulegan-Carpenter number, defined as:

$$KC = \frac{U_m T}{D}. \tag{2.3}$$

Now assuming that in a harmonic motion $x_4 = X_4 sin(\omega t)$ the velocity experienced by the bilge keel is denoted as:

$$U(t) = l f \omega X_4 cos(\omega t) \tag{2.4}$$

with f being a certain correction factor depending on hull geometry, X_n the amplitude of the motion in the n^{th} direction and ω the oscillation frequency. Continuing with this assumption the characteristic length of twice the bilge keel height a KC number and quadratic damping moment is found in the form of:

$$KC = \frac{f l \pi X_4}{2 h_{bk}} \tag{2.5}$$

$$M = \frac{1}{2} l \rho C_D L h_{bk} f^2 X_4^2 \omega^2 cos(\omega t)|cos(\omega t)| \tag{2.6}$$

The hull pressure damping is determined by assuming a certain hull pressure distribution and the dimensionless pressure coefficient:

$$P = \frac{1}{2}\rho C_P U(t)|U(t)| \tag{2.7}$$

Rewriting and integrating over the hull surface equals to

$$M_{hp}(t) = \frac{1}{2}\rho \int_S C_P(S) l_m(S) dS U(t)|U(t)| \tag{2.8}$$

with l_m the moment lever and S the hull surface. Here C_P is again obtained from experiments lending the method its empirical nature. For further reading reference is made to the summary by Himeno [3] and the original works by Ikeda, Himeno and Tanaka [6] and [7]

2.1.1. WEAKNESSES

The theory of Ikeda has a few weaknesses, where the most prominent are listed below:

1. global motions,
2. free-surface,
3. memory effects,
4. the maximum pressure not being at maximum roll velocity, and
5. semi-empirical nature.

The weaknesses are discussed in the following Sections. It should furthermore be noted that in the most applied variation of the ITH method that certain assumptions are made about the geometry and roll axis. Vertical side walls, a horizontal bottom and quadrant bilges are assumed. It is assumed that the bilge keel is in line with the line from the bilge keel base to the roll axis and the bilge keel is placed at the center of the bilge. This allows easy evaluation of the integral in Equation 2.8 and moment arm l. These assumptions hold when the breadth of the ship over twice the draft is relatively close to unity (H_0), the distance from the roll axis to the free surface over the draft is small (OG/d) and the bilge keel is under a 45 degree angle. This is

Vessel	H_0	OG/d
FPSO loaded	1.4	0.11
FPSO intermediate	2.12	-0.37
Ikeda #1	1.25	0
Ikeda #2	1.15	0
Ikeda #3	1.232	0
Ikeda #4	1.036	0

Table 2.1: Comparison of FPSO and Ikeda vessel characteristics.

not always true for an FPSO as it has a greatly varying draft and CoG which is taken as the roll axis. If these assumptions do not hold exact evaluation is more appropriate. Values for an example FPSO and for the Ikeda et al. experiments can be found in Table 2.1. It can be seen that for the experiments done by Ikeda et al. the assumptions hold, while for a typical FPSO they do not.

GLOBAL MOTIONS

The ITH method is based around the roll motion of the vessel itself instead of the water velocities and was deduced from experiments using forced oscillations. The velocity is corrected to account for the hull geometry, but does not account for local kinematics of the fluid, such as wave orbital velocities and fluid velocities from previous cycles. The fluid velocities and other effects caused by a causal connection are grouped under the term memory effects and are discussed in a later Section. The influence of wave orbital velocities can most markedly be appreciated as a difference between the leeward and windward bilge keel forces, assuming a vessel oriented in a beam direction. Here much higher local velocities can be observed at the windward keel. This results in uncertainty of application of the ITH method in waves. Furthermore influence of velocities caused by other DoF are relevant as well. To stress the importance of local velocities the results of tests of a vessel in regular waves where the bilge keel loads were measured are plotted in Figure 2.1 for the leeward and windward side and compared to the ITH method method. It can be noted that in reality the bilge keels loads have a very significant difference between them, while the ITH method predicts equal loads on both sides, which results in a large difference for the windward side and a still significant difference for the leeward side. In situations where a bilge keel is for example asymmetric this can lead to different responses depending on the which side of the vessel is the windward side. This shown by Seah [8] and Bigot [9] where a 15% difference in the starboard and port-side RAO is observed.

FREE-SURFACE

The tests performed by Ikeda et al. were performed in a vertical manner instead of a horizontal floating vessel, eliminating the influence of the free surface. From literature it becomes apparent that the free surface, as well as the draft of a vessel, have an impact on the roll damping. The first item of importance is the roll center that varies with draft and is crucial for the roll damping. Secondly the free surface influences the pressure distribution on the hull of the vessel, and thus directly influences the roll damping. This effect is mitigated in the ITH method by the factor f but it is unclear how well this factor performs for various geometries and in waves.

MEMORY EFFECTS

Memory effects are all effects on the roll damping that can be attributed to the previous cycles. Overall it can be said that if a large wave follows a smaller wave the drag coefficient will be lower, while with a small wave following a larger wave the drag coefficients will be higher [10] and [11].

MAXIMA

In the ITH method it was assumed that the maximum roll pressure distribution would occur at the highest roll velocity and thus at the moment that the roll angle was zero degrees. From experiments and CFD results it becomes apparent that this is not valid. This is due to two factors: first the roll moment caused by hull pressures is not entirely in phase with the normal velocity on the bilge keel, and the normal velocity on the bilge keel is not entirely in phase with the roll velocity.

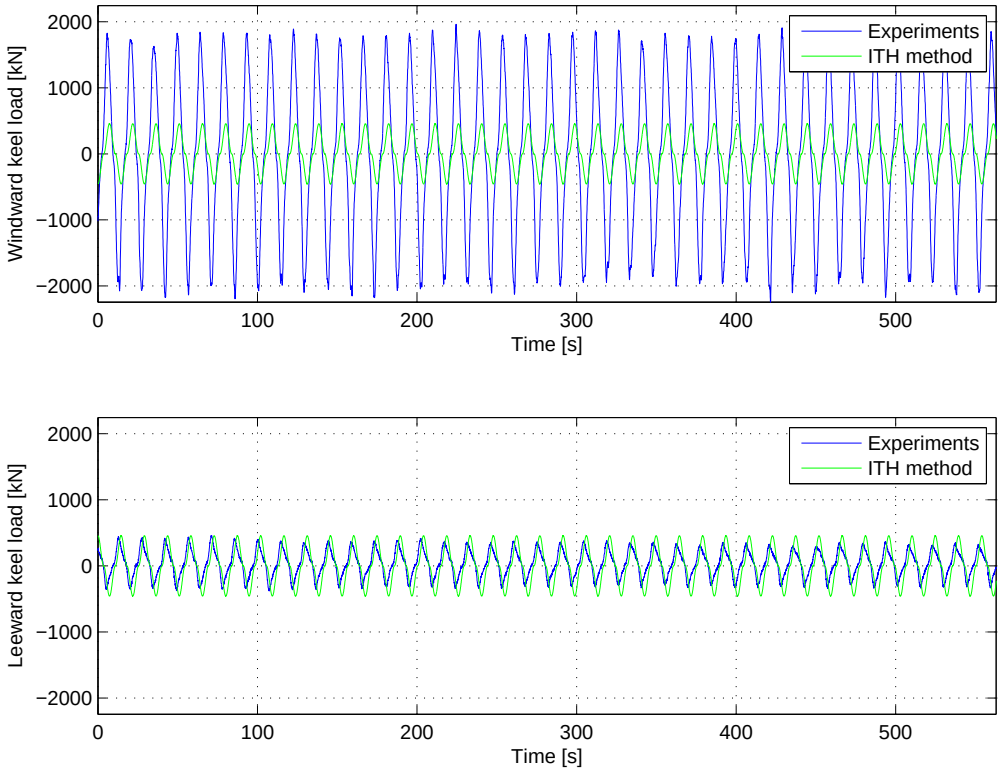

Figure 2.1: Schematic overview of the various components influencing bilge keel generated moments.

EMPIRICAL NATURE

The empirical nature of the ITH method allows only hull shapes and keel geometries within certain limits, as well as no other appendages. This limits the applicability to relatively small bilge keels and simple hull shapes as encountered on small cargo vessels and fishing ships.

2.2. ON ROLL DAMPING

This Section is aimed at recent literature on roll damping, especially of FPSO-shaped hull types.

2.2.1. IN GENERAL

On a general note Oliveira suggests that regular quadratic damping is not applicable to FPSO roll damping and proposes bilinear or hyperbolic damping to get better results as roll damping becomes linear at larger angles [12]. It should be noted that Oliveira focuses on roll-decay test and subsequent damping coefficients as well as roll damping in general and not separate components.

Van Dijk showed that with a properly tuned damping coefficient good agreement can be reached between theory and full-scale measurements if wave-spreading is taken into account. He further notes good agreement between model tests and full-scale measurements which shows adequate handling of scaling effects [13].

Korpus used CFD and potential theory to investigate the difference between potential theory and RANS [14]. By subtracting the potential theory roll moment from the RANS roll moment the shear and vortex effects could be captured. The shear roll moment was negligible, while the vortex effect was identified to have significant difference in phase and magnitude compared to the potential theory. Furthermore for tests including bilge keels higher harmonics (third and fifth) were identified as significant.

Recently a paper was submitted by van 't Veer [15] detailing results on hull pressures and bilge keel loads. It was identified that to describe the normal load, higher harmonics and inertia terms are required. If these are included in the ITH method the resulting loads seem well in line with measurements. Furthermore frequency dependency was observed for inertia coefficients. These results are based on a cylinder-shape hull and not necessarily directly applicable to a more real hull.

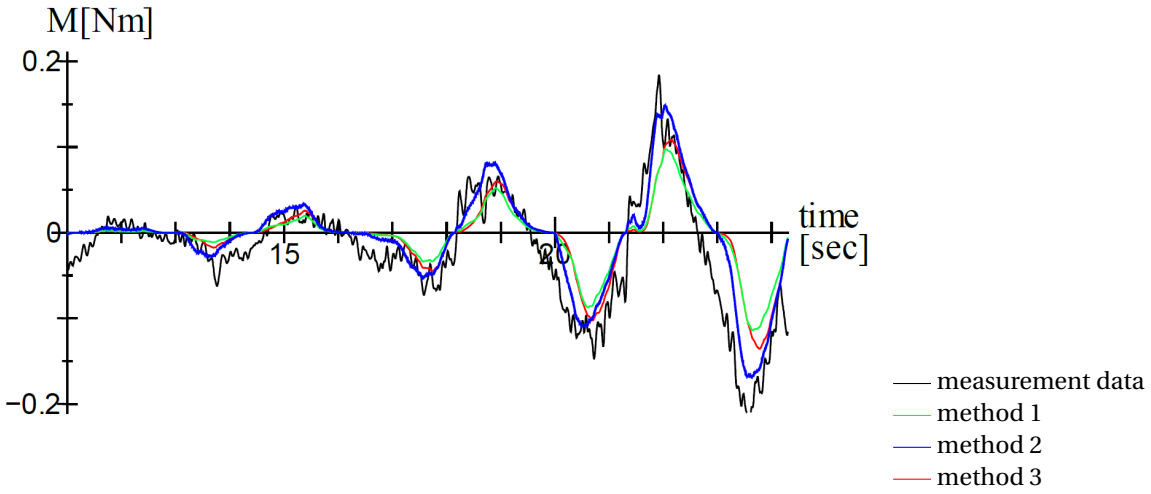

Figure 2.2: Comparison of estimation methods and measured data [18].

2.2.2. MEMORY EFFECT

Flow memory effects are due to flow velocities and thus vortices from previous cycles. This means that if the system is not in a steady state the velocity field depends on one or more previous cycles, as well as the roll motion itself. Van 't Veer [16], Katayama [10] and earlier Ikeda [11] confirmed that memory effects are present and Schut [17] showed that the results from regular oscillations are not directly applicable on irregular oscillations.

Katayama et al. proposed a manner relying on global roll velocity to cope with memory effects and irregular oscillations [18]. In a 2010 paper of Katayama it was shown during the drag coefficient changes when a test device undergoes a forced oscillation from rest [10]. It is found that after the fourth swing the drag coefficient stabilizes. Various formulations were made to incorporate the memory effect and changing drag but a definite conclusion is not made. Three estimation methods are tested against measured data:

1. Method one uses a C_D number that is based on a position dependent KC number and is updated with each time step. It excludes memory effects.
2. Method two expands on method one by including memory effects.
3. Method three utilizes constant KC and C_D numbers but does include a factor f for flow velocity at the bilge.

It seems that the results from method two are in best agreement with the measurements as seen in Figure 2.2.

Cummins outlines a method to incorporate the pressure and thus force created by waves generated in previous cycles [19], a method which is commonly used for example by Ibrahim [20]. It utilizes a convolution integral in the following form:

$$F = -\alpha\dot{V} - \int_{-\infty}^{t} K(t-\tau)V(\tau)d\tau \tag{2.9}$$

with α being the added mass, V the ship velocity and K the retardation or memory function.

$$K(t-\tau) = \rho \int\int \frac{\delta\Phi(t-\tau)}{\delta\tau} s d\sigma \tag{2.10}$$

with s being the normal vector of the surface element $d\sigma$. This method does not take into account viscous effects but perhaps could be modified for use with viscous damping.

2.2.3. (IR)REGULAR WAVES

Roll damping in irregular waves is observed to be four times as high during regular oscillations or decay tests by Orozco [21], which is largely attributed to the local kinematics. Orozco applied the method of Ikeda et al. to irregular waves. For this he linearized the non-linear damping coefficients using stochastic linearization

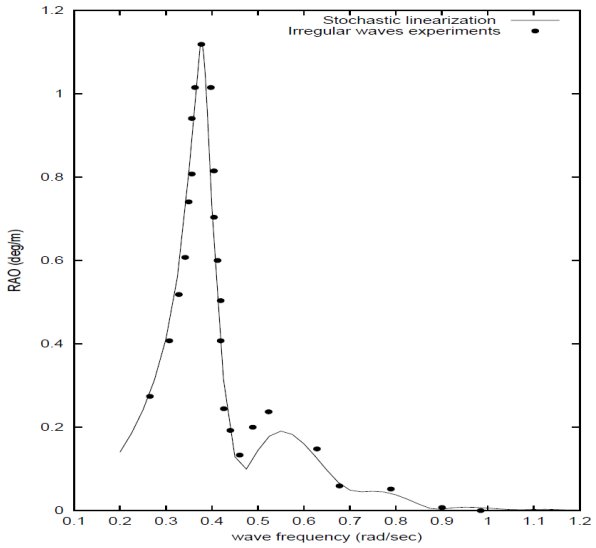

Figure 2.3: Results from Orozco where Ikeda's formulation for roll damping was stochastically linearized and multiplied by four to account for irregular waves as became clear from experiments and using HydroStar to solve [21].

which takes into account the spectra of the incoming waves. This yielded better results than the regular wave linearization where the quadratic damping is assumed to dissipate the same energy as the linear damping in one oscillation cycle. Using the method of applying a Rayleigh distribution to the maximum values of roll a estimate can be found for the roll motion maxima, although it should be noted that this is only valid for linear damping. It is used in Orozco's research as it provides an indication which should be sufficient for determining the influences of various different sizes bilge keels. After applying a factor of four to the roll damping the numerical model, which utilizes the BV package HydroStar, showed good agreement with the experimental results. Reference is made to Figure 2.3.

Jung identified in an experiment that local kinematics dominates the generation of the vortices and not ship motions, when the wave period is longer than the natural roll period. I.e. the flow velocities are higher than the body's roll velocities [22]. Jung continued his research for a larger range of period for a rolling barge fixed in other DoFs in regular waves [23]. He concluded that for waves at the roll natural period the generated vortices were behind the body's motion, resulting in viscous damping. The same results applied for waves with shorter periods than the roll natural period. It was confirmed that for longer periods damping became negative and thus viscous effects added to the body's motions instead of reducing. Although it should be noted that damping does not dominate far from the resonance frequency.

Van 't Veer [24] uses a similar approach as Orozco, but instead of relying on global motions use is made of local kinematics as an input for the Morison/Ikeda formula resulting in a calculation scheme as in Figure 2.4. Instead of using the velocity increment factor as proposed by Ikeda, velocities are obtained directly from potential flow theory. This allows van 't Veer to incorporate the local kinematics missing in the research done by Orozco. Van 't Veer remarks that there still is quite some work to be done regarding the complex flows around the appendage:

> "It is for seen that such a development [an heuristic damping model] will utilize a (local) KC-dependent drag coefficient in combination with a local flow velocity obtained from potential flow. Among others one difficulty lies in finding a proper relationship between the complex flow behaviour seen around the appendage and the potential flow velocities in wave conditions."

Another advantage of using local velocities is the ability to differentiate between the bilge keels on both sides which is relevant in for example beam seas where one keel will experience much higher local velocities than the other.

Van 't Veer continued research on bilge keels leading to a 2012 paper on bilge keel normal forces [25]. The goal of this research was to provide insight into the forces on the bilge keel for structural calculation, not roll damping. Nonetheless these results are relevant for this research. The bilge keel forces are calculated using local fluid velocity RAOs, the drag equation with a KC-dependent drag coefficient and a correction factor to account for unknowns such as the memory effect and the free surface. The local relative velocity is dependent

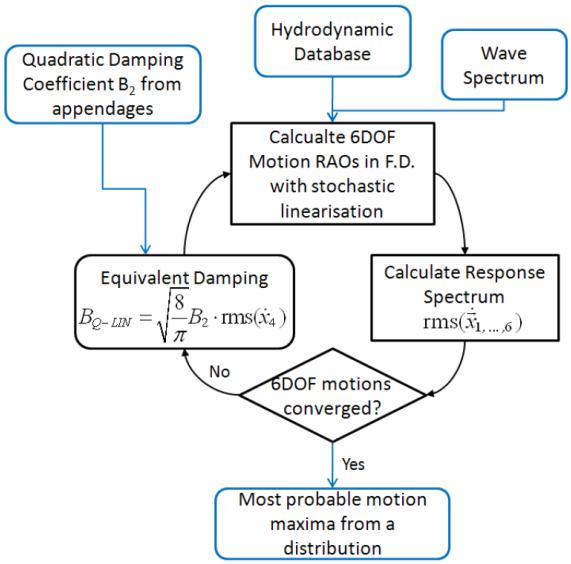

Figure 2.4: Calculation scheme utilizing stochastic linearization by van 't Veer [24].

on vessel motions, radiation velocities, diffraction velocities and wave orbital velocities. Another point that was raised is the difference between exposed and leeward bilge keel velocities and thus loads in mostly beam seas.

In 2013 van 't Veer published another paper [26]. The focus was on irregular waves and bilge keel forces (not pressures on the hull). In this research van 't Veer used the BV software HydroStar to calculate the total local velocity RAOs around the bilge keel composed of wave orbital velocities, diffraction velocities and radiation velocities. The peak of this relative velocity is used to calculate the maximum force on the bilge keel. Further research is mostly aimed at determining bilge keel forces in irregular waves after the tuning of the roll motions, including the inertia term and higher harmonics. Loads are well predicted.

Brown and Patel [27] developed a theory using the Direct Vortex Method (DVM). This method entails the use of potential flow in combination with discreet vortices to model viscous effects within an inviscid model. Reference is made to the literature review for more information [1]. The results of the model were captured in the following formula which can be used in the frequency domain:

$$M_{vs} = -f_1(\phi_0) f_2(r/d) e^{i(\omega t + \alpha)} \tag{2.11}$$

Where M_{vs} is the vortex shedding induced moment, ϕ_0 the roll amplitude, r the roll center measured upwards from the keel, d the draft and α the phase. Brown and Patel thus state that the roll moment and thus damping is dependent on the roll frequency, amplitude, roll center and draft. Their results seem to yield a fair estimate but differ at resonant frequency with large amplitude motion. A disadvantage of this method is that the roll center needs to be estimated as the roll center is determined from the motions of the vessel.

Downie and Graham developed a method using the DVM to perform an one-off calculation to determine a vortex shedding moment coefficient to be used in potential flow calculations to estimate roll damping [28] which is based on the work of Brown and Patel [27]. Hajiarab continued this work with Downie and Graham as documented in [29] and [30] and finished his PhD thesis recently which involved a black box model compatible with most potential flow-based hydrodynamics software [31]. The focus was on rectangular cylinders with sharp corners and not round corners with bilge keels. The results are promising when compared to experiments, reference is made to Figure 2.5 and Figure 2.6. There seems to be an overestimation of the RAOs at wave periods higher than the natural period and underestimation at wave periods lower than the natural period for the Hajiarab model tests, while comparison to the Brown et Al. data is the other way around.

2.2.4. SPECTRAL ANALYSIS

One of the goals is to develop a tool to determine roll damping and more specifically to predict the Most Probable Maximum (MPM) roll amplitude, for this purpose spectral analysis is employed. To determine these roll maxima it is common to assume a Gaussian distribution for the incoming waves, assume a narrow-band spectrum and a Rayleigh distribution for the wave height and through a linear system thus the MPM of the

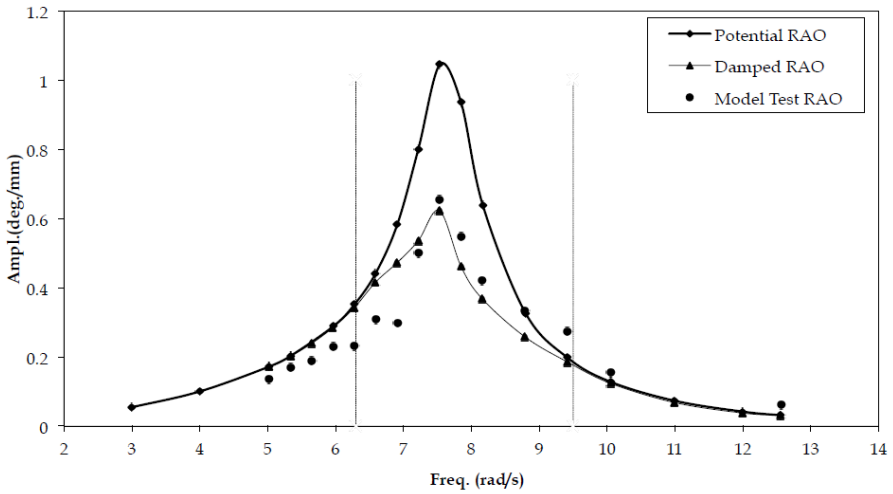

Figure 2.5: Regular wave RAOs for potential diffraction-refraction based software, using the method by Hajiarab and from experiments by Hajiarab [31].

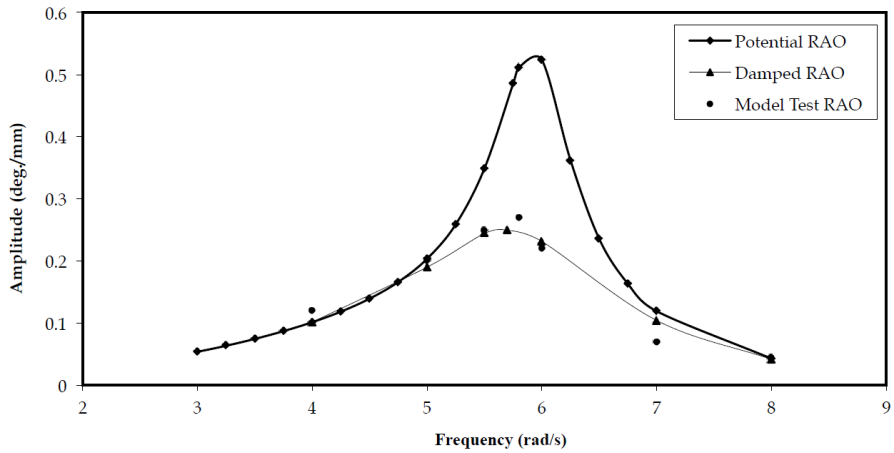

Figure 2.6: Regular wave RAOs for potential diffraction-refraction based software, using the method by Hajiarab [31] and from independent experiments by Brown et Al. [32].

motions [2]. While this is valid for most motions it is not for roll, as the Rayleigh distribution is only valid for a linear process and roll is non-linear. To solve this issue various solutions have been proposed which can broadly be divided in two areas: the linearization or a different distribution that can cope with non-linearities.

The linearizations for irregular waves are stochastic linearizations which are based on maintaining the stochastic properties of the non-linear damping in the linear damping. This means that the wave state is incorporated in the damping and iteration has to be performed, solving and converging the Equation of Motion (EoM) to obtain the proper equivalent linear damping coefficient, reference is made to Orozco [21] and Drobyshevski [33]. This iteration can be avoided by using an approximation as proposed by Drobyshevski [33], but is mostly useful as an initial approximation. After linearization usually the Rayleigh distribution is applied.

Leloux compared a two-parameter Weibull and the Rayleigh distribution but are both found lacking for the MPM roll [34]. Leloux makes reference to a third method, which is the so called Linearize, Match and Iterate (LMI) method which approximates a non-linear system with a non-linearity in the form of $u|u|$ by another non-linear system which is based around a cubic polynomial, reference is made to Prevosto [35] and Minko [36]. The system is then supplemented with a variety of linear systems to ensure statistical equality.

Gachet and Kherian assessed the impact of stochastic linearization on ship operability [37]. It is compared to constant damping and is found to be more favorable as it yields higher operability. Unfortunately Gachet does not evaluate the accuracy of stochastic linearization.

Choi attained good agreement when using regular wave linearization of a damping coefficient obtained from experiments [38].

Leloux concluded that spectral linearization is more applicable than the harmonic, regular wave approach. It seemed to yield reasonable results compared to the experiments, but it seemed to underestimate the roll damping when the wave peak frequency was not located near the roll natural frequency.

An alternative is selecting a distribution that is more fitting for the response and the MPM values. It should furthermore be noted that the non-linearities are also introduced due to changing underwater geometry and non-linearities in the waves. The spectrum of the waves of furthermore often assumed to be narrow-band while it often is more medium-band. This implies that just linearization of the system is not sufficient to justify the use of the Rayleigh distribution. Nonetheless the combination of linearization and a Rayleigh distribution is often used for roll as it yields reasonable results as long as roll angles are not too large [39].

2.3. ON VORTICES

Sarpkaya and O'Keefe [40] performed experiments based on a flat plate attached to a wall in an oscillating flow. Three vortex shedding regimes depending on the Keulegan Carpenter number were identified:

1. $KC < 3$
2. $3 < KC < 8$
3. $KC > 8$

For $KC < 3$ when a new vortex is created it sheds away with the vortex created in the previous motion cycle, creating a counter-rotating pair that moves away at a 45° upwards angle to the left or right of the tip of the plate. The direction is random and dependent on starting conditions, once a direction is established it is continued for an indefinite period of time.

For $3 < KC < 8$ the vortices of the previous cycles have started decaying and thus will start orbiting around the newly shed, stronger vortices. This results in a more complex flow pattern that does not reset itself each cycle such as is the case with $KC < 3$. This means that on each side of the plate a new vortex is generated each half cycle around which the older vortex starts orbiting. The time for shedding a fully developed vortex and the decay time are identified to be crucial to determine flow and pressure characteristics.

For $KC > 8$ the vortex shedding approaches a steady state in which one large vortex is shed each half cycle in addition to various smaller ones which develop if the longer duration of a cycle allows them to. Increasing the KC number leads to more vortices being shed.

Yeung utilized a different approach, using a vertical, partially submerged plate with an angular forced oscillation at the emerged end, which thus includes the free surface and an angular movement [41]. Yeung's results are not directly comparable due to differences between the setup and KC number. What can be compared are the identified flow regimes. Yeung observed two flow regimes, the so-called symmetrical and asymmetrical regimes. The asymmetrical regime is similar to the area identified by Sarpkaya for $KC < 3$

with a shedding of vortex pairs in one 45° direction. The symmetrical flow regime is similar to the $3 < KC < 8$ regime, which is described by Yeung as a vortex pair which is not strong enough to move away from the plate and where the older vortex is absorbed by the newer, stronger one. While there are discrepancies between the work of Sarpkaya and the work of Yeung, the identified regimes are similar.

Various experiments very similar to the work of Yeung have been done by Klaka et al. [42]. A distinct difference is that Klaka et al. compares 2D and 3D effects. Unfortunately the flow is not visualized and only forces, moments and damping coefficient are considered. One important note is made. Klaka et al. found a transition in the 2D model at a certain frequency that caused a (relatively) large shift in the roll moment generated, which was not encountered in the 3D model. They theorized that the transition observed from symmetric to asymmetric vortex shedding by Yeung is the most likely source of the transitional phenomenon. This brings into question the results of Yeung for a 3D case. It should be noted that a long bilge keel is more similar to a 2D setup as end effects will be very small.

Aloisio performed a PIV analysis of a ship model with a bilge keel during a free roll decay test [43]. At a Froude number of zero (no forward speed) Aloisio identifies the formation of the Kelvin-Helmholtz instability (mostly found at the separation between two fluids). This instability is characterized by acceleration instead of velocity. The intensity of the vortex is found to be dependent on the roll amplitude. The vortex behavior seems similar to that identified by Sarpkaya and O'Keefe where in the beginning the flow regime is similar to the $3 < KC < 8$ regime as identified by Sarpkaya, although from the data provided by Aloisio it is impossible to determine to relevant KC number.

Oliveira studied the effect of vortex shedding due to large bilge keels on the roll damping on an FPSO using numerical methods and experiments with PIV [44]. During a decay test the behavior of the vortices is analyzed. A 45° shedding angle is observed, which gives the impression of the $KC < 3$ area identified by Sarpkaya. This holds for smaller roll angles, but at larger angles the interaction between the vortices becomes too strong, resulting in a split of the pair into two pairs. One pair will move away from the hull while the other hugs the wall. This separation can explain the limit on roll damping at large angles where it seems to reach saturation. After some periods a vortex street can be observed. It is furthermore determined through regular wave experiments that the size of the bilge keel has a influence of the natural roll frequency, i.e. larger bilge keels lead to lower natural frequency. This is most likely due to additional added mass.

Avalos performed experiments and numerical calculations to study vortex shedding and roll damping around bilge keels on sharp and rounded bilges [45]. After the first one-and-a-half oscillation the last vortex interacts with the previous vortex through which both are dissipated. From this point on the flow field seems to reach a steady state similar to the regime identified by Sarpkaya for $KC < 3$ with pairs shedding at a 45° angle, most likely as the outer vortex is less strong. It should be noted that from simple calculations the KC number belonging to Avalon's data seems higher that three. It should also be noted that the KC-number is hard to determine as the roll center position is unclear. It was identified that as the bilge keel becomes smaller the flow becomes more complex and the vortices shed start 'hugging' the hull, similar to other experiments.

2.3.1. NEAR-SURFACE INFLUENCE

From sources such as Bernal [46] it is stated that as a vortex approaches the surface, the vortex lines open, resulting in vortex lines that run from and to the surface. Ohring numerically shows that a vortex can connect and be absorbed by the surface, connect and create a secondary vortex or bounce from the surface while creating multiple secondary vortices [47]. This depends on the vortex velocity and the amount of surface tension present.

Rood performed similar research in 1994, with similar results [48]. He shows with a thought experiment that vorticity is not conserved, while not ignoring any physical laws such as conservation of momentum and mass. Imagine an infinite horizontal plate with a fluid on top and bounded by another plate on top of the fluid. If the lower plate starts moving a velocity gradient will be created which will results in a steady-state of constant vorticity. If the upper plate is replaced with a free surface the flow velocity will become equal to that of the moving plate resulting in zero vorticity as no gradient is present. In reality the free surface is an interface between two fluids where vorticity is transferred from one fluid to another. In his paper Rood reviews other literature (including Bernal's work) that confirm this hypothesis.

2.3.2. INFLUENCE OF (IRREGULAR) WAVE-INDUCED ORBITAL VELOCITIES

While studies have been done towards vortices generated by a fully submerged cylinder under wave action, less work has been done on bluff bodies, bodies with appendages and partially submerged bodies.

Jung performed an experiment in 2002 with a fixed rectangular structure in waves [49] and [50]. PIV

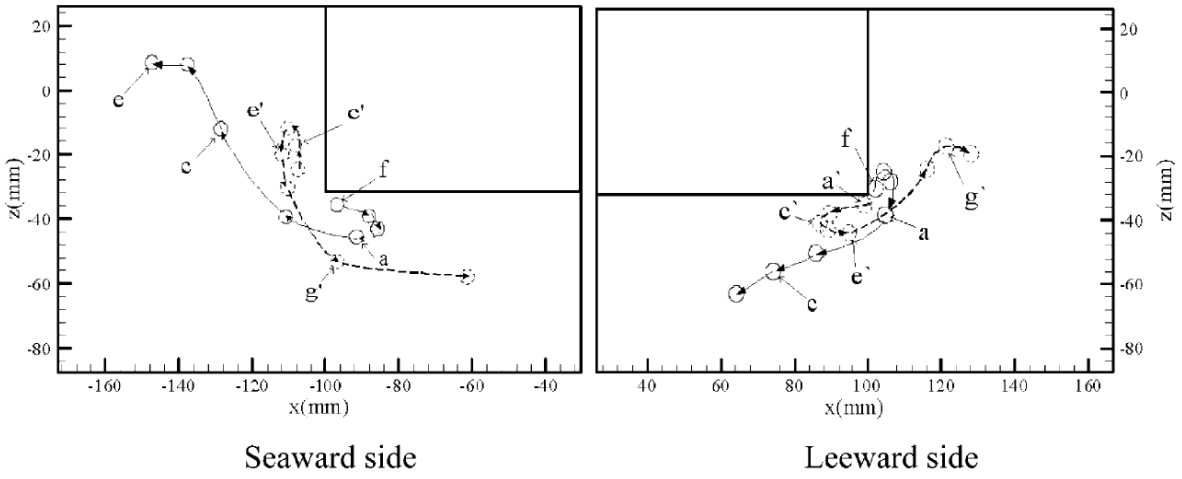

Figure 2.7: Path of the highest vorticity concentrations of a fixed rectangle in a regular wave. The solid line and circle is positive vorticity, while the dotted line and circle are negative vorticity. The points a through e represent the time of the snapshots. For the seaward side this is an inverse cosine and for the leeward side this is an inverse sine for wave elevation 8 cm before the barge (seaward) and 8 cm behind the barge (leeward). From Jung [50].

recordings were made and analyzed. Vortex paths were analyzed and presented as in Figure 2.7. The paths seem to venture quite far from the hull, but the vorticity extends quite far from the center of intensity. Significant differences were found between the leeward and seaward sides. It is observed that water surface level and velocities around the barge have a large impact on the shedding and path of the vortices. The absolute vorticity on the leeward side is observed to be roughly half of that on the seaward side. Jung does not discuss pressure, so no conclusions can be made on the impact on hull pressure damping.

In 2005 Jung continued work on the rectangular body (without keels) in waves, but now instead of fixed it was free on the roll axis using a hinge through the CoG [22]. In waves with a period longer than the natural period of the structure is was identified that the rolling body moved in the same direction as the fluid flow, but the fluid flow had a larger magnitude. This means that the relative velocity was lower leading to less strong vortices, as opposed to what was described in Section 2.2. For a wave with the natural period this is not valid and the vortices are generated in the wake of the body roll motion and cause positive damping. The vortex shedding patterns at the natural period were not discussed while these are of interest for this review. Other patterns were found to be similar to the fixed case, reference is made to the previous paragraph.

In 2006 Jung continued his research but with a larger spread of wave periods and aimed at viscous damping [23]. The research contains PIV images, from which it is identified that the vortices at the leeward and seaward side are the same size and magnitude for the natural roll period. At shorter periods the leeward side shows a decrease of size and magnitude of the vortices compared to the seaward side.

In 1999 Oshkai and Rockwell applied PIV to a submerged cylinder at various depths, subjected to wave action [51]. It is noted that decreasing the depth of the cylinder resulted in the retardation of the orbital motion and variations in the shedding point of the vortices.

Chen performed RANS simulations and used PIV measurements by Jung [49] on a fixed and rolling rectangular barge subjected to wave motions. The validated RANS code was used to simulate a barge in regular waves that capsized due to extreme roll motions [52] and one DoF large amplitude roll motions of a barge in a regular wave [53]. Unfortunately the discussion about the large amplitude roll motions in a regular wave is limited to the influence of the wave period, where it was identified that waves with the same period as the free-decay period were causing resonance. As for the capsizing simulation more results were visualized. It is surmised that the wave-induced velocities are strong enough to generate vortices due to flow separations at the barge corners, with a strong positive vortex being created when the surface elevation rises. As the surface level drops the positive vortex decays and an elongated negative vortex is created which is subsequently shed as the flow velocity forces it downward.

2.4. ON CFD

Bilge keels or similar problems have recently [16], [24], [34], [54], [55], [56], [57], [58], [59], [60], [61], [62], [63], [64] and not so recently [27], [28], [65] and [66] been modeled using CFD code.

Van 't Veer used the STAR-CCM+ software and experiments in combination with a Unsteady Reynolds-Averaged Navier-Stokes (URANS) and a Finite Volume Method (FVM) method with Rhie and Chow interpolation to create a 3D model of an FPSO section [24] and [16]. The presence of air was modeled using the VoF method. Coupling was achieved using the SIMPLE algorithm and accelerated using a Multigrid algorithm. The SST turbulence model was employed. Three grids were used to determine the discretization error, although a full study remains to be done. The mesh is adapted each time-step to incorporate the roll motion using a inner and outer mesh.

Davis employed STAR-CCM+ and experiments to study the various RANS turbulence models for a flow over a wall-mounted cylinder [54]. The FVM was used for discretization with polyhedral elements. Three meshes were utilized and a mesh dependence study was performed. It was concluded that for a wall-mounted cylinder the Realizable $\kappa-\epsilon$ model is superior over the $\kappa-\omega$ and V2F model as it captured certain flow phenomena absent in the other models. It should be noted that the Realizable model seemed to keep mesh dependence, allowing the use of fine meshes.

Quérard studied a RANS application to bilge keels and baffles. Various meshes, timesteps and turbulence models were compared. In general the best results were obtained by using an SST model over a $\kappa-\epsilon$ model. It was observed that the RANS code was suitable to predict the forces on the keel, as well as the newly formed vortices. The convected vortices required a more refined mesh and timestep to correctly predict the size, center and velocities of the vortices. As the influence of the convected vortices decreases with distance they are less relevant.

Khatir utilized a boundary element method with a vortex method to simulate a near-wall fluid flow and is focused on boundary conditions [56]. It is mostly relevant for flows over arbitrarily shaped bodies and complex geometry implemented in DVMs and is compared to the method of images. The results are compared to experiments and good agreement is found.

Yeung focused on finned bodies and the FSRVM [57]. The Free-Surface Random-Vortex Method (FSRVM) is a hybrid Lagrangian-Eulerian method similar to the DVM and potential flow combination as the flow is seperated in a irrotational and rotational part. Diffusion is simulated by giving each vorton blob a random path using a Gaussian distribution. The results are compared to experiments for a bilge keel. The hydrodynamic moment seems to reach reasonable agreement after one and a half period, with some over-prediction in the negative moment. The delay in agreement could be caused by different initial conditions, as the water in a basin in never fully at rest. Roll damping coefficients are estimated well at lower frequencies, while at higher frequencies the experiments and model start to deviate. This can be attributed to less accuracy in the experiments. Excellent agreement was attained in free decay experiments for a short period after which the bearing friction could not be neglected anymore. It seems FSRVM is a good method for 2D models of bilge keels. In research by Seah, reference is made to [62], the FSRVM was used to model FPSO sections similar to the experiments performed by Na [67]. There is good agreement between the model trend and the experimental trend, although model damping values are higher than experimental values. It should be noted that the measured values are assessed as low compared to inviscid theory.

Leloux has brought attention to the Principia EOLE code to simulate a "Clarom" barge [34]. EOLE utilizes the FVM for discretization and the VoF method for the free-surface and is based around Pseudo-Unsteady Systems (PUS) and RANS using the Gorski turbulence model which combines the $\kappa-\epsilon$ model with algebraic equations for the near-wall viscous layer. Results for the roll damping coefficients seem in good agreement with the experiments, except for small angles, where a finer mesh is recommended. The validation is discussed quite summarily so it is hard to validate the results from a third party perspective.

Kinnas modeled an oscillating flow past a vertical plate [58]. In this method Euler and Navier-Stokes equations were used in combination with FVM. The resulting drag and inertia coefficients were close to measurements at low KC numbers but a turbulence model was not implemented. Reference is made to later papers that incorporate these turbulence models for more relevant results. The same model was applied to study bilge keel flow separation, but was not experimentally verified, only against flow past a wall-mounted vertical plate [59]. In a paper by Kinnas [60] the above mentioned solver was compared to the FLUENT software and good agreement was achieved. Various solvers were compared but no experimental validation took place. Yu compared the results to published experimental data for box and step shaped hulls [61]. Good agreement was found.

Graham tried to apply DVM combined with the panel method to predict the hydrodynamic damping of

floating bodies [63]. The method is compared to DNS and experimental results. The roll RAOs for regular waves compare well to wave-flume tests around resonance frequency.

Huijsmans aimed to provide an insight on the water velocities and pressures around an FPSO using PIV for use in CFD techniques [64]. RAOs were determined for the water velocities at two points near the bilge keel and compared to linear potential flow theory. As expected the linear theory overestimates the flow velocities, especially at point A located at the bottom of the hull and at lower frequencies. The PIV data should be sufficient for CFD validation.

Miyake looked at bilge keels for a new type of non-ballast ship with a rounder cross section [55]. The commercial code Fluent is used to calculate a vertical plate on a wall and two vertical plates in tandem on a wall. A CFD study is performed to visualize the effects taking place. It it shown that two bilge keels in tandem have large effects on each other when placed close enough. The results are not validated.

Brown developed a theory for vortex shedding from marine vehicles using DVM [27]. In his paper he provides an extensive overview of previous work. The paper focuses on showing that the DVM correctly shows the vortex shedding component and allows good prediction when combined with potential flow theory. Potential flow theory is compared to experimental data and vortex shedding influence is evaluated but no direct comparison between the DVM and experiments is made. It is furthermore concluded that the roll center determined from potential flow theory is sufficient to be used in vortex shedding applications.

Downie used the DVM similar to Brown, including potential flow theory for far-field calculations to evaluate the effect of vortex shedding on roll response [28]. The DVM was used to evaluate the vortex shedding forces to be used in addition with potential theory resulting in a new equation of motion. The results were compared with experimental data based on a round-edged barge instead of a sharp edge.

Taylor based his research around the DVM as well [65]. He aimed to provide an insight into the unsteady flow around square and rectangular section cylinders. The results show good agreement with various experiments, including pressure distributions. It should be noted that only stationary bodies were evaluated. Reference is made to a future report for moving bodies.

Graham utilizes a Cloud-in-Cell vortex method (ViC) to evaluate vortex shedding from edges resulting in a mixed Lagrangian-Eulerian method [66]. The method is used to identify flow phenomena which are summarily compared to experiments.

Lian used a method a developed by Graham in 1977, not dissimilar to DVM [68]. Good agreement is found for a long bilge keel for C_D and C_M. In other cases the drag coefficient is underestimated up to 20%

Avalos used the FVM method with an upwind TVD Roe-Sweby scheme to simulate the roll decay of an FPSO with bilge keels [45]. The free surface is considered flat and thus radiation waves are neglected. Good results are obtained compared to experiments with a slight underestimation most likely due to neglecting the radiated waves.

Kim employed RANS with a $\kappa - \epsilon$ to recreate the experiments done by Jung, reference is made to [49] and [22]. This included the roll motion of a rectangular body in a regular wave with a wave period longer than the natural period of the body. Results were in good agreement with experiments, even close to resonance.

2.5. DISCUSSION

As the discussion aims to answer the research questions posed in the literature review a recap is given:

1. What is the current state-of-the-art in the field of roll damping?
2. Which approaches have been taken to solve the roll damping of an FPSO and what angles seem promising?
3. What are the physical workings of vortices, dependency on velocity and their influence on hull pressure?
4. What is an appropriate CFD method that balances accuracy and computation time with the capability to accurately compute hull-pressures and vortex shedding?

The first and second questions have been answered in Chapter 2.2. An overview has been provided of the current state-of-the art as well as of the various issues that still remain to be solved for roll damping to be properly calculated in waves. The most promising angle at this point in time seems a combination of empirical data and\or CFD with potential flow programs based around local kinematics.

The third research question is challenging as the basics of vortices and the generation are understood, but there is not a lot written on the influence of (ir)regular wave orbital motions. The conclusion is that vortices

can be assumed to dissipate or be removed from influence when reaching the free surface. Furthermore they are impacted by local velocities but the influence on the hull pressure is not clear. Dependency on local velocities and accelerations has been observed. The conclusion is that while the flow patterns can be captured from experiments and CFD and certain patterns can be identified the problem is too complex to generate proper formulations to capture the various phenomena on a analytic or flexible semi-empirical formulation.

The last question has been appropriately answered in Section 2.4. The problem with the answer is that it is not definitive as a method for a certain application can only be evaluated properly after it has been applied. The method of choice now is the model based on RANS with an SST turbulence model by J.L. Pelerin as it is readily available. Other options include a RANS model with a Realizable $\kappa - \epsilon$ model or the DVM method. A thorough and proper evaluation of the method selected and the resulting model should be performed.

3

Proposed Methodology

In this Chapter a methodology is proposed based on the results of the previous Chapter. This method should allow the goals of this thesis to be reached.

3.1. Alternatives

While the ITH method definitely has its merits, it has shortcomings as shown in the previous Chapter. The various alternatives to predict roll damping and motion are discussed in the subsequent Sections.

3.1.1. Full CFD

As nowadays CFD is becoming more and more readily available, it seems to make sense to utilize CFD in ship motions. Unfortunately CFD is still a very time consuming with computation requirements steeply increasing with added features such as three dimensions, ship motions, waves etc. This means that while CFD might be a useful tool for analyzing and researching ship motions, computational and thus time constraints do not allow usage during for example a tender period.

3.1.2. Expanding the ITH method

The limitations of the ITH method could perhaps be circumvented by expanding on it. For example by adjusting the assumed pressure distributions and basing them on local kinematics instead of global motions. It remains difficult to capture the influence of complex hull and bilge keel geometry into single or range of (semi-empirical) formula, as the flow complexities created due to a bilge keel are not easily defined, let alone their influence on the hull pressure. The ITH method method is strictly speaking applicable to only fishing and small cargo vessels, where the semi-empirical formulation was based upon. It so happens that it seems applicable to some extent to other vessels, but this is limited by bilge keel sizes and geometries. Converting the ITH method to work with local kinematics is trivial and is thus worth analyzing. So instead of utilizing regular motions to describe the local velocity the ITH method is written as:

$$M_{ITH}(t) = \frac{1}{2}\rho L\left(\int_S l_m C_P dS + h_{bk} C_D\right) U(t)|U(t)|. \tag{3.1}$$

Here C_P and C_D both depend on the frequency and amplitude of the local velocity. For further details on C_P reference is made to Ikeda [7].

3.1.3. Combining CFD and an ITH-based approach

Another method would be to combine results from CFD with linear potential theory to incorporate complex hull and bilge keel geometry influence from CFD into a model that could take simpler parameters such as draft into account as input parameters. This is similar to the work done by Hajiarab [31], but instead of relying on a less flexible DVM a more flexible and widely used RANS approach based on the ITH method separation of damping is possible which allows for easier integration of complex geometries and general application.

3.2. PROPOSED METHODOLOGY

In the next Sections the framework of the methodology that is proposed is presented.

3.2.1. OVERALL

The proposed methodology uses the method of Ikeda where the bilge keel damping is split in three components and groups them into two categories:

- bilge keel normal force moment, and
- bilge keel hull pressure moment and bilge keel wave moment.

The basic premise is that the empirical coefficients used in the ITH method cannot be applied to a general situation. It is furthermore recognized that especially the hull pressure cannot be properly described analytically and is furthermore hard to parameterize without requiring a stupendous amount of expensive and time-consuming experiments.

The proposed solution for this issue is the application of CFD. CFD has the advantage of allowing any combination of bilge keel and hull shape to be simulated. One of the disadvantages is old engineering dilemma of time versus accuracy. It is possible to simulate the motions of a vessel in all DoF and in 3D, including waves, using CFD, but this would result in a exceedingly complex simulation and impractical computational time-spans. This is why the problem is simplified in a manner similar to the strip theory. The problem is reduced to 2D slices of the vessel, where the relevant slices are simulated in the roll DoF undergoing forced oscillations with a certain amplitude and frequency. This allows the desired coefficients to be obtained in a relatively short period of time, around twenty hours on a 2012 desktop computer and much faster and in parallel on a computing cluster. Furthermore a database can be built by collecting old runs and thus possibly a semblance of parameterization in the future.

The need to base a methodology around local velocities, incorporating waves as well as velocities due to other motions, is also recognized. Ir-rotational, non-viscous velocities in waves can be obtained using linear potential theory and superposition. The local velocities are divided into four separate components:

- rigid body velocities,
- radiated wave velocities,
- incoming wave velocities, and
- diffracted wave velocities.

Here the rigid and radiated velocities can be calculated depending on the six rigid body motions of all six DoF. The incoming and diffracted wave velocities are assumed to be independent of motion. The general assumption that is made here is that the velocities obtained from linear potential theory can be used to estimate the undisturbed velocities 'felt' by the tip of the bilge keel.

The governing formula for the moments and forces caused by the bilge keel are similar to those assumed in the ITH method but are somewhat adjusted, which is discussed in the next two Sections. Three main items to discuss arise from this approach:

- the implementation of the methodology,
- the CFD, and
- the validation of the methodology.

The implementation will be discussed in the subsequent Sections. The CFD will be discussed in Chapter 4. As for validation of the methodology reference is made to Chapter 5.

3.2.2. KEEL FORCES

It has been shown by van 't Veer [26] and in a more basic sense by Keulegan and Carpenter [69] that the the loads acting on the bilge keel can accurately be predicted using a Morison equation with higher harmonics:

$$M(t) = l\left(\frac{1}{2}\rho C_D(KC)AU(t)|U(t)| + \rho V C_M(KC)\dot{U}(t) + \Delta R\right). \tag{3.2}$$

Here ΔR is a remainder function containing the third and fifth linear in and out of phase harmonics.

While higher harmonics are necessary to predict loads properly their impact on the effective damping is not directly clear. The amount of damping performed can be determined through mean work performed, thus energy removed or added from the system:

$$P = \int \frac{M\dot{x}_4}{T} dt. \tag{3.3}$$

Replacing M by a moment with a sine wave with an arbitrary phase ϕ and frequency Ω and $\dot{x}_4$ by a representative harmonic roll velocity as higher harmonics are linear results in the following evaluation:

$$\frac{\omega}{2\pi}\int_0^{\frac{2\pi}{\omega}} \underbrace{Bsin(\Omega t+\phi)}_{\text{Moment}}\underbrace{X_4(\omega)\omega sin(\omega t)}_{\text{Roll velocity}} dt = BX_4(\omega)\frac{\omega^2\left(sin(\phi(\omega)) - sin(2\pi\frac{\Omega}{\omega}+\phi)\right)}{(\omega-\Omega)(\omega+\Omega)}. \tag{3.4}$$

Examination of Equation 3.4, which was obtained using Wolfram Alpha, shows that there is a normalized envelope present of:

$$\pm\frac{\omega^3}{\pi}\frac{sin\left(\pi\frac{\Omega}{\omega}\right)}{(\omega+\Omega)(\omega-\Omega)}. \tag{3.5}$$

Reference is made to Figure 3.1 for a plot of this function. It can be noted that in regular waves higher harmonics do not play a role in damping, there is no energy added or removed from the main motion of the system.

In irregular waves this is a bit different. The dominating higher harmonics are the third and fifth harmonics. The relation between the energy removed by the third and fifth harmonics and a certain frequency lower than the frequency of the dominating motion in review is shown in Figure 3.2. The combination of a narrow-banded roll response, relatively small third and fifth harmonic coefficients in comparison to the first and the fact that at half the motion frequency the effectiveness of the third harmonic is at maximum half leads to the conclusion that higher harmonics are likely to have a small impact in irregular waves. Of course a different spectrum and the combination of all terms could still lead to a more significant influence thus this theory is best evaluated using actual coefficients and integrating over ω, but in this thesis the remainder function is assumed to have a small influence and thus the moment caused by the keel force is evaluated as:

$$M(t) = l\left(\frac{1}{2}\rho C_D(KC)AU(t)|U(t)| + \rho V C_M(KC)\dot{U}(t)\right). \tag{3.6}$$

Here the inertia coefficient C_M is assumed to be only dependent on the KC number although a small dependency on frequency is observed.

3.2.3. HULL PRESSURES

The bilge keel hull pressures are observed from experiments to be mostly proportional to local velocity and have a dependency on the amplitude of that velocity. Experiment particulars can be found in Appendix A. This is thus assumed to simplify the selection of a proper coefficient and reasonable implementation. There is furthermore a dependency on which side the vortex forms, i.e. during a negative velocity cycle the pressure on the hull is different than during a positive velocity cycle. This results in a asymmetric damping moment during a motion. Higher harmonics are present but small. This results in the following Equation:

$$M(t) = B_h(sgn(U), U_a)U(t) + A_h(sgn(U), U_a)\dot{U}(t). \tag{3.7}$$

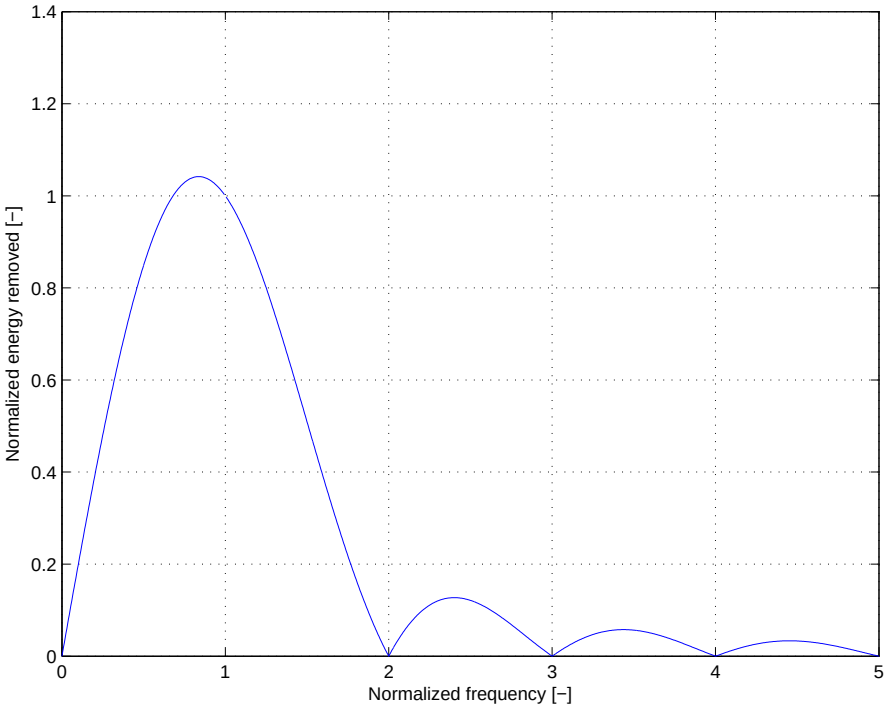

Figure 3.1: Normalized energy removed due to moments at a certain frequency normalized against the frequency of the motion. Here one is the frequency of the motion. So a moment with a frequency of 2.5 times the motion frequency removes only one-tenth of the possible energy removal.

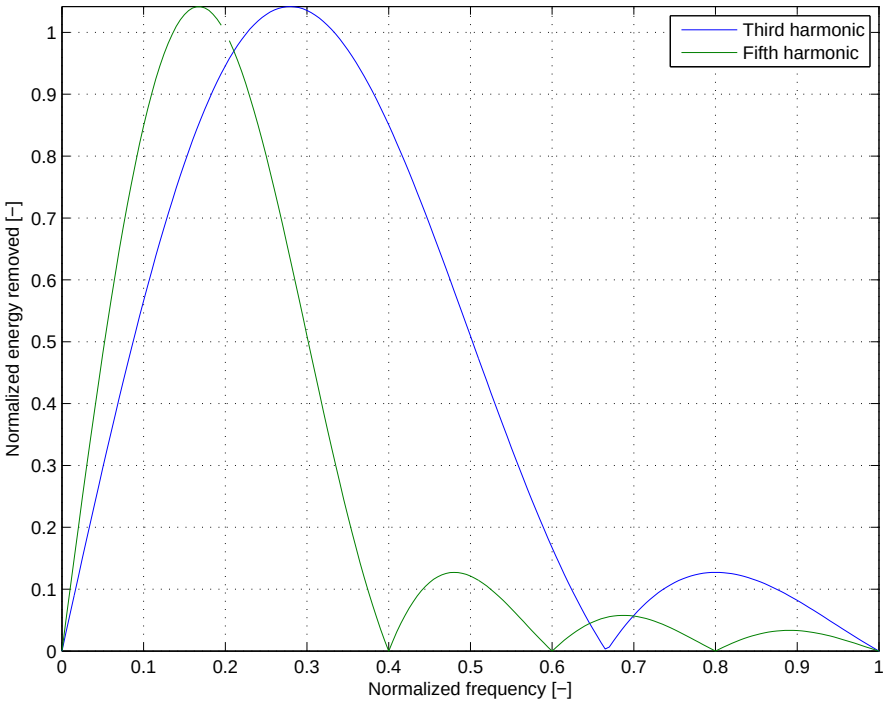

Figure 3.2: Normalized energy removed due to moments at the third and fifth harmonic caused by a certain frequency normalized against the frequency of the motion. Here one is the frequency of the motion. So the third and fifth harmonics of a motion only remove half and one eight of the possible energy removal respectively.

3.2.4. COEFFICIENTS

From the above equations the unknowns are C_D, C_M, A_h and B_h. These coefficients are determined using CFD. C_D and C_M are less dependent on the hull shape and more dependent on the bilge keel geometry and can be applied in a more general fashion or used as obtained from literature, validation from CFD is possible. B_h and A_h are dependent on the hull geometry and bilge keel geometry. While the pressure drop over the bilge keel can be determined from the normal force acting on the bilge keel the pressures from the subsequently generated vortex cannot. This is where theory is supplemented by CFD as the CFD calculations can accurately describe the vortex-induced pressures, allowing B_h and A_h to be obtained. As B_h and A_h are coupled to actual local velocities, not only rigid body velocities are used in the CFD to extract the coefficients but radiated velocities as well.

3.3. IMPLEMENTATION PATHS

While the methodology described in the previous Section results in constants and equations for roll moment and damping that can be solved, the methodology to implement these equations needs to be determined as well. In general two paths are available when ship motions are concerned: the frequency domain and the time domain. Both methods have their advantages and disadvantages. The difference is best characterized as the frequently encountered problem of time versus accuracy. The frequency domain allows for rapid calculation as it is independent on time and time steps, but allows only linear systems and the results are based around a host of assumptions. This results in reduced accuracy and reduced applicability.

The time domain has little constraints in complexity, but comes with a cost of a much higher computational time. As the goal is to obtain information about the probability of large vessel motions some statistical information needs to be obtained. In the time domain this usually means that one calculation of not enough, but that a multitude of realizations need to be performed to obtain a sufficiently accurate Cumulative Density Function (CDF) of the value of interest, i.e. a Monte Carlo simulation needs to be performed.

A third option is the combination of the frequency and the time domain. Various sources show that when a proper coefficients are chosen, solutions in the frequency domain can yield quite satisfactory results. It might be possible to obtain these coefficients more easily in the time domain than in the frequency domain from a few short realizations which should be acceptable time-wise and apply these coefficients in the time domain.

3.4. TIME DOMAIN

In this Section the implementation of a time domain methodology will be discussed. The basic equation to describe roll motion in the time domain, based around the Cummins equation [19], is:

$$(M+A)\ddot{x}_4(t) + \int_0^\infty B(\tau)\dot{x}_4(t-\tau)d\tau + Cx_4(t) = M_{wave}(t) + M_{hp}(t) + M_{bk}(t) + M_{mem}(t) \tag{3.8}$$

where the coupling terms are omitted for clarity. The left side of Equation 3.8 and the $M_{wave}(t)$ terms are well known and applied and thus reference is made to Journée [2] for further details. The other terms require some additional information to make sense. The M_{hp} and M_{bk} are the hull pressure and keel force induced moments as described in Equations 3.7 and 3.6 respectively. The issues that remain are the correct selection of the coefficients C_D, C_M, B_h and A_h and the calculation of the local velocities U and acceleration $\dot{U}$ for use in Equations 3.7 and 3.6.

Ogilvie shows a method to relate linear frequency domain damping coefficients from potential theory to the retardation function $B(\tau)$ in Equation 3.8, reference in made to Ogilvie [70]:

$$B(\tau) = \frac{2}{\pi}\int_0^\infty b(\omega)cos(\omega\tau)d\omega. \tag{3.9}$$

This method allows for any excitation to be used, however irregular. In regular waves and forced oscillations, or other harmonic motions, the retardation function can be replaced by $b(\omega)$ and A by $a(\omega)$. Other functions become dependent not only on time, but on frequency as well.

3.4.1. VELOCITIES

The local velocities in the time domain can be split into four components:

- rigid body velocities,

- radiated wave velocities,
- incoming wave velocities, and
- diffracted wave velocities.

Rigid body and radiated velocities in the global coordinate system in regular waves are obtained using Equations 3.10, 3.12 and 3.11 where x_{bk}, y_{bk} and z_{bk} are the coordinates of the tip of the bilge keel and A and B are the in- and out-of-phase terms of the radiated velocities obtained from HydroStar after transformation. The total relative velocities are obtained through Equation 3.13 where diffracted and incoming velocities are readily obtained. The bilge keel normal vector is obtained and corrected for rotations in Equation 3.11 after which the magnitude of the total normal vector and thus rigid body velocities can readily be obtained. The R_n matrices in Equations 3.14a-c are the standard right-hand-rule rotational matrices for use in a Cartesian coordinate system and allow for the non-linear implementation of the rigid body velocities. In linear calculations such as performed in HydroStar all components are evaluated separately, i.e. the pitch has no influence on velocities caused by heave, the rotation matrices have their angles set to zero. The impact of this assumption is evaluated in Chapter 5.

$$\begin{bmatrix} U_{rig,x} \\ U_{rig,y} \\ U_{rig,z} \end{bmatrix} = \begin{bmatrix} 1 & 0 & 0 & 0 & z_{bk}sin(x_5) & -y_{bk}sin(x_6) \\ 0 & 1 & 0 & -z_{bk}sin(x_4+a) & 0 & x_{bk}cos(x_6) \\ 0 & 0 & 1 & y_{bk}cos(x_4+a) & -x_{bk}cos(x_5) & 0 \end{bmatrix} \begin{bmatrix} \dot{x}_1 \\ \dot{x}_2 \\ \dot{x}_3 \\ \dot{x}_4 \\ \dot{x}_5 \\ \dot{x}_6 \end{bmatrix} \tag{3.10}$$

$$U_{rig} = \begin{bmatrix} 0 & -sin(\alpha_{bk}) & cos(\alpha_{bk}) \end{bmatrix} \boldsymbol{R}_x(x_4)\boldsymbol{R}_y(x_5)\boldsymbol{R}_z(x_6) \begin{bmatrix} U_{rig,x} \\ U_{rig,y} \\ U_{rig,z} \end{bmatrix} \tag{3.11}$$

$$\begin{bmatrix} U_{rad,x} \\ U_{rad,y} \\ U_{rad,z} \end{bmatrix} = \sum_{n=1}^{6} \begin{bmatrix} B_{x,n} & A_{x,n} \\ B_{y,n} & A_{y,n} \\ B_{z,n} & A_{z,n} \end{bmatrix} \begin{bmatrix} \dot{x}_n \\ \ddot{x}_n \end{bmatrix} \tag{3.12}$$

$$U = \begin{bmatrix} 0 & -sin(\alpha_{bk}) & cos(\alpha_{bk}) \end{bmatrix} \begin{bmatrix} U_{rad,x} + U_{diff,x} + U_{inc,x} \\ U_{rad,y} + U_{diff,y} + U_{inc,y} \\ U_{rad,z} + U_{diff,z} + U_{inc,z} \end{bmatrix} + U_{rig} \tag{3.13}$$

$$\boldsymbol{R}_x(x_4) = \begin{bmatrix} 1 & 0 & 0 \\ 0 & cos(x_4) & -sin(x_4) \\ 0 & sin(x_4) & cos(x_4) \end{bmatrix}, \tag{3.14a}$$

$$\boldsymbol{R}_y(x_5) = \begin{bmatrix} cos(x_5) & 0 & sin(x_5) \\ 0 & 1 & 0 \\ -sin(x_5) & 0 & cos(x_5) \end{bmatrix}, \tag{3.14b}$$

$$\boldsymbol{R}_z(x_6) = \begin{bmatrix} cos(x_6) & -sin(x_6) & 0 \\ sin(x_6) & cos(x_6) & 0 \\ 0 & 0 & 1 \end{bmatrix}. \tag{3.14c}$$

In irregular waves the velocities are influenced by the memory effect as described by Cummins, while the connection to the frequency domain is made as described by Ogilvie [70], resulting in:

$$U_{rad}(t) = A\ddot{x}(t) + \int_0^t K_U(\tau)\dot{x}(t-\tau)d\tau. \tag{3.15}$$

The incoming and diffracted velocities are independent of rigid body motions and only dependent on time are are thus obtained directly from potential theory and diffraction calculations.

3.4.2. ACCELERATIONS

Accelerations are determined in a similar manner as the velocities, taking the derivative off all velocity terms. In case of the radiated velocities this results in dependence on jerk $\dddot{x}$ which is physical less relevant and suspicable to numerical noise. In a harmonic motion such as forced oscillations or regular waves A is reduced to $A_{red} = -A\omega^2$ which reduces the dependence to the first order derivative, velocity.

In irregular waves the radiated accelerations are again different and determined using again the method as by Ogilvie [70]:

$$\Phi(t) = \dot{x}(t)\Psi + \int_{-\infty}^{t} \chi(t-\tau)\dot{x}(\tau)d\tau, \tag{3.16}$$

$$\dot{U} = \frac{\delta^2\Phi}{\delta t^2} = \ddot{x}(t)\Psi + \int_{-\infty}^{t} \frac{\delta^2\chi(t-\tau)}{\delta t^2}\dot{x}(\tau)d\tau. \tag{3.17}$$

Rewriting to a more practical form:

$$\dot{U} = A'\ddot{x}(t) + \int_{0}^{\infty} K'_U(\tau)\dot{x}(t-\tau)d\tau. \tag{3.18}$$

Substituting $x = 1.0cos(\omega t)$, splitting the $sin(\omega t - \omega\tau)$ term and rewriting while comparing to the frequency domain equation yields:

$$b(\omega) = -\frac{1}{\omega}\int_{0}^{\infty} K'_U(\tau)sin(\omega\tau)d\tau, \tag{3.19a}$$

$$a(\omega) = A' - \frac{1}{\omega^2}\int_{0}^{\infty} K'_U(\tau)cos(\omega\tau)d\tau. \tag{3.19b}$$

An inverse fourier transform is applied to the first Equation while the second is rewritten.

$$K'_U(\tau) = \frac{2}{\pi}\int_{o}^{\infty} -\omega b(\omega)sin(\omega\tau)d\omega, \tag{3.20a}$$

$$A' = a(\omega) + \frac{1}{\omega^2}\int_{0}^{\infty} K'_U(\tau)cos(\omega\tau)d\tau. \tag{3.20b}$$

An alternative is to simply take the derivative Equation 3.15 resulting in:

$$\dot{U}_{rad}(t) = A\ddot{x}(t) + \int_{0}^{t} K_U(\tau)\ddot{x}_4(t-\tau)d\tau \tag{3.21}$$

Both approaches have the disadvantage of relying on the third derivative or jerk which is not known directly at time t, it can be estimated using a backward-difference method, but will be sensitive to time-step size.

3.4.3. KEEL AND HULL COEFFICIENTS

As the coefficients C_D, C_M, B_h and A_h depend on the maximum velocity and the period of the local velocities and both of these depend on the motion of the vessel an iterative procedure is necessary over the entire simulation run. After a run has finished the local velocities are known and thus KC and Re can be determined, after which convergence can be evaluated.

In an irregular motion the definition of the velocity amplitude, period and thus KC-numbers is not entirely clear. There are a few options to determine the values in an irregular motion, it is possible to

- estimate the amplitude and period using FFT on the time history to determine the most important regular component present and use that to compute the desired values [71]; or
- estimate the values from the period and maxima between two zero crossings [15].

The first option has a computational cost, but it should not be excessive. Its disadvantage is the lag introduced. This means that the velocity amplitude and period will lag behind the actual values until sufficient data has been gathered to allow the recognition of a new dominant regular component from the FFT computations. An iterative loop can solve this issue, but at the cost of additional computational effort.

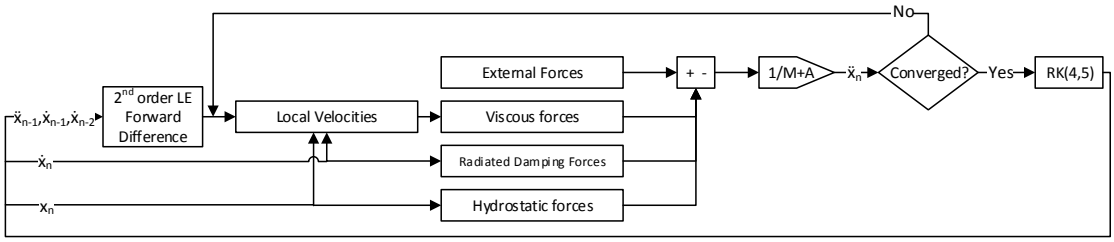

Figure 3.3: Diagram of the implemented differential equation.

The second option requires an iterative procedure which can be in the outer loop or inner loop. It can be determined after each complete run, the outer loop. This results in a time trace of the desired values or a single value representative for that time trace. It is also possible to calculate a values for each encountered zero crossing resulting in back-stepping in time to the previous zero crossing and recalculating until convergence is reached. The second method, i.e. inner iteration, has yielded good results for the prediction of bilge keel forces and is thus preferred.

Overall the second option with an inner iteration is more reliable and proven as shown by van 't Veer [26]. Computational effort might be higher, if it proves prohibitive the first approach or an outer iteration method can be performed.

3.4.4. IMPLEMENTATION

The various numerical implementations and issues are discussed in this Section for regular and irregular waves.

FORCED OSCILLATIONS AND REGULAR WAVES

As the Equations governing the system are known, reference is made to the previous Section, a numerical implementation can be designed. The numerical method used is in the form of a Runge-Kutta(4,5) integrator scheme, which is available by default in the MATLAB environment. The MATLAB implementation requires a single or set of first order ODEs. A second order ODE can be simplified to two first order ODEs using

$$y_1 = x_n, \tag{3.22a}$$
$$y_2 = \dot{x}_n, \tag{3.22b}$$
$$dy_1 = y_2, \tag{3.22c}$$
$$dy_2 = f(x_n, \dot{x}_n, \dot{x}_{n-1}, \dot{x}_{n-2}, \ddot{x}_{n-1}, t_n, t_{n-1}, t_{n-2}). \tag{3.22d}$$

Equation 3.22d is shown graphically in Figure 3.3. There are two loops visible: the internal loop in the RK(4,5) solver and the loop for the accelerations, as the forces and moments depend on the accelerations. Another loop is present over the entire system to allow the selection of the proper coefficients based on the local velocity amplitude and frequency. The convergence criteria is the Keulegan-Carpenter number, i.e. local velocity amplitude and period for each keel.

To provide an initial estimate for the local accelerations a second order fixed leading coefficient finite difference scheme can be used:

$$\dot{y}_n = \frac{3y_n - (3+\rho^2)y_{n-1} + \rho^2 y_{n-2} + (\rho-1)h_n\dot{y}_{n-1}}{2h} + O(h^2) \tag{3.23}$$

with $\rho = \frac{h_n}{h_{n-1}}$ and $h = max(h_n, h_{n-1})$, after which a loop can be performed to converge to a suitable acceleration.

IRREGULAR WAVES

While the regular wave application allows the use of the standard ODE45 solver used within MATLAB this is not applicable in irregular waves. The standard solver is customized allowing for zero and maxima detection

of the local velocity as well as internal iteration steps for the KC-number. It is furthermore changed to allow implementation of the convolution integrals, thus incorporating the values of previous time steps. The second order differential equation as given in Equation 3.8 is reduced to a system of first order equation, where only the roll DoF is shown:

$$y_1 = x_4, \tag{3.24a}$$
$$y_2 = \dot{x}_4, \tag{3.24b}$$

$$dy_1 = y_2, \tag{3.25a}$$
$$dy_2 = f(x_n, \dot{x}_n, \dot{x}_{n-1\ldots N}, \ddot{x}_{n-1\ldots N}, t_n, t_{n-1\ldots N}), \tag{3.25b}$$

with N depending on the length of the retardarion functions. This equation can then be solved in a similar manner to the regular waves.

The retardation functions have to evaluated using an integral from zero to infinity. As radiation-diffraction software is limited to a certain frequency Ω due to computational time the tail of $b(\omega)$ for values higher than Ω is assumed to be proportional with $\frac{1}{\omega^3}$ which allows analytic evaluation of the error. For functions where the tail is different extrapolation is used and integration is performed up to high ω. Visual appreciation is used to estimate the validity of these assumptions.

3.5. FREQUENCY DOMAIN

The basis of calculations in the frequency domain for vessel motions is the assumption that an irregular sea can be decomposed in many harmonic waves with a random phase and an unique frequency, using the assumption of linearity and thus superposition. This results in a 2^{nd} order ODE with is easily solved when harmonic motions are considered:

$$(\boldsymbol{M} + \boldsymbol{A}(\omega))\ddot{\vec{x}}(\omega) + \boldsymbol{B}(\omega)\dot{\vec{x}}(\omega) + \boldsymbol{C}\vec{x}(\omega) = \vec{F}(\omega). \tag{3.26}$$

Solving this equations results in a response amplitude with respect to wave amplitude, an RAO. Using RAOs an energy density spectrum can be constructed where the amplitude squared is divided by the frequency. The amplitude squared for waves is proportional with the energy, reference is made to Journée [2]. It is furthermore assumed that the response of a vessel to these waves can be described using a linear system. When the assumption of a narrow banded spectrum is made a Rayleigh distribution can be assumed for the maxima, which results in a cumulative probability distribution for the vessel motions.

The frequency domain approach simplifies the equations to be solved, but involves some assumptions and requirements that need to be solved. Most of these issues arise from the non-linear damping present which can be treated in a manner as described in Appendix B.

Another issues is that in the frequency domain the KC-number cannot be evaluated directly, as it depends on the maximum total velocity and frequency and is not a sum of the individual wave components, i.e. the superposition principle does not apply. This means the KC-number has to be determined in a different manner. There are two options: utilizing the stochastic properties of the velocity spectrum to determine a representative velocity and zero-crossing period, or by determining the proper KC, or even drag and inertia coefficients from a number of time domain realizations and taking a representative value, for example the dominant harmonic, i.e. determining the stochastic properties in the time-domain.

While the methodology for the time-domain determination of the KC-number is similar to that described in the Section 3.4.3 the stochastic approach is less clear. While good agreement is reached for the mean between the two methods the simplest stochastic methods does not provide information about values other than the mean. Furthermore the mean velocity is most likely not to match with the mean period. To obtain information about at other points than the mean, the joint probability density function of the zero-crossing amplitude and zero-crossing period are necessary. It is recognized that realizations from the JONSWAP spectrum allow a good estimate of real sea-states and thus the KC-number [72].

The joint PDF of the wave period and amplitude which is applicable to a signal with a slowly varying envelope is given by Longuet-Higgins as [73]:

$$p(R,\tau) = \frac{2}{\pi^{\frac{1}{2}}\nu}\frac{R^2}{\tau^2} exp\left[-R^2\left(1 + (1-\frac{1}{\tau})^2/\nu^2\right)\right] L(\nu) \tag{3.27}$$

and by Stansell as [74]:

$$p(R,\tau) = \frac{4}{\nu(1+\sqrt{1+\nu^2})}\sqrt{\pi}\frac{R^2}{\tau^3}exp\left[-\frac{R^2}{\nu^2}\left(\frac{1}{\tau^2}-\frac{2}{\tau}+\nu^2+1\right)\right] \tag{3.28}$$

with

$$\nu^2 = \frac{m_0 m_2}{m_1^2} - 1 \tag{3.29a}$$

$$R = \frac{U}{(2m_0)^{\frac{1}{2}}} \tag{3.29b}$$

$$\tau = \frac{Tm_1}{2\pi m_0} \tag{3.29c}$$

$$L \approx 1 + \frac{1}{4}\nu^2 \tag{3.29d}$$

Then dimensionless amplitude and period R and τ can be rewritten to the relevant KC-number:

$$R\tau = UT\frac{m_1}{\pi(2m_0)^{1.5}} \tag{3.30}$$

$$KC = \frac{R\tau}{c}\frac{\pi(2m_0)^{1.5}}{m_1} \tag{3.31}$$

The Rohatgi integral describes the probability density function of two (in)dependent random variables multiplied with each other [75]:

$$p(C) = \int_0^\infty p\left(R, \frac{C}{R}\right)\frac{1}{|R|}dR \tag{3.32}$$

Using this Equation leads to the cumulative probability density function of the KC number based on the zero-upcrossing period and the amplitude:

$$P\left(KC = \frac{\pi(2m_0)^{1.5}}{cm_1}C\right) = \int_0^{KC} -R^2\int_0^\infty p\left(R, \frac{C}{R}\right)\frac{1}{R}dRdC \tag{3.33}$$

The various methods are compared in Figure 3.4. It can be immediately noted that all methods have considerable differences. Both time-domain methods where one is based on full periods (zero-upcrossings) and the other on half-periods (zero-crossings) vary considerably. This is due to lower amplitudes and usually periods being discarded in the full period method, a half period or quarter period can usually be considered more accurate. The frequency domain methods do not fare better, the mean KC-number from the mean wave-height and the mean zero-upcrossing period yields a low KC-number. This can be explained as the values are dependent, i.e. simply multiplying both means does not yield the mean KC-number as $p(x,y) \neq p(x)p(y)$. The Longuet-Higgins method seems as it usually overestimates larger periods. The Stansell method seems to be more accurate and close to the half-period time-domain results. It should be noted that the upper limit of the frequency during numerical integration for m_2 should be taken high enough to incorporate the high frequency tail of the spectrum.

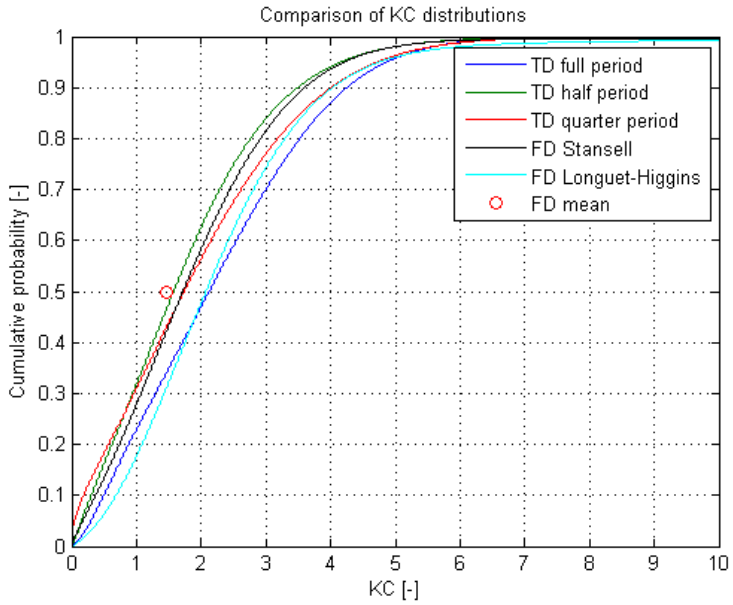

Figure 3.4: Comparison of the various methods to determine the KC-number in irregular flows

3.6. MEMORY EFFECTS

In the time-domain memory effects are partially incorporated as the influence of radiated waves. These effects can be incorporated using the retardation function. This method does not include viscous memory effects as induced by the vortices shed by bilge keels. Reference is made to Section 2.2.2 for a method described by Katayama. This method relies on adjusting the drag coefficient depending on previous cycles. While the proposal is interesting it remains unclear on applications in waves, especially highly irregular waves. Furthermore validation in waves is absent and incorporation of hull pressure damping is not discussed. As the memory effect is very complex and depends on the entire viscous flow history it is not incorporated in the current model as the influence of local kinematics is deemed to have a larger influence.

In frequency domain the memory effects are even more difficult to properly implement, as a stochastic implementation would be necessary. One possibility would be to adjust the frequency dependent damping coefficient based on the chance of the next wave being higher or lower than the current.

3.7. SELECTED IMPLEMENTATION

As the implementations vary in complexity and depend on each other the following order of implementation is adhered:

1. time domain: forced oscillations;
2. time domain: regular wave;
3. time domain: irregular wave; and
4. frequency domain.

Where the regular wave and forced oscillation implementations are simply the irregular wave implementation with instead of the convolution integrals, the frequency domain constants and without an internal iterative for the KC number, but only an outer step over the entire simulation. As for the particulars of the frequency domain a lot of unknowns need to be evaluated through experiments and simulations as to determine which approach is most effective and is thus left for later investigation.

3.8. POTENTIAL FLOW CALCULATIONS

The Bureau Veritas (BV) HydroStar software is utilized to perform the relevant radiation-diffraction calculations. There are two sets of calculations done in HydroStar: for the CFD the relevant midship section and for

Parameter	2D	3D
Radiated velocity	x	x
Potential damping	x	x
Potential added mass	x	x
Exciting forces	-	x
Incoming velocities	-	x
Diffracted velocities	-	x
Hyd. properties	-	x

Table 3.1: Desired parameters from HydroStar

the time domain/frequency domain model the full ship. The results relevant are detailed in Table 3.1. For further details reference is made to Appendix C.

4

CFD Model Verification and Validation

A CFD model was created by Jean-Luc Pelerin from SBM Offshore in CD-Adapco's STAR-CCM+ with an interface designed so it can be used by engineers inexperienced with CFD. This model was used during this thesis to obtain the C_D, C_M, B_h and A_h coefficients of a section of a vessel. Before application becomes feasible validation is required. Two types of experiments are available for validation. Experiments by X. Schut on a 2D circular hull with a variety of bilge keels with forced oscillations in roll with all DoF restricted except roll. The second experiment was a one in forty model of an FPSO in a decaying motion, a forced oscillation, regular waves and irregular waves free in all DoF with soft moorings to counter wave drift forces. Both are discussed in the following Sections after which validation is attempted.

4.1. Experiments by Schut

The experiments performed by Schut were designed to evaluate the influences of complex bilge keels, the validation of the ITTC procedure, slamming, the use of regular motion coefficients in irregular motions and frequency-dependence of the various coefficients. Nonetheless the experiments seem well suited to validate CFD simulations. A circular hull was attached to a moving frame. The hull was semi-2D, i.e. constant radius, using endplates with bilge keels with varying geometry attached over the entire length. The frame with the hull was then oscillated around the CoG to establish a forced roll motion. Reference is made to Appendix A for more information.

Four parameters are varied during the experiments, as such four parameters are used in the CFD simulations. These four parameters are:

- keel geometry,
- draft,
- frequency, and
- amplitude.

As evaluating all possible combinations would require to much computational time, a selection is made in the next Section.

4.1.1. Runs for validation

The various criteria with which the CFD and experimental results are compared are discussed in the Sections that follow. The resulting relevant experiments are listen in Table 4.1. Here ω is the oscillation frequency, d the draft, bk the used bilge keel, reference is made to Appendix A, and X_4 the amplitude of the motion.

Code [#]	$\omega[rad/s]$	$d[m]$	$bk[\#]$	$X_4[deg]$	Purpose
111120	2.62	0.364/0.476	1	12	Various
112120	2.62	0.364/0.476	2	12	Bilge keel
113120	2.62	0.364/0.476	3	12	Bilge keel
114120	2.62	0.364/0.476	4	12	Bilge keel
111060	2.62	0.364/0.476	1	6	Amplitude
111080	2.62	0.364/0.476	1	8	Amplitude
111100	2.62	0.364/0.476	1	10	Amplitude
211120	3.14	0.364/0.476	1	12	Frequency
311120	2.10	0.364/0.476	1	12	Frequency
121120	2.62	0.278/0.371	1	12	Draft
131120	2.62	0.148/0.187	1	12	Draft

Table 4.1: Experiments to be compared to CFD results.

4.2. EXPERIMENTS PERFORMED IN THE ROLL JIP

The FPSO modeled for the Roll JIP was the Bluewater Glas Dowr FPSO.

A multitude of tests were performed:

1. roll decay tests (forced, transient and manual),
2. forced roll tests,
3. regular wave tests, and
4. irregular wave tests.

For the validation of the CFD model the forced oscillation tests are relevant. The forced oscillations were performed using a moment applied at the CoG by accelerating and decelerating an electric engine. The motions in all six DoF were unrestricted which means that a coupling between sway, roll and yaw would be present. Combined with the complex geometry and 3D effects present some deviation in correlation between the CFD and experiments can be expected. After examination of the results from the Roll JIP it was concluded that the differences between the Roll JIP setup and the setup of the CFD simulations are too fundamentally different to allow accurate validation. It was furthermore noted that the obtained coefficients from the Roll JIP are too fundamentally different from literature again showing the influence of the other motions. Reference is made to Appendix A for more information.

4.3. EVALUATION CRITERIA

In the light of roll damping two criteria are important: the hull pressures and the keel forces. These can then be directly incorporated into the methodology proposed in Chapter 3.

4.3.1. KEEL FORCES

The keel forces are assumed to be described by the well known Morison equation:

$$F(t) = \frac{1}{2}\rho C_D A U(t)|U(t)| + \rho V C_M \dot{U}(t) \tag{4.1}$$

While higher harmonics are neglected, reference is made to Section 3.2.2, they are still relevant in determining the proper C_D and C_M values. This means that to obtain the correct coefficients from the data the higher harmonics should be included. Two methods can be used: non-linear least squares fitting and the method described by Keulegan and Carpenter [69] which relies on Fourier decomposition. As the Fourier decomposition does not rely the amount of higher harmonics taken into account it is preferred. Reference is made to Appendix D. The values used for verification and validation are the C_D and C_M coefficients. A note should be made that while in the circular model used by Schut no radiated wave velocities are present, the experiments performed in the Roll JIP do have radiated wave velocities present. This means that these velocities should be a part of U(t) in Equation 4.1 and they are obtained using the radiation calculations performed by HydroStar.

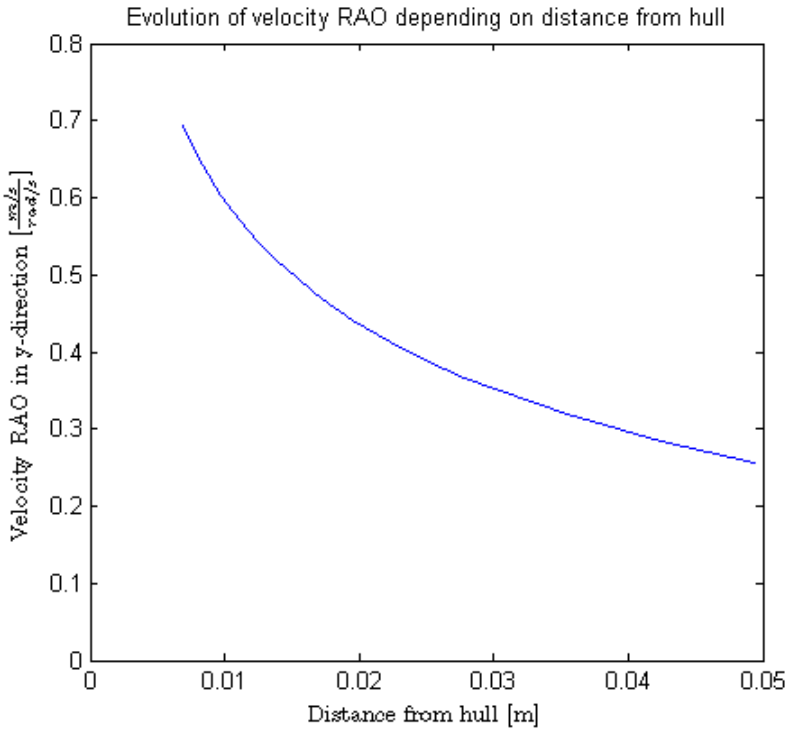

Figure 4.1: Radiated velocity RAO in y-direction at various distance perpendicular from the hull on model scale.

It should be noted that the velocities obtained at a point through HydroStar vary as the point is chosen closer to the hull, reference is made to Figure 4.1. This is why as a representative velocity, the velocity at the tip of the bilge keel, is taken. If this is done consistently proper results should be obtained. It is furthermore a physical logical location.

4.3.2. HULL PRESSURE MOMENT

The other criteria for evaluation is the hull pressure moment. To obtain this value the pressures acting on the hull are multiplied with an arm and integrated over the hull:

$$M(t) = \int_S p(t,S) l_m(S) dS \tag{4.2}$$

This moment is a time trace which is not very suitable for verification and validation. Instead suitable coefficients are obtained in a similar manner as for the keel forces. There is one difference, as the Fourier analysis requires a full period it cannot generate different coefficients for a positive and negative velocity over the keel. While for the forces acting on the keel this is not necessary as the moment generated is almost symmetric, hull pressure damping can be quite asymmetric. This results in the need to perform a least-squares fitting instead of a Fourier analysis, reference is made to Appendix D. In the Roll JIP results and simulations the moment caused by the potential damping and added mass is removed to obtain the damping purely from viscous effects.

As a circular keel used in the experiments by Schut [17] does not generate any moment due to the pressure distribution on the hull a different measure is used. Instead of a regular moment an equivalent moment is defined where the pressure distribution of the equivalent circular hull is projected onto the 303 FPSO hull, reference is made to Figure 4.2. This way the effect of the reduced moment arm and thus importance of pressures further from the hull are accounted for. This is relevant as both CFD and experiments have reduced accuracy further from the hull. This moment can be reduced to a single number: the hull pressure coefficient B_h.

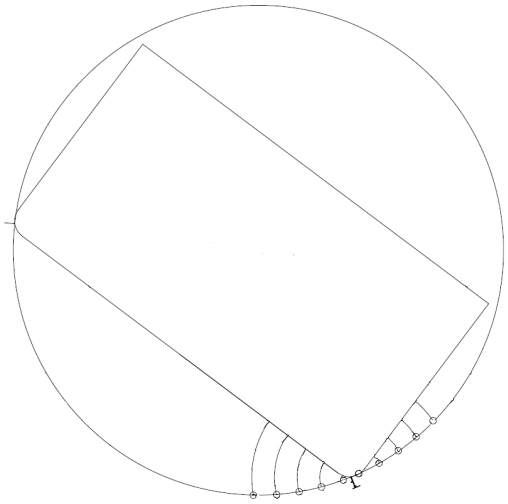

Figure 4.2: The circular 303 hull with projection onto the rectangular 303 FPSO hull.

4.4. MODEL

The used model was built by J.L. Pelerin from SBM Offshore. The global modeling methodology used is based around the URANS method with a $\kappa-\omega$ SST turbulence model which seemed favorable from literature, reference is made to the literature review [1] and Chapter 2. A segregated solver is employed which solves the separate governing equations separately and iterating until proper convergence is reached or the maximum iterations are reached. A 2^{nd} order discretization scheme is used is space and an implicit unsteady 2^{nd} order scheme in time.

The surface is modeled using the VoF method with a High Resolution Interface Capturing (HRIC) convection discretization scheme to capture the (sharp) interface for Courant numbers smaller than 0.5. A combination between HRIC and Upwind Difference (UD) between 0.5 and 1.0 and UD for Courant number higher than 1.0. This is why the Courant number is limited to smaller than 0.5.

The motion is modeled by dividing the domain in two regions: stationary and rotating. An interface is present between the moving part of the mesh and the stationary part to allow transfer of mass and energy. A prism layer in combination with a trimmer mesher is used to mesh the volumes to allow the solver to properly solve near-wall effects using hexehedral cells.

A ramp function is used when deemed necessary and is defined between $t = 0$ and $t = \frac{T}{2}$ as:

$$x_4(t) = \frac{1}{2}(1 - cos(\omega t))sin(\omega t)), \tag{4.3a}$$

$$\dot{x}_4(t) = A\omega sin^2\left(\frac{\omega}{2}t\right)(2cos(\omega t) + 1), \tag{4.3b}$$

$$\ddot{x}_4(t) = \frac{1}{2}A\omega^2 sin(\omega t)(4cos(\omega t) - 1) \tag{4.3c}$$

An example mesh can be found in Figures 4.3 and 4.4 for the Schut experiments and the Roll JIP experiments respectively. The typical number of cells for the Roll JIP is 4e4 for the entire domain, which is depicted in Figure 4.5. The inner region contains around 24000 cells and the outer region 16000. A single run takes approximately ten hours depending on server configurations, motion velocity, mesh size etc.

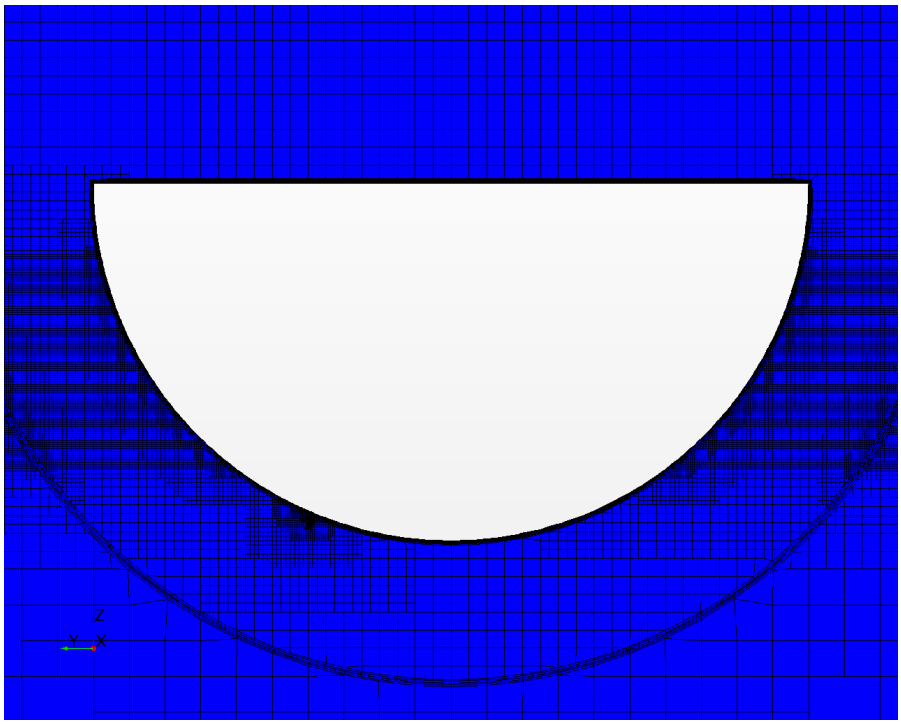

Figure 4.3: Mesh as used in the CFD simulations for the circular hull.

Figure 4.4: Mesh as used in the CFD simulations for the rectangular hull.

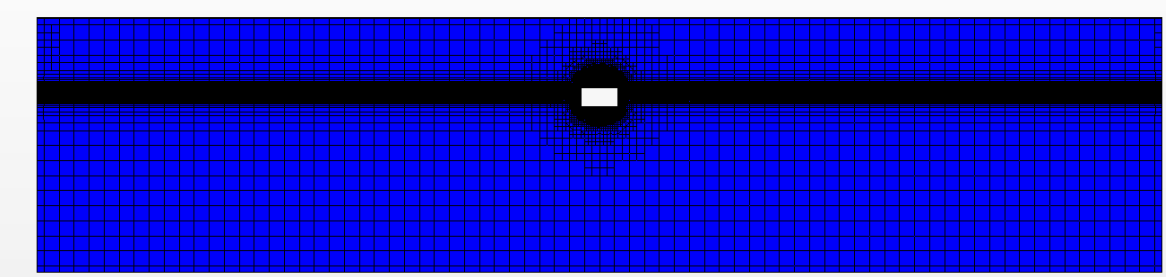

Figure 4.5: Overview of the domain including mesh as used in the CFD simulations for the rectangular hull hull.

4.5. VERIFICATION & VALIDATION

A detailed description of the verification and validation is given in the accompanying literature review preceding this report, reference is made to the literature review [1] and the papers by Eça [76], [77] and [78].

4.5.1. VERIFICATION

Code verification is the verification of the general code, i.e. the detection and removal of programming errors or bugs. This verification is assumed to be done by the creators of STAR-CCM+, CD-Adapco. The solution verification is a process that depends on the problem at hand and aims to quantify the error due to round-off, iterative and discretization errors. The STAR-CCM+ software utilizes double precision floating point data, resulting in a very small round-off error that is negligible compared to the likely discretization error. Convergence is such that the iterative error is considered very small. The discretization error is usually the largest numerical error and thus should be properly evaluated. The method used is a mesh convergence study, where the influence of the grid size on the results is evaluated. The uncertainty of a certain flow quantity can be defined as:

$$U_\phi(\phi_i) = \begin{cases} F_s\epsilon_\phi(\phi_i) + \sigma + |\phi_i - \phi_{fit}| & \text{if } \sigma \leq \Delta_\phi \\ 3\frac{\sigma}{\Delta_\phi}(\epsilon_\phi(\phi_i) + \sigma + |\phi_i - \phi_{fit}|) & \text{if } \sigma > \Delta_\phi \end{cases}$$

where U_ϕ is the uncertainty of flow quantity ϕ. F_s a safety factor to account for uncertainty in the error estimation ϵ_ϕ and σ the standard deviation of the fit to the various grid points. $|\phi_i - \phi_{fit}|$ is the measure of the error of the fit. Δ_ϕ is a tool to evaluate the uncertainty of U_ϕ by evaluating the standard deviation of the fit σ.

4.5.2. VALIDATION

To validate a certain model three uncertainties need to be determined to compare model to the experiment. The uncertainties are:

- numerical uncertainty,
- experiment uncertainty, and
- parametric uncertainty.

The numerical uncertainty is evaluated through the verification process. The experiment uncertainty depends on the accuracy of the sensors used during an experiment, as well as the control on outside disturbances. Parametric uncertainty is uncertainty in the input parameters, such as the KC-number, geometry etc. With these uncertainties the overall validation uncertainty can be calculated using:

$$U_{val} = \sqrt{U_{num}^2 + U_{input}^2 + U_{exp}^2} \tag{4.4}$$

With this and the validation error E which is defined as:

$$E = S - D \tag{4.5}$$

where S equals the simulation value and D the experimental value a model can be validated.

If $|E| >> U_{val}$ the error of the simulation is greater than the uncertainty so the model cannot be considered validated as the error cannot be explained statistically.

When $|E| \leq U_{val}$ the error is within the 95% confidence range and the model can be considered validated for this particular case.

4.6. VALIDATION RESULTS

The CFD seems to perform within the experimental uncertainty. It should be noted that validation for one case does not validate the CFD for all cases, even within a single hull and keel configuration. Unfortunately it is impractical to validate every case and defies the use of CFD to replace experiments. This means that whenever the unvalidated CFD is used the final results should still be validated against experiments, although this can then be done at a later stage with a more definitive design. The criteria are discussed below.

4.6.1. EXPERIMENTS BY SCHUT

The following subsections will show the results and considerations of the performed validation.

EXPERIMENTAL UNCERTAINTY

The largest source of uncertainty within the experiments performed by Schut [17] seem to come from sensors, especially the pressure sensors. Calibration was performed by Schut and from this the error was determined but uncertainty was not. The error is estimated at 15%, although it may be larger this is not verifiable. Furthermore some unusual oscillations are present which most likely can be attributed to start-stop phenomena or sensor dynamics. Unfortunately these are not quantifiable and thus not taken into account. Another error source would be an error in calculated hydrostatics. As the viscous effects are small compared to the pressure changes due to hydrostatics a small error in hydrostatics can lead to large errors in viscous pressures. This error is not evaluated.

PARAMETRIC UNCERTAINTY

The largest parametric uncertainties seem the initial conditions of the water as well as the actual roll angle, in which measurement show a 5% higher value than specified.

MESH CONVERGENCE

A mesh convergence study shows that the mesh can be considered converged. Reference is made to Table 4.2 for relative changes and Figure 4.6 for the mesh convergence plot. The small variations when increasing the mesh size from the default make a verification as described in Section 4.5 impractical. Numerical uncertainty is taken conservative and thus assumed to be very small. Figures 4.7 and 4.8 show the reference mesh and a refined mesh with half the characteristic mesh size.

DAMPING AND WORK

As linearized damping is determined through work, reference is made to Section B, they are not evaluated separately. In Figure 4.9 the bottom two graphs show the linearized damping/hull pressure coefficients for various frequencies and amplitudes, and constant draft and bilge keel geometry. In Figure 4.10 the same is visible but then for various drafts and geometries and constant amplitude and frequency. It first should be noted that instead of the KC number which is usually employed for oscillatory motions the Reynolds number which depends on local velocity seems more appropriate, resulting in an almost linear dependence.

The results from the CFD seem to be consistently between the estimates by the ITH method and the results from the experiments. It consequently overestimates the experimental results. It is within the range of the sensor inaccuracies, as the pressure are underestimated up to 15% according to Schut [17].

Grid size	C_D [%]	C_M [%]	B_h [%]
0.5	-0.0809	0.4893	-1.9005
0.75	-4.577	-4.3274	0.1453
1	10.35	33.9053	-15.4658
1.25	0	0	0

Table 4.2: Change from previous grid size

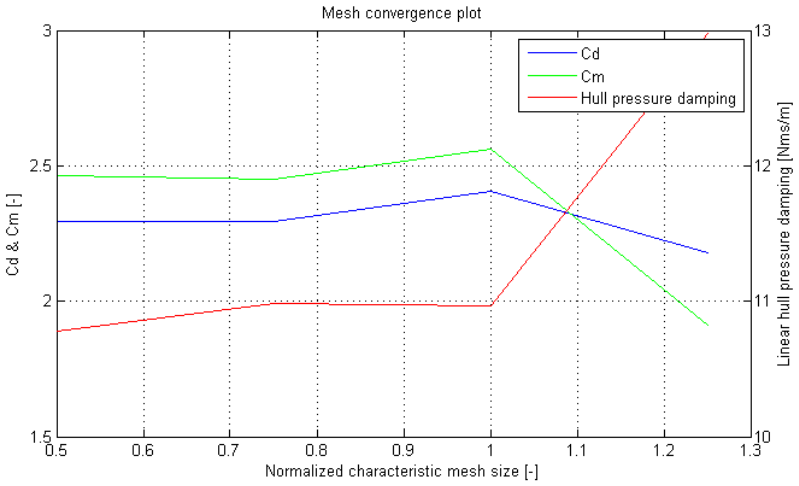

Figure 4.6: Mesh convergence plot based on C_D, C_M and the hull pressure damping coefficient

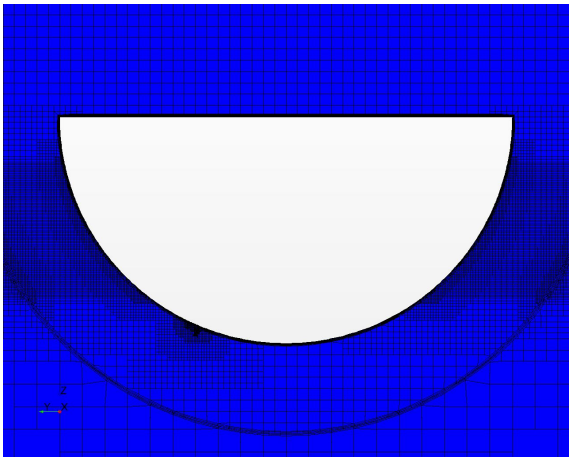

Figure 4.7: Circular mesh with reference mesh size.

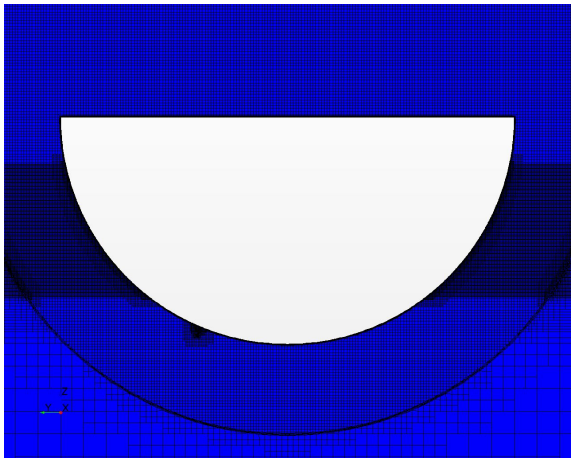

Figure 4.8: Circular mesh with half the reference characteristic mesh size.

One part that can be identified in the experiments is a additional oscillatory pressure at the maximum roll angle. This might be caused due to inertial effects or a start-stop phenomena. This pressure will reduce the moment at the peaks, possibly resulting in a smaller amount of damping. Furthermore a low frequency oscillatory component seems to be present in the CFD which suggest reflections.

Overall it can be concluded that while the CFD and experimental results are in good agreement close to the bilge keel, uncertainty increases when sensors further from the bilge keel are evaluated. This is expected as RANS models turbulent effects instead of simulating them, while this results reasonably accurate approximation of large scale structures some errors are to be expected. None the less, pressures farther from the bilge keel are in general smaller and have a smaller moment lever, reducing their relevance in the generation of the moment. In all the model is considered validated as trends are captured well and there is some uncertainty in the measurements.

DRAG AND INERTIA COEFFICIENTS

The drag and inertia coefficients caused by the bilge keels can be seen in Figure 4.9. Here good agreement is found between the experiment and the CFD results. For the drag coefficient no comments are necessary, while for the inertia coefficient it can be noted that the inertia coefficient from the experiments seems more sensitive to frequency than from CFD. As the experiments have a harder to define start moment of the motion and a slightly irregular period this is attributed to phase shifts in the measurement data which are hard to post-process. These have an impact on the inertial coefficients as these represent the out-of-phase terms of the bilge keel normal force.

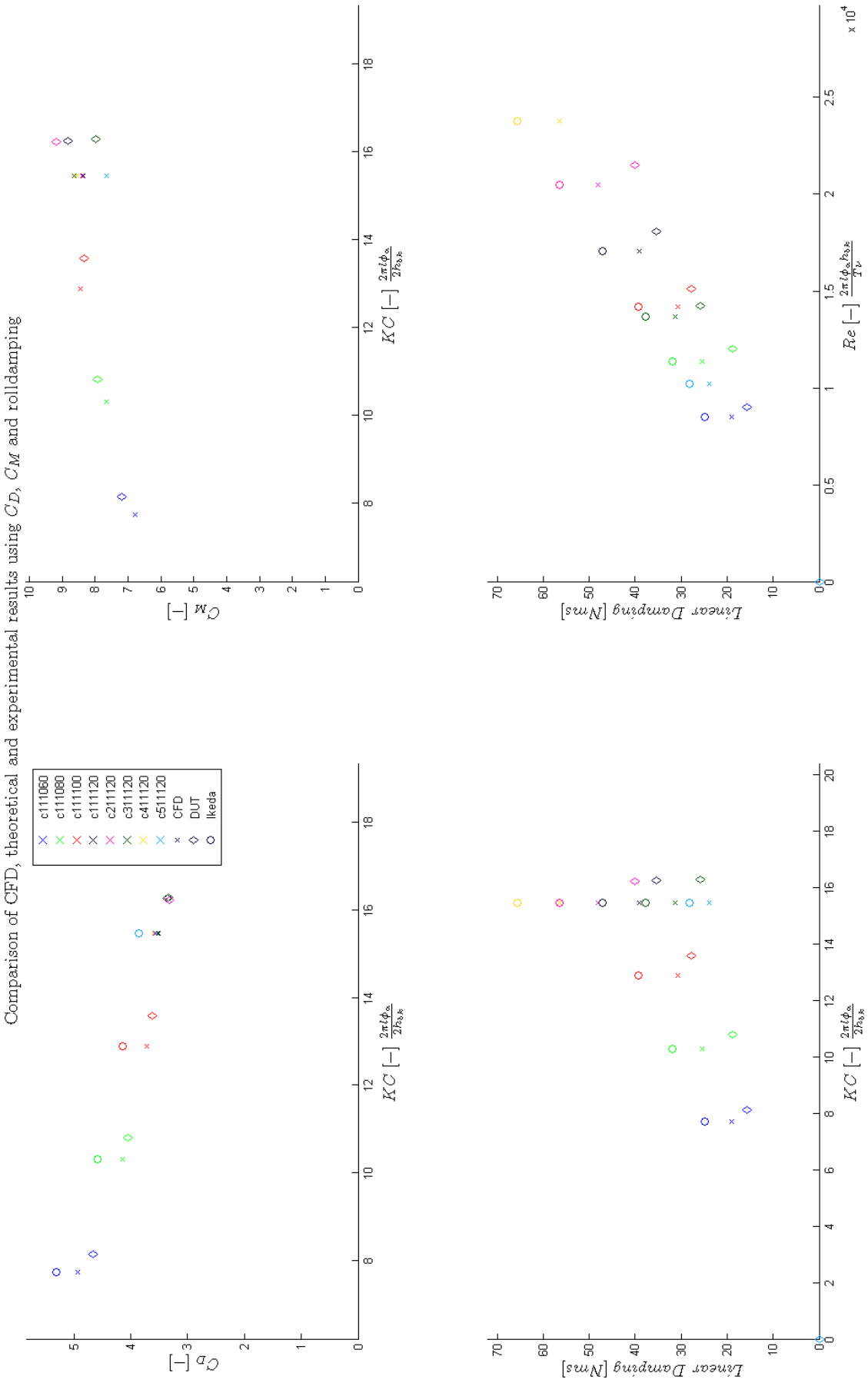

Figure 4.9: Comparison of CFD, the ITH method and the results of Schut for linear roll damping, the coefficient of drag and the coefficient of inertia for various frequencies and amplitudes.

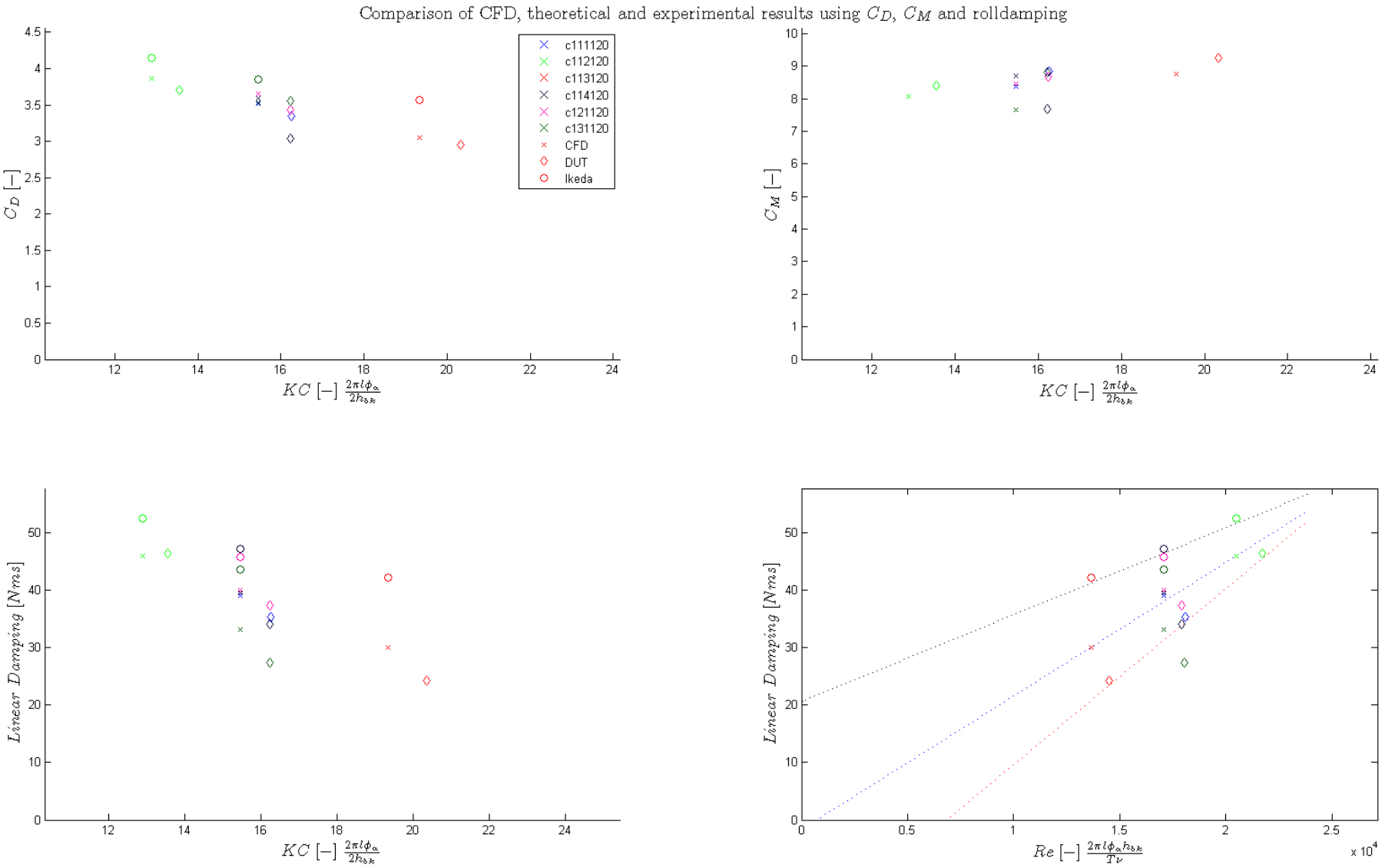

Figure 4.10: Comparison of CFD, the ITH method and the results of Schut for linear roll damping, the coefficient of drag and the coefficient of inertia for various drafts and bilge keel geometries.

4.6.2. EXPERIMENTS IN THE ROLL JIP

While the experiments performed in the Roll JIP did entail forced oscillations as well, they were performed in a free-floating situation. This results in motions in the other DoF besides roll. This results in a rather ineffective comparison between the CFD and the experiments. One could argue to model the other DoF in the current model, although the round sliding interface makes this impractical. This would require either another interface or a different kind of mesh. Furthermore a 3D situation is compared to a 2D situation. While the time-trace of the hull pressure moment in Figure 4.11 seems to compare quite well, the slight differences, especially after subtraction of the added mass and damping and looking at each keel separately, lead to differences in the obtained coefficients.

At higher amplitudes the CFD results become less reliable, there are furthermore slowly varying oscillations present in the hull pressure moment. The most likely cause of errors at higher amplitudes are optimizations in the sliding interface. A possible solution would be to utilize an overset or Chimera mesh. While this kind of mesh requires the Courant number (Cu) to be below 0.5 the HRIC scheme already has this requirement. Another option is eliminating the interface by replacing it with a morphing mesh, although this limits the range of motion that can be simulated. The sub-harmonics are most likely reflections.

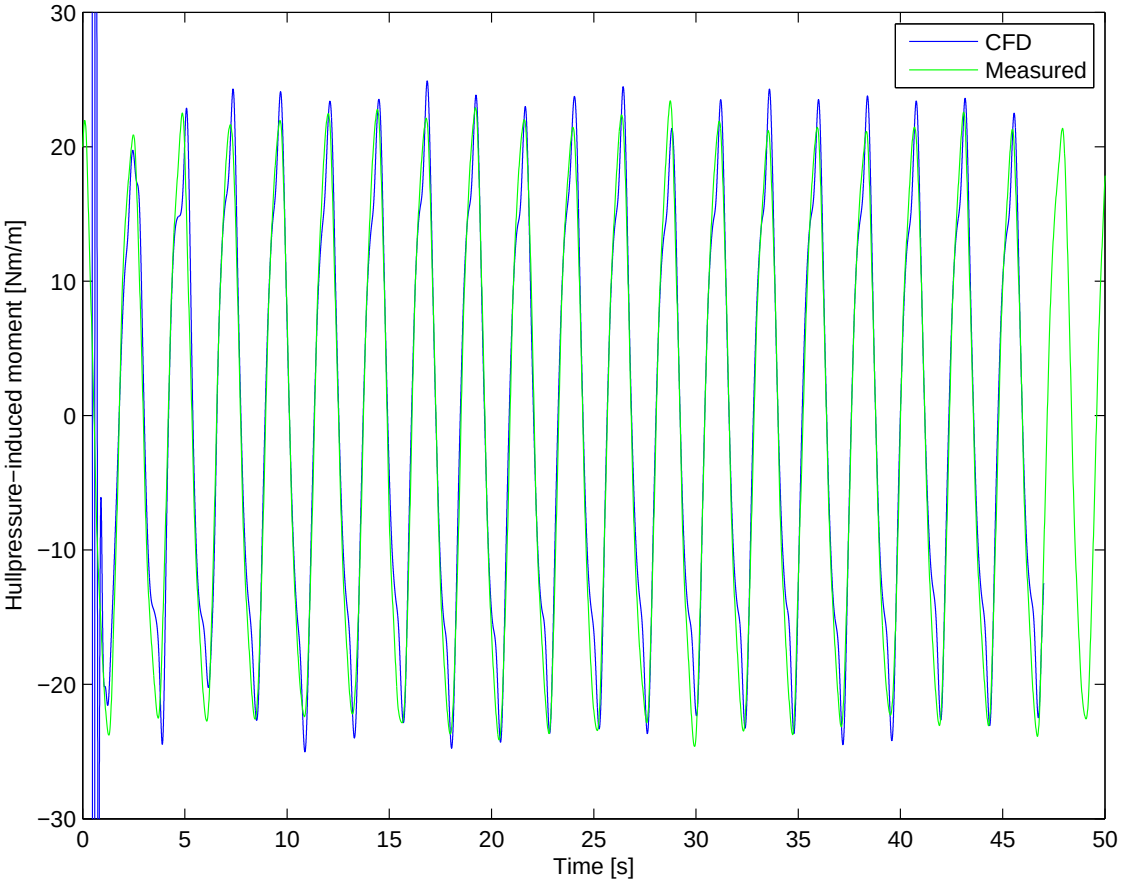

Figure 4.11: Hull pressure moments as obtained from CFD compared to measured experiments from the JIP.

4.6.3. TURBULENCE MODEL

To evaluate the performance of the $\kappa-\omega$ SST turbulence model it is compared to the Realizable $\kappa-\epsilon$ model. The comparison is done through visual inspection and the Normalized Root Mean Squared Error (NRMSE) which is:

$$NRMSE = \frac{RMSE}{M_{max} - M_{min}}. \tag{4.6}$$

Both keel forces and hull pressure moment have an NRMSE of less than 1% when the steady state is reached. Reference is made to Appendix E for example time-traces.

4.7. COMPARISON TO THE ITH METHOD

In this Section the validated CFD results are compared to the ITH method. The ITH method seems to follow trends quite well. It consistently overestimates the damping predicted by the experiments and even the CFD, this could be due to the fact that a circular hull is used. The hull geometry is not incorporated in the ITH method when considering the C_p curve and the fact that the free surface is present. When looking at the C_p curve is can quickly be seen that the ITH method does not have the same distribution which can account for the overestimates.

It can furthermore be noted that the ITH method method does not take into account the difference in bilge keel geometries, only bilge keel height. Influence of draft is only accounted for in C_p distribution length and not distribution shape, which is the result of the type of experiments that were performed. This leads to underestimation of the effect of draft.

5

Methodology Verification and Validation

In this Chapter the code to implement the methodology is verified and the results are validated using the Roll JIP results.

5.1. Implementation and assumptions

Due to time limitations and computational time limits a few assumptions were made. First the number of sections used in the CFD was only one as geometry varied little over the length of the bilge keel. Secondly only local velocities at the section where the CoG was located were used and thus the influence of pitch and yaw motions on the bilge keel were neglected. This was done to save time as well as the assumption that due to the proximity of the bilge keel to the CoG the influence would be limited. Damping due to parts of the hull other than the part simulated in CFD were calculated using the ITH method as implemented in HydroStar.

5.2. Verification

The basic time domain code can be verified against the results obtained in the frequency domain. In theory the time domain simulations should reproduce the RAOs as produced by the frequency domain calculations. For this purpose a one meter regular wave is simulated in the time domain after which the steady state amplitude and phase should equal the frequency domain RAO. The calculation of the retardation functions can be verified by recalculating the original frequency-dependent added mass and damping coefficients. The radiation-diffraction software used is the BV HydroStar package. The HydroStar code is assumed to be verified for basic calculations such as this.

5.2.1. RAO verification

There are two sets of code that can be verified: forced oscillation/regular wave and irregular wave, i.e. with frequency domain coefficients and with retardation functions. Both methods should return the same roll RAO when compared to the HydroStar RAO.

Regular wave model

When the relative and absolute error tolerances are set to 1e-6, the time domain model reproduces the frequency domain RAO amplitude and phase with a NRMSE of less than 0.1%. Reference is made to Appendix F for all results.

Irregular wave model

This verification has not yet been performed.

5.2.2. Retardation function verification

The retardation functions are verified by reconstructing the frequency dependent added mass and damping from the retardation functions which are appreciated visually and using the NRMSE. Reference is made to Table 5.1 and Appendix F.

Degree	Added mass error [%]	Damping error [%]
11	0.3462	0.0289
22	0.4563	0.0080
33	1.7529	0.0922
44	1.2333	0.0148
55	1.1191	0.0381
66	0.4709	0.0076
13/31	0.5024	0.0206
15/51	0.4570	0.0377
24/42	0.5526	0.0069
26/62	0.4941	0.0027
35/53	0.7434	0.0341
46/64	0.4759	0.0093

Table 5.1: Error in the recalculation of the added mass and damping

5.3. VALIDATION

The validation can be performed three-fold and in six DoF for the following cases:

- forced oscillations,
- regular waves, and
- irregular waves.

Here each scenario adds new effects. The forced oscillations only incorporate the damping coefficients and radiated wave velocities, and a really small part due to other DoF motions. In regular waves incoming and diffracted wave water velocities are added, in addition to velocities caused by other motions such as heave and sway. In irregular waves, the added mass and damping, as well as radiated wave velocities are now incorporated using retardation functions. Furthermore a different mechanism is implemented to evaluate the KC and Re numbers, iterating over each zero-crossing.

5.3.1. FORCED OSCILLATIONS

Forced oscillations are performed in the Roll JIP using not a prescribed motion but by using a roll exciting moment generated by the inertia of an electric drive. As forced oscillations are performed using only one frequency, coefficients from the frequency domain can be employed directly without resorting to retardation functions. The addition that is made to regular simulations is in the form of additional non-linear forces and moments supplementing potential theory and an exciting moment similar to the experiments applied to the CoG of the model. In the forced oscillations only two local velocities and accelerations are present, namely the rigid body and radiated wave motions. The experiments of interest are tabulated in Table 5.2.

5.3.2. REGULAR WAVES

The regular wave situation is similar to that of the forced oscillations, with the exception of added diffracted and incoming wave induces water velocities, as well as the exciting forces in the other DoF. In Table 5.3 the

SBM id.	Marin id.	X_4[°]	$h_{bk}[m]$	T [s]	M_e [Nm]	LC
122044	318002	4.4	0.7	2.308	14.43	intermediate
122066	318003	6.6	0.7	2.308	25.77	intermediate
122081	318007	8.1	0.7	2.308	37.19	intermediate
122117	318004	11.7	0.7	2.308	70.25	intermediate
122135	318008	13.5	0.7	2.308	85.20	intermediate
122174	318005	17.4	0.7	2.308	117.35	intermediate
122190	318006	19.0	0.7	2.308	137.31	intermediate

Table 5.2: Selected forced oscillation parameters for validation

Marin id.	θ_a[°]	$h_{bk}[m]$	T [s]	ζ_a [cm] ([m])	Heading [°]	LC
318001	6.2	0.0175	2.308	2.47 (0.989)	intermediate	270
318002	11.0	0.0175	2.308	8.75 (3.5)	intermediate	270
318003	16.0	0.0175	2.308	14.75 (5.9)	intermediate	270

Table 5.3: Selected regular wave parameters for validation on model scale

parameters used for the regular wave validation are summarized. The parameter of highest interest is the roll angle. As the experiments were done at only a single frequency close to but not at the natural frequency the comparison is very sensitive to shifts in the natural frequency, which is why a range of frequencies should be plotted.

5.3.3. IRREGULAR WAVES

In the irregular waves the main difference with regular waves are the retardation functions that are employed, which are validated in Section 5.2.2, and the evaluation of the KC and Re numbers. To validate the irregular wave pattern a FFT is performed on the timetrace of the undisturbed waveheight. From this spectrum and phases the timetraces of the various wave forces, velocities and accelerations can be constructed. These are then used as input for the time domain solver. The output of the solver can then be compared to the results of the experiments. While of course a close agreement between the timetrace would be preferable other values can be compared and are perhaps more important such as the deviation of the roll, the distribution of the maxima and others. These are the parameters which are of interest during design.

5.3.4. FREQUENCY DOMAIN

The frequency domain solution can be compared in a similar manner as the irregular wave solution. Again using timetraces although these are not very likely to match well, as well as more interesting values such as a response spectrum or significant roll.

5.4. RESULTS AND DISCUSSION

In this Section the obtained results of the time-domain and CFD simulations will be depicted followed by a discussion of the obtained results.

5.4.1. CFD

In Figures 5.1, 5.2 and 5.3 and Table 5.4 the results of the CFD simulations can be found as used in the implemented methodology. The C_D plot is consistent with expected values as it contains a correction for the potential flow velocities which are of only an approximation of actual velocities 'felt' by the keel. The applicability of a velocity correction seems in line with literature as by van 't Veer [25]. The C_M value shows a slight sensitivity to frequency, which was also observed during experiments by Schut [17]. This scatter should not influence the roll damping a great deal. The B_h coefficients seem to be as expected, with a (small) difference between an upwards and downwards motion. As subharmonics are present, most likely due to reflections, the standard deviation due to these subharmonics is plotted as an error bar for each run. Scatter is observed in the A_h coefficients. As these coefficients are quite small and suspicable to small phase shifts, constant coefficients are assumed.

Code	Period [s]	Amplitude [°]	KC [-]	Re [-]	C_D [-]	C_M [-]	B_h (+/-) $[Nms]$	A_h (+/-) $[Nms^2]$
GD122035	2.308	3.5	11.5	3.0e3	4.64	2.52	6.0/9.0	0.32/0.44
GD122050	2.308	5.0	16.4	4.4e3	3.70	3.36	7.7/9.1	0.64/0.64
GD122060	2.308	6.0	19.7	5.2e3	3.32	3.57	9.1/10.0	0.65/0.68
GD122066	2.308	6.6	21.7	5.7e3	3.16	3.86	10.6/10.7	0.75/0.65
GD122081	2.308	8.1	26.6	7.1e3	2.92	4.18	14.7/13.6	0.73/0.75
GD222050	2.000	5.0	16.6	5.1e3	3.67	3.69	10.3/11.1	0.53/0.49
GD222075	2.000	7.5	24.8	7.6e3	2.95	4.73	17.5/16.0	0.71/0.48
GD322050	2.600	5.0	16.4	3.9e3	3.86	4.08	7.1/8.4	0.80/0.47
GD322075	2.600	6.5	24.6	5.8e3	3.00	4.92	12.2/11.8	0.98/0.37

Table 5.4: Results from CFD simulations of a FPSO section.

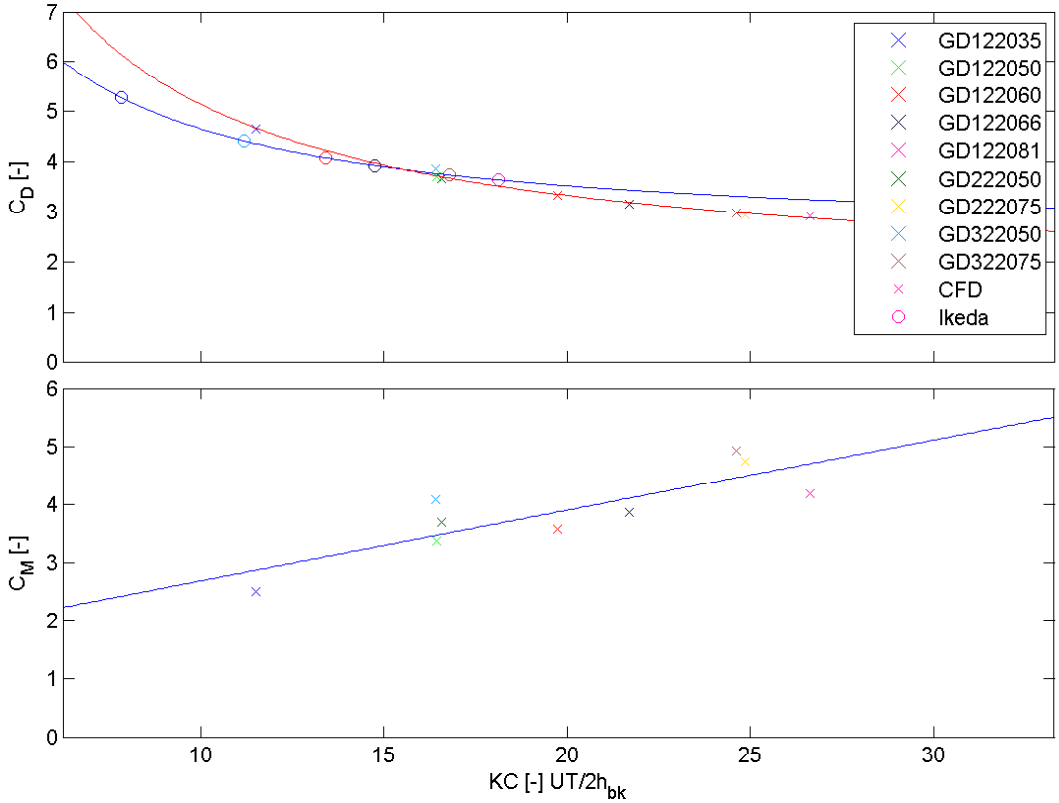

Figure 5.1: C_D and C_M coefficients as obtained from CFD including fitted lines.

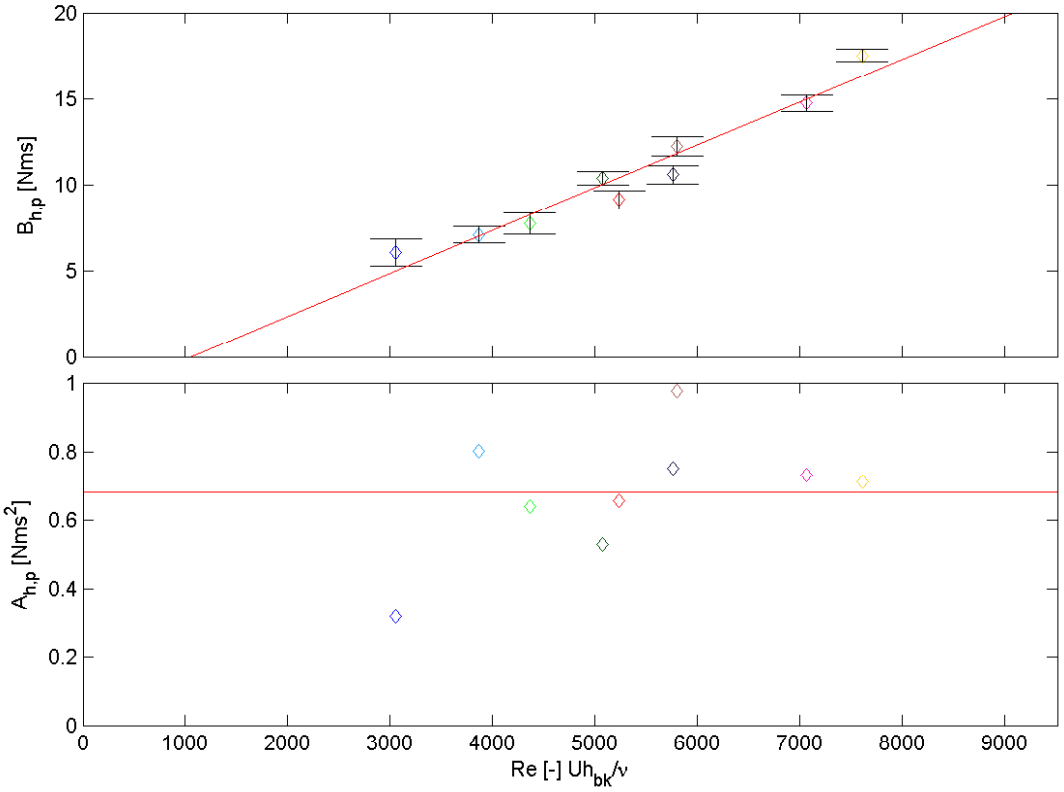

Figure 5.2: Positive hull pressure coefficients as obtained from CFD including fitted lines, the legend is the same as Figure 5.1. Error bars denote the standard deviation due to variations within one run.

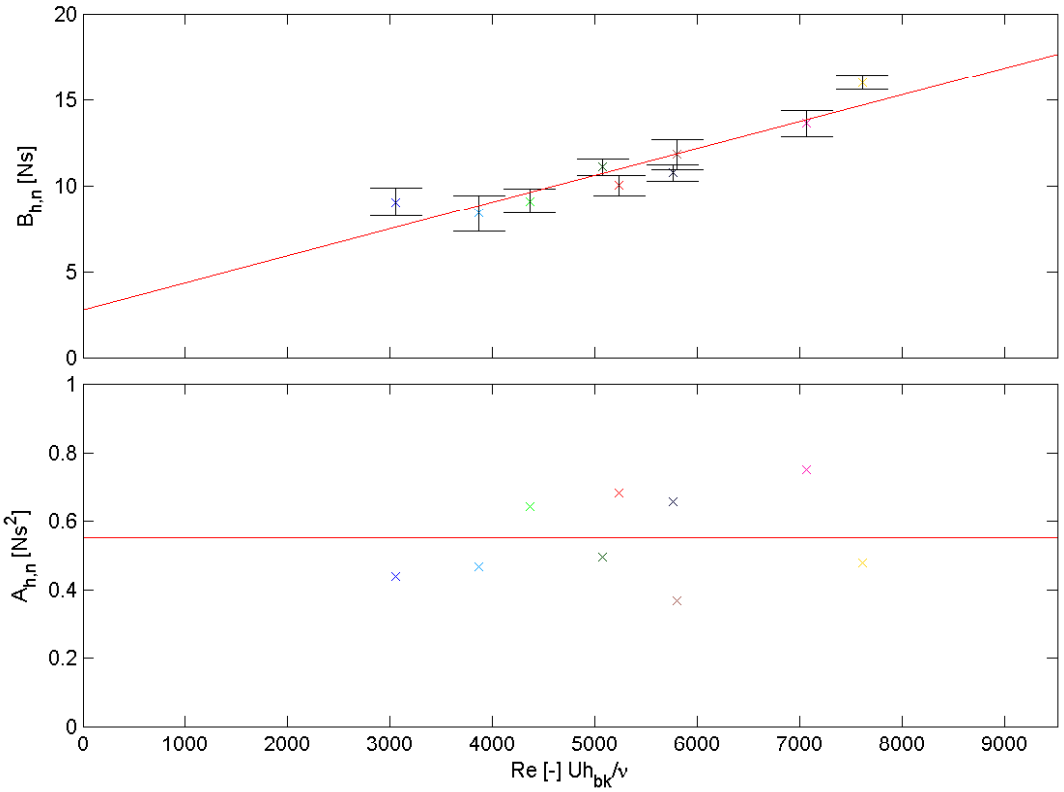

Figure 5.3: Negative hull pressure coefficients as obtained from CFD including fitting lines, the legend is the same as Figure 5.1. Error bars denote the standard deviation due to variations within one run.

5.4.2. FORCED OSCILLATIONS

The forced oscillations performed for the Roll JIP using a exciting moment generated by an electric drive are simulated using the same exciting moment without restrictions in any DoF. In Table 5.5 the results of the forced oscillation experiments can be viewed. During the forced oscillations the roll motions of the vessel are overestimated. There are various possible reasons for this issue, such as

- due to viscous damping caused by the hull geometry, i.e. besides the bilge keel;
- due to other motions present in the experiments such as heave and sway; which also result in additional local velocities and thus damping;
- due to 3D effects;
- due to an underestimation of the keel force and/or hull pressure coefficients; and
- due to a high forcing moment.

The damping in item one is estimated using HydroStar and should not have a large impact and be reasonably well estimated. Adding more damping that way would results in underestimations at the higher amplitudes. Item two seems most likely as sway motions measured can be ten times as high during the experiments than the simulations and heave motions are completely absent in the simulations. Their impact on the total local velocity would be a maximum of approximately 10-14%. Allowing for this increase new roll angles are determined which paint a picture that is more logical. Higher amplitudes are not well predicted but this is expected as keel and hull damping are most likely to reduce in trend as higher amplitudes cause the keels become near to the surface and thus the vortex shedding and damping becoming saturated. Other effects are the shedding of multiple smaller vortices and vortices moving further away from the hull resulting in reduced influence. The results can be viewed in Table 5.7.

Measured [°]	CFD [°]	Error [%]
4.4	5.2	18
6.6	7.4	12
8.1	9.1	12
11.7	12.9	10
13.5	14.4	7
17.4	17.1	-2
19.0	18.6	-2

Table 5.5: Results from forced oscillations.

Measured sway [m]	Simulated sway [m]	Measured heave [m]	Simulated heave [m]	Local velocity influence [%]
0.04	0.02	0.07	0	6
0.11	0.03	0.15	0	11
0.26	0.04	0.19	0	11
0.32	0.06	0.29	0	11
0.50	0.06	0.32	0	12
0.76	0.07	0.38	0	13
0.89	0.08	0.45	0	14

Table 5.6: Measured sway and heave motions versus simulated sway and heave motions and the influence on the local velocity.

Target [°]	CFD [°]	Error [%]
4.4	4.8	9
6.6	6.8	3
8.1	8.4	4
11.7	11.9	2
13.5	13.3	-1
17.4	15.8	-9
19.0	17.1	-10

Table 5.7: Results from forced oscillations corrected for sway and heave motions.

5.4.3. REGULAR WAVE

To clearly present the results in waves the most relevant parameter is compared: the resulting roll angle. There are five datasets available for comparison:

- the simulated results using the proposed methodology,
- the simulated results using measured damping from experiments,
- the simulated results using ITH method damping,
- the simulated results using modified ITH method damping, and
- the measured roll angle from the experiments.

All the simulated results are presented as amplitudes at various frequencies. Unfortunately the experiments were performed at only one frequency and these are thus presented as points at these frequencies. Experiments were performed at multiple wave heights, for which reference is made to Table 5.3. RAOs are not used due to the non-linear nature of the problem. Figure 5.5 shows the obtained roll amplitudes at various frequencies. The phase difference between heave and roll is shown in Figure 5.6. The maximum roll amplitude is the value of highest interest and is tabulated in Table 5.8 with the roll exciting moment from HydroStar. In Figure 5.7 a comparison of bilge keel loads as measured, as simulated using the CFD coefficients and local velocities and as predicted by the traditional ITH method. The exciting moment in the roll DoF is adjusted to allow for the same roll angle as measured without compromising the other motions which were predicted correctly. The agreement is quite good considering that the higher harmonics and 3D effects are neglected.

A large underestimation of the roll amplitude is present when compared to measured roll angles. When simulating again with the roll damping coefficients obtained from the experiments a similar underestimation is found. The source of this error is not clear and can have some potential sources such as:

1. incorrect wave-height from experiments,
2. incorrect exciting moment,
3. viscous roll-sway coupling [79],
4. drift motions [80], and
5. incorrect damping from experiments.

Item number one, incorrect wave-height, seems unlikely as heave is very well predicted and sway only with minor discrepancies, most likely due to the smaller roll angle. An increase of at least 50 % would be required to attain the correct roll angle, which leads to incorrect heave and sway.

The second item, the incorrect exciting moment seems more likely. Comparing the measured roll angle and exciting moment of the forced oscillations with the theoretical roll exciting moment from radiation-diffraction calculations and the measured roll in waves, the roll exciting moment in waves is significantly lower, while the opposite would be expected, reference is made to Tables 5.2 and 5.8. A possible cause would be incorrect measurement of the roll exciting moment during forced oscillations. This seems unlikely as the roll damping obtained from forced oscillations and decay tests is very similar, as expected. Another option would be an error in the potential theory calculations, which seems equally unlikely as HydroStar is a widely

used package and is considered verified and validated. Linear potential theory is also widely used and wave forces are assumed to be properly predicted. Especially as other motions such as heave are correctly predicted. This leaves the input to HydroStar being incorrect. The mesh seems to be in-line with the body plan as presented in the documentation of the Roll JIP, as the results from independently created meshes by the author and R. van 't Veer show almost the exact same results, reference is made to Appendix C. The only others parameters besides the mesh that have influence on the exciting forces are the water-depth and density. Both are set correct and the water-depth does not have enough influence to explain the difference. Scaling is not an issue, full scale HydroStar models give the same results as model scale models.

Items three and four are neglected, but would have a very limited impact, not nearly enough to explain the difference.

Item five would require an overestimation of the damping of at least 30% from the experiments. Considering the consistency of the obtained damping from the experiments this should be a systematic error which cannot be evaluated ten years after date. Furthermore considering the performance in the forced oscillations this seems unlikely. Concluding, a likely source cannot be identified thus an alternate path is taken to benchmark the results.

If the simulations with the experimentally obtained damping are used as a reference the various methods perform as expected. The traditional ITH method produced by HydroStar shows an underestimation of the damping and as such a very conservative roll angle. This is expected due to the neglect of local velocities, reference is made to Figure 2.1 for the impact. There is furthermore no sign of a shift in resonance frequency, which is also expected as only damping is added. The ITH method based on local velocities performs much better which makes sense as damping is increased due to the additional incorporated velocities. A small shift in peak amplitude can be found due to the velocities not being entirely in phase with the roll velocity. The CFD-based methodology seems to perform even better with peak amplitudes close to the predicted value and an expected shift of the peak response. Performance in the highest wave degrades for the CFD-based method, as well as the ITH method based on local velocities. KC numbers will run well into a range of over fifty and up to ninety. This explains the better estimate by the modified ITH method method as the C_P value drops at high KC numbers, reference is made to Figure 5.4. This while the results from the CFD are proportional to the local Reynolds number and thus local velocity amplitude. It does not reach the same 'barrier' as the C_P. This behavior (saturation) is observed in literature as well. As the ITH method is not based on high KC number such as these it also enters a range of uncertainty. The results are furthermore in line with what was expected from the forced oscillations. It can additionally be considered that higher waves results in higher diffracted and incoming wave velocities which partly determine the path. If this path is further removed from the hull the influence of the vortex declines, reference is made to Section 2.3.2.

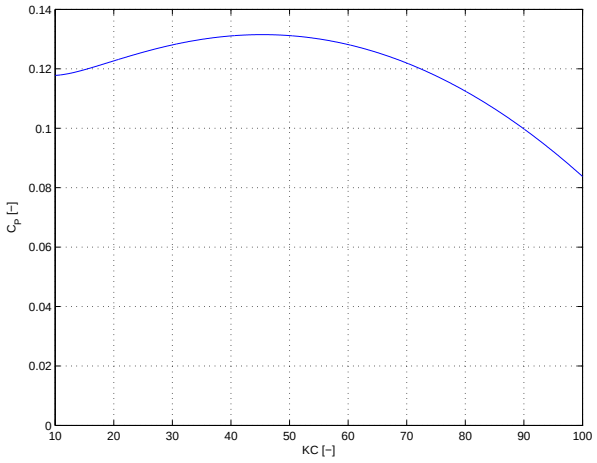

Figure 5.4: The C_P value of the Glas Dowr FPSO plotted versus the KC number.

5.4.4. IRREGULAR WAVE

Unfortunately due to time constraints the irregular wave simulations have not yet been performed.

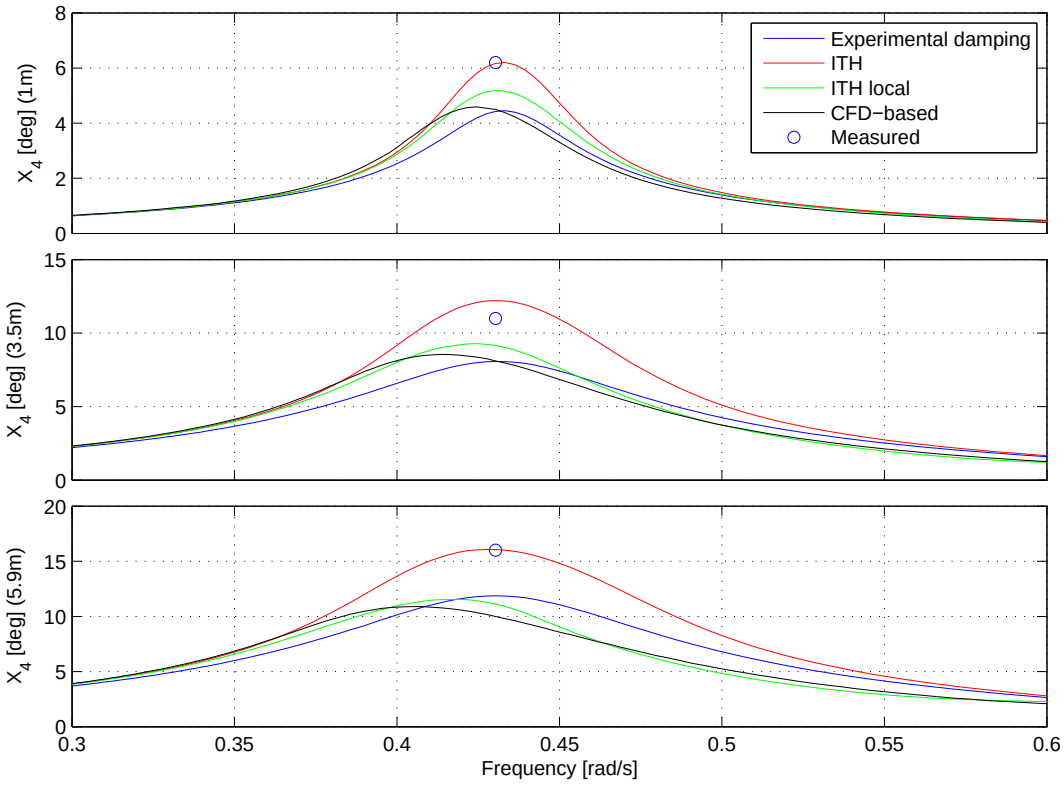

Figure 5.5: Various roll amplitude plots for a 1, 3.5 and 5.9 meter amplitude incoming wave.

Wave amplitude [m]	Experiment [°]	CFD-based [°]	ITH local [°]	ITH [°]	F_4 [Nm]
1.0	4.5	4.6	5.2	6.2	15.0
3.5	8.1	8.5	9.3	12.2	53.3
5.9	11.9	10.8	11.5	16.1	89.8

Table 5.8: Maximum roll amplitude and potential roll exciting moment in regular waves.

5.4.5. FREQUENCY DOMAIN

Unfortunately due to time constraints the frequency domain simulations have not yet been performed.

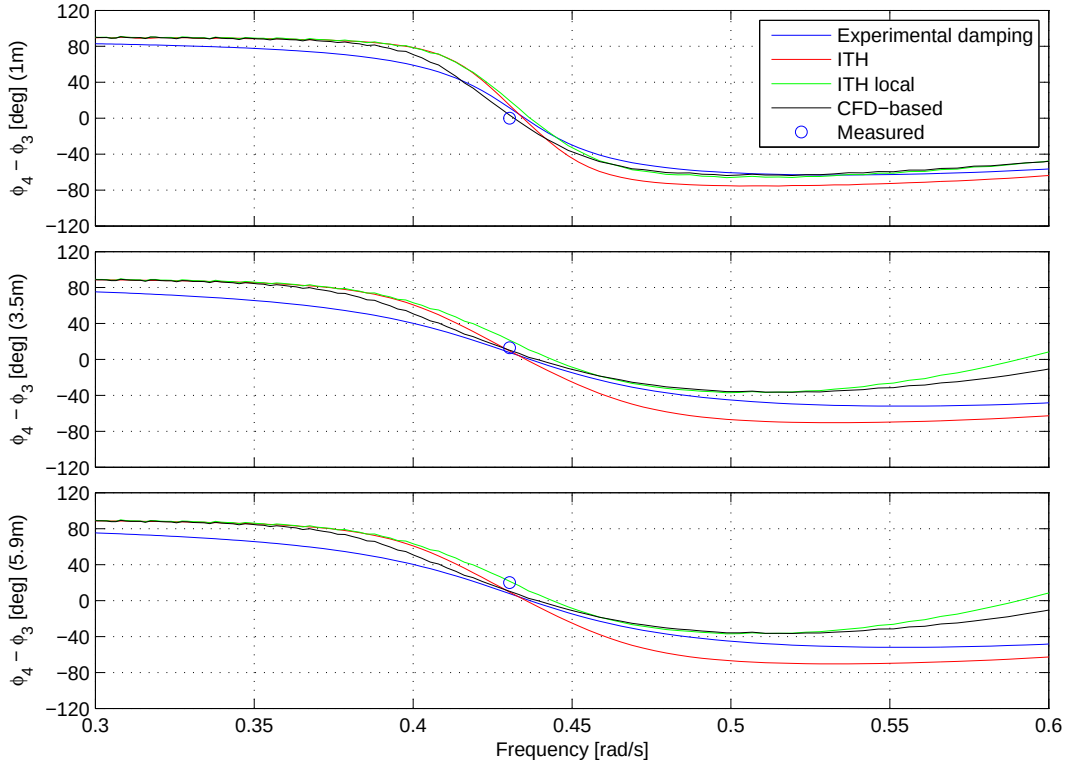

Figure 5.6: Phase difference between heave and roll for a 1, 3.5 and 5.9 meter amplitude incoming wave.

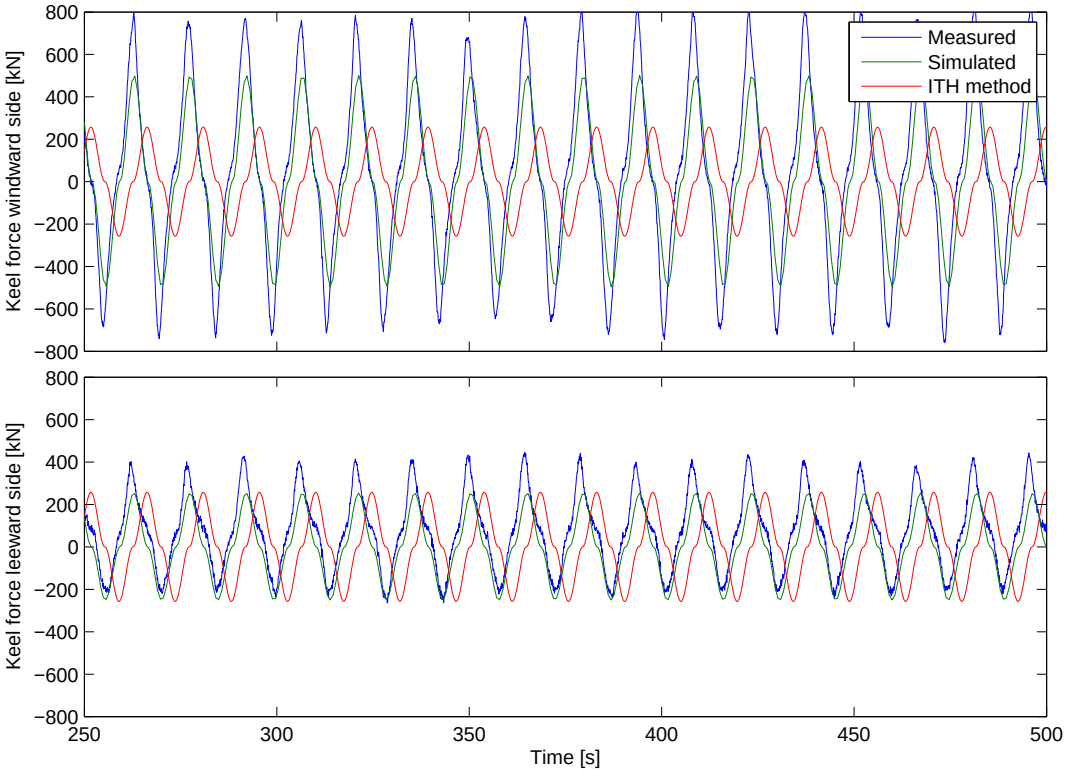

Figure 5.7: Predicted bilge keel loads in waves with adjusted forcing moment in roll.

5.5. SENSITIVITIES

Tested sensitivities are:

- ±20% hull moment coefficients,
- ±20% keel force coefficients,
- ±20% local velocities, and
- linear or non-linear rigid body motion velocities.

Besides the sensitivities shown in Figures 5.9 and 5.10 a sensitivity plot around the natural frequency without bilge keel (0.43 [rad/s]) is shown in Figure 5.8. It can be concluded from Figure 5.9 that using non-linear rigid body motions velocities or linear, superposed rigid body motion velocities does not make a large difference in beam seas. While it seems safe to say that thus the linear, superposed approach is sufficient this assumption needs to be validated in head waves or quartering waves as well, as pitch and surge motions are very small in beam waves.

As expected the both the keel and hull coefficients have a significant impact on the roll motions, reference is made to Figures 5.8 and 5.10 , and as expected hull coefficients have a larger impact as the hull damping is larger at higher amplitudes than keel force damping. The largest impact is due to the local velocities, again as expected. The large dependency on local velocities is expected as the hull pressure and keel force influences are both impacted and this impact is quadratic in nature. The large impact is worrisome for correct prediction. Each velocity component should be singled out and evaluated as it is unlikely that all components are simultaneously predicted wrong by 20%. It should be noted that a wrong prediction of the radiated velocities will have an effect on the CFD results as well, compensating a potential error.

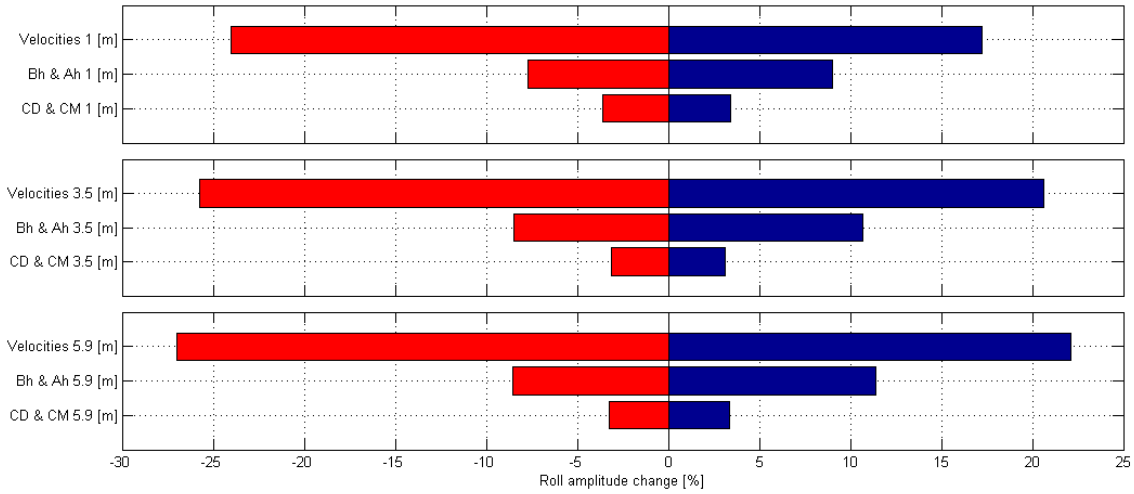

Figure 5.8: ±20% sensitivity plot for a 1, 3.5 and 5.9 meter amplitude incoming wave.

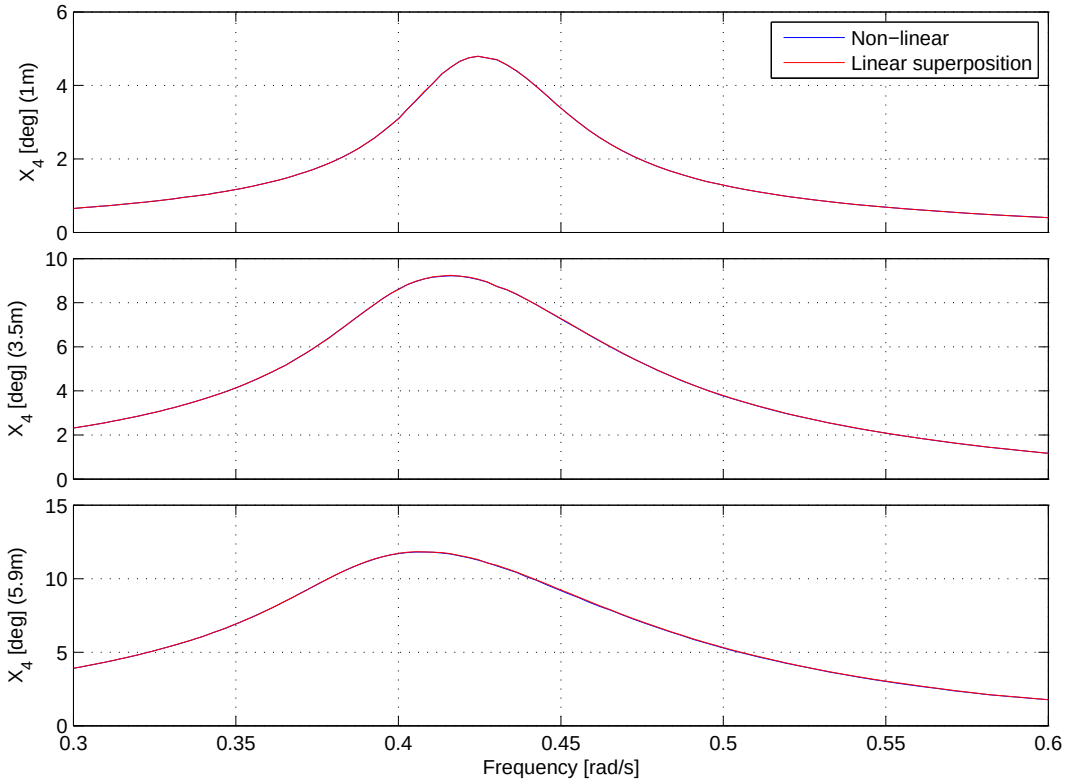

Figure 5.9: Non-linear and linear rigid body velocity roll amplitude plots for a 1, 3.5 and 5.9 meter amplitude incoming wave.

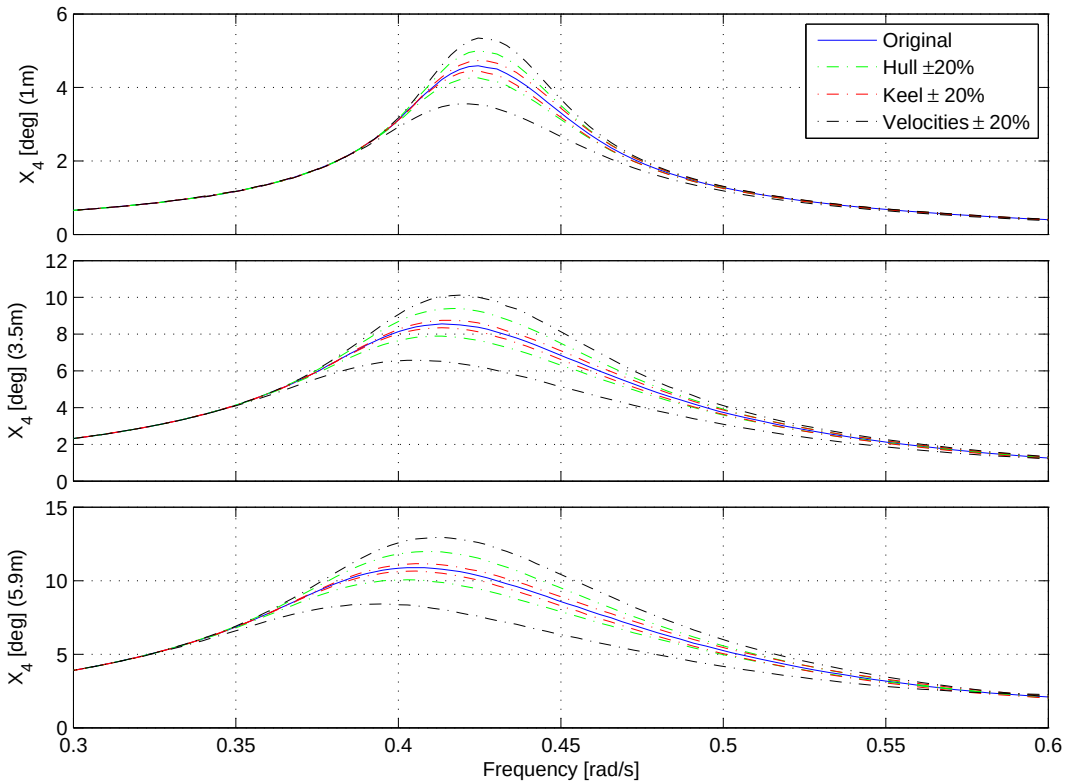

Figure 5.10: ±20% hull ,keel and local velocity coefficients roll amplitude plots for a 1, 3.5 and 5.9 meter amplitude incoming wave.

6

Conclusion and Recommendations

The conclusions and recommendations are presented in this Chapter.

6.1. Conclusions

Roll damping and motions of vessels with bilge keels are in general predicted using theories based on rigid body motions and with empirical foundations. These do not always yield the correct results when applied to vessels in waves and with the aberrant hull and/or bilge keel geometry typical for vessels without forward speed such as an FPSO. The only alternative available at this time is wave tank experiments, which are expensive, time-consuming and require reservations months ahead. Thus the question that is the focal point of this report is:

> *"How can the roll damping and roll motion of an FPSO with aberrant bilge keel geometry in waves be determined within a time-frame reasonable for a tender/design stage (2-4 weeks)?"*

From the performed literature review it is concluded that:

- The current methodologies as recommended by the ITTC (the ITH method) are insufficient for accurate and physical correct prediction of roll motions in waves and configurations that deviate from the empirical basis of the methodologies.
- The largest potential sources for errors in the ITH method are the velocities based on the global roll motion and thus exclusion of local water velocities and limitations in the empirical foundations. To a lesser extent memory effects and other factors have an influence.
- Local velocities as obtained using linear potential theory can be used to accurately predict loads on bilge keels.
- CFD can be used to predict effects caused by bilge keels. A wide range of methods can be used, but in general DVM or URANS with a $\kappa-\omega$ SST or Realizable $\kappa-\epsilon$ turbulence model are preferred.
- The hull pressure moment generated by bilge keels is significant in terms of damping, but is not well described analytically or in a semi-empirical manner.

From these conclusions a methodology is proposed based on CFD as a substitute for the empirical basis and local velocities from linear potential theory as a substitute for rigid body motions to predict roll motions of vessels with bilge keels in waves.

The CFD calculations are performed in a 2D setup with forced oscillations in the DoF and all other DoFs fixed. The rotation axis is through the DoF and a URANS method with a $\kappa-\omega$ SST turbulence model is utilized. From comparisons to a Realizable $\kappa-\epsilon$ turbulence model; to 2D forced roll oscillation, single DoF experiments with a circular hull and various bilge keels; and to a 3D forced roll oscillation, six DoF experiments with a typical FPSO hull and simple bilge keels it is concluded that:

- The difference in this particular application between $\kappa-\omega$ SST and Realizable $\kappa-\epsilon$ turbulence models in negligible with a NRMSE of less than 1%.
- Keel forces and hull pressures close to the keel of 2D forced roll oscillations of a circular hull with a variety of bilge keels are well predicted by URANS simulations with a $\kappa-\omega$ SST turbulence model.
- Including radiated wave velocities from potential theory in forced oscillations CFD simulations to extract drag coefficients yield reliable drag coefficients when compared to literature, i.e. compares well to $C_D = 22.5/KC + 2.4$.
- At high amplitudes the sliding interface between the moving and stationary mesh has optimalizations that render the results unreliable.

The results of the CFD are in the form of relations between the keel forces and local velocities as well as the hull pressure moments and local velocities. These relations are represented as coefficients which are functions of local water velocity amplitude, local water velocity period, bilge keel geometry and hull geometry. These coefficients were combined with local velocities from potential theory, including diffracted, incoming, radiated and 6 DoF rigid body motions, to obtain a roll moment due to bilge keels in waves. This method was implemented in the time domain to allow non-linearities between vessel motions, keel forces and hull pressure moments to be present. The results are compared to forced roll oscillations using an exciting moment generated by an electric drive installed in a free-floating scale model of an FPSO. Further comparison was performed in regular waves. As a discrepancy was observed between measured values in regular waves and simulated values using experimentally obtained damping, comparison is made between simulated values using experimental damping, using the ITH method, using the ITH method with local velocities implemented and using the proposed methodology. It can be concluded that:

- Forced oscillations can be predicted using coefficients obtained using CFD.
- A linear relation between hull pressure coefficients and local velocity amplitude is only valid for a certain range of velocity and roll amplitudes.
- When comparing to simulations with experimental damping coefficients the proposed methodology provides an accurate prediction at low to medium amplitudes.
- When comparing to simulations with experimental damping coefficients the ITH method based on local velocities provides a drastically improved prediction over the ITH method based on only rigid body motions
- The proposed and modified ITH method both are more representative of the actual physics, including phenomena such as different loads on windward- and leeward side bilge keels.
- When comparing to simulations with experimental damping coefficients the forced oscillations simulation results seem to be representative in waves as well.
- The method in waves is sensitive to changes in local velocities and to a lesser extend hull pressure coefficients. The impact of keel force coefficient changes is relatively small.

Summarizing it can be concluded in general that methodologies based on local velocities seem to provide a better prediction of vessel response in calm water and in regular waves. Furthermore incorporation of coefficients obtained from CFD show good results. It mush be emphasized that the method has not been validated. As the discrepancy between actual measured results and simulated results is very large further investigation and, if possible, validation is required. A step has been taken towards a practical method that can be used before final design experiments have been done, but there are issues that need to be addressed which will be discussed in the following Section.

6.2. RECOMMENDATIONS

Following the conclusion there are some recommendations regarding future work on roll motion prediction and continuation of development of a methodology based on local velocities and CFD. The recommendations are divided in two sections: CFD and the methodology.

6.2.1. CFD

The CFD model was identified to have some issues of which three are discussed. As it seems that most problems, especially at higher amplitudes, were caused by the sliding interface it is recommended to eliminate this potential source of error. There are in general two options to eliminate the sliding interface: a morphing mesh and a chimera or overset mesh. A morphing mesh deforms the mesh to allow for motions. This could lead to instability and cannot cope with very complex or large displacements. The advantage is that there are no additional requirements on the time-step. The alternative the overset mesh utilizes two meshes: a background mesh that spans the entire domain and a mesh around the body of interest. These meshes overlap one another and information is passed between them. The advantage of overset meshes is that they allow all motions to be simulated and do not have a risk of badly deforming cells. The disadvantage is that the motion cannot be more than half a cell size per timestep, i.e. a Courant number smaller than 0.5. As the Courant number needs to smaller than 0.5 for the HRIC interface the overset mesh is recommended. This would furthermore allow a three DoF (roll, sway and heave) motion to be simulated. Another possibility would be to depart from the Eularian RANS method and move to a Lagrangian method such as DVM which relies only on a mesh positioned on the surface of the hull. This would be more complex to implement as it is a complete departure from the current method but is a very sensible methodology for this particular problem. Both a Lagrangian and overset mesh method would allow more freedom in the choice of experiments to validate with as other motions can be simulated as well.

Further validation is recommended as well. While the model is validated for a circular hull, no validation has been performed for other hull shapes. The best option would be to perform more controlled experiments similar to the ones performed by Schut, i.e. a hull section with a one DoF forced oscillation through the CoG. This way other influences such as heave motions, sway motions and 3D effects are eliminated or minimized.

Finally besides the moment generated by the roll motions and thus vortex shedding there is also a sway and heave force generated. These are currently neglected but could result in a roll-sway and roll-heave coupling and should be possible to extract from the CFD results.

Summarizing the recommendations are to:

- implement an overset mesh;
- validate with a ship-shape hull; and
- evaluate generated sway and heave forces.

6.2.2. METHODOLOGY

One of the largest flaws in the results is the large discrepancy between measured roll angles and roll angles simulated using either the proposed methodology or damping coefficients obtained from the experiments. This is an issue that is still unexplained, as such an alternative route has been taken to validate against simulated results based on experimental data, but this does not solve the issue. As the time domain code is verified using HydroStar and HydroStar is assumed verified through the years of use, this leaves the input to HydroStar, the output of the experiments or some unidentified phenomena as the source of the error. The simplest solution is to evaluate if the same discrepancy is found when simulations are performed of other experiments, but this requires new experiments to be done or a different data set of already performed experiments.

A discrepancy is also found at higher amplitudes where the predicted roll amplitude is too low. This is most likely due to the limited range of velocity amplitudes in which the CFD simulations were performed. Looking at the ITH method the hull pressure coefficient is expected to decline after velocity becomes too high (with a constant period). This is not reflected in the CFD. This would require investigation with CFD simulations at higher roll velocities or by introducing velocities in the CFD that are independent of the roll motions. These results could then possibly be incorporated to predict the hull pressure coefficient saturation at higher local velocities.

The out-of-phase coefficient C_M requires further validation as well. In the C_M coefficient a sensitivity to frequency was observed but not incorporated and the coefficient was again not evaluated at higher velocities while results from Schut [17] and Keulegan [69] both show a decline in steepness at higher KC numbers. The same is valid for the hull pressure out-of-phase component. It is now assumed constant for pragmatic reasons, but a variance is observed which should if possible be coupled to a appropriate dimensionless number.

Wave drift effects are not evaluated and incorporated while they are shown to have an influence on roll motions and should be possible to implement. Another parameter that was not evaluated are the memory

effects. While they are not present in regular waves, they can play a role in irregular waves and should be implemented if shown relevant.

Another consideration is the validation for actual aberrant bilge keel geometries, riser balconies and asymmetric configurations. This will show the effectiveness of the proposed methodology in scenarios such as these, which should be an improvement over traditional methods. Some issues are expected such as the shedding point of the vortex from the riser balcony as it is much thicker than a bilge keel. This should be evaluated from CFD simulations.

Finally irregular waves were not simulated. The methodology to perform these simulations has been outlined and an argumentation why higher harmonics can be neglected is presented, but these are both not validated. This is an essential step to complete a model that can predict maximum roll motions and thus evaluate the design criteria and is recommended to be performed. It can be argued that the regular waves can be used to construct RAOs but the problem is non-linear and thus requires a specific RAO for a specific sea-state. The results of the irregular wave simulations can then be used to implement a frequency domain method as the ultimate goal and tool that is usable for prediction of roll motions for a wide range of sea-states and wave directions while not being as time consuming as running many time domain simulations.

Summarizing the recommendations are to:

- apply the methodology to other regular experiments or identify the source of the discrepancy in the current comparison;
- evaluate hull pressure coefficients at higher roll amplitudes/velocities;
- evaluate out-of-phase components for frequency sensitivity and at high roll amplitudes/velocities;
- evaluate and if necessary implement wave drift effects and memory effect;
- implement and validate for aberrant bilge keel geometries, riser balconies and asymmetric configurations;
- implement the methodology in irregular waves to enable a more broad validation as a great deal of data is available for irregular waves and to validate certain assumptions; and
- eventually parameterize the coefficients to make the CFD obsolete.

While it becomes apparent from the recommendations the methodology is far from finished and validated a foundation has been laid and a clear path for the future has been set.

A

EXPERIMENT PARTICULARS

A.1. ROLL JIP

The FPSO Roll JIP was commissioned in 2004 by Maritime Research Institute Netherlands (MARIN). The objective was to: "quantify the roll damping of the Glas Dowr FPSO" including the motions and the contribution of the separate damping components. The Glas Dowr FPSO was scaled with a factor of one over forty, the midship deck was heightened slightly and a rudder was not fitted. The midship was fitted with pressure sensors over the entire section, relative waveheight sensors were fitted bow and center, as well as force sensors in the soft mooring system. The bilge keel normal forces were measured by fitting force transducers at the aft and front of a bilge keel section which was about half of the total bilge keel.

To perform the free-floating forced oscillations a electric servo engine was installed which could be accelerated and decelerated to provide the desired pure roll moment. A six-component force transducer was used to determine the roll damping. The six DoF motions were measured at the CoG. A photograph of an example setup can be viewed in Figure A.1.

Figure A.1: A photograph of the Glas Dowr model in regular waves.

A.1.1. OVERVIEW

In Tables A.1 and A.2 the particulars at full loaded and intermediate draft can be found.

BILGE KEEL GEOMETRY

In the tests three geometries were used: no bilge keel, a 0.35 [m] bilge keel and a 0.7 [m] bilge keel. Both bilge keels were a simple plate. A bilge keel length of 72 [m] was realized.

DRAFT

Two drafts were tested an intermediate loaded draft and a fully loaded draft.

Parameter	Unit	Glas Dowr	Model
Length between perpendiculars	m	232	5.8
Breadth	m	42	1.05
Depth	m	21.2	0.531
Draft	m	14.85	0.37125
CoG z-direction	m	13.22	0.3305
Transverse radius of gyration	m	14.29	0.35725
Longitudinal radius of gyration	m	56.36	1.409
Yaw radius of gyration	m	60.62	1.5155
Displacement	kN	1187501	18.555
Roll period	s	14.91	2.356
Bilge keel location y	m	20.43	0.510761
Bilge keel location z	m	-14.28	-0.357101

Table A.1: Fully loaded Glas Dowr and model parameters

Parameter	Unit	Glas Dowr	Model
Length between perpendiculars	m	232	5.8
Breadth	m	42	1.05
Depth	m	21.2	0.531
Draft	m	9.9	0.2475
CoG z-direction	m	13.599	0.339975
Transverse radius of gyration	m	15.98	0.3995
Longitudinal radius of gyration	m	59.34	1.4835
Yaw radius of gyration	m	60.62	1.5155
Displacement	kN	761354.0	11.896
Roll period	s	14.6	2.308
Bilge keel location y	m	20.43	0.510761
Bilge keel location z	m	-9.33	-0.233351

Table A.2: Intermediate loaded Glas Dowr and model parameters

FREQUENCY

All tests were done at the natural frequency, although this is a disadvantage, especially when constructing overviews, the damping is most critical at the natural frequency.

AMPLITUDE

A variety of amplitudes was tested ranging from two to twenty degrees in calm water, regular waves and irregular waves.

A.1.2. DISCUSSION

The Roll JIP experiments are quite extensive. Unfortunately the forced oscillation results are not suitable to validate the CFD as the other motions besides the roll are not restricted. The experiments are suitable to validate the proposed methodology as they include the wide range from forced oscillations to regular waves and irregular waves. Almost raw sensor data is available. Performed experiments can be found in Tables A.3, A.4 and A.5. It should be noted that loaded condition experiments were performed with a 14.9 [s] period and intermediate with a 14.6 [s] period.

SBM id.	Marin id.	$\theta_a[deg]$	$h_{bk}[m]$	LC
113024	220001	2.4	0	loaded
113043	220002	4.2	0	loaded
113060	220003	6.0	0	loaded
113113	220004	11.3	0	loaded
113148	220005	14.8	0	loaded
111021	213005	2.1	0.35	loaded
111042	213004	4.2	0.35	loaded
111061	213001	6.1	0.35	loaded
111112	213002	11.2	0.35	loaded
111160	213003	16.0	0.35	loaded
112063	204005	6.3	0.7	loaded
112114	204006	11.4	0.7	loaded
112154	204007	15.4	0.7	loaded
123019	304006	1.9	0	intermediate
123043	304002	4.3	0	intermediate
123058	304003	5.8	0	intermediate
123110	304004	11.0	0	intermediate
123178	304007	17.8	0	intermediate
123212	304008	21.2	0	intermediate
123240	304009	24	0	intermediate
121019	313001	1.9	0.35	intermediate
121041	313002	4.1	0.35	intermediate
121062	313004	6.2	0.35	intermediate
121115	313005	11.5	0.35	intermediate
121171	313006	17.1	0.35	intermediate
121186	313009	18.6	0.35	intermediate
121200	313007	20	0.35	intermediate
122020	318001	2.0	0.7	intermediate
122044	318002	4.4	0.7	intermediate
122066	318003	6.6	0.7	intermediate
122081	318007	8.1	0.7	intermediate
122117	318004	11.7	0.7	intermediate
122135	318008	13.5	0.7	intermediate
122174	318005	17.4	0.7	intermediate
122190	318006	19.0	0.7	intermediate

Table A.3: Performed calm water forced oscillation experiments with their respective parameters

MARIN id.	$H_s[m]$ (dist./undist.)	$\theta_a[deg]$	$h_{bk}[m]$	LC
205011	0.75/1.00	6.5	0.70	loaded
206005	2.40/2.73	11.6	0.70	loaded
206007	3.30/3.70	13.7	0.70	loaded
319001	0.84/0.98	6.2	0.70	intermediate
319002	2.88/3.50	11.0	0.70	intermediate
319003	5.04/5.90	16.0	0.70	intermediate

Table A.4: Performed free floating regular experiments with their respective parameters only beam waves with a 0.7 [m] bilge keel are included.

MARIN id.	$H_s[m]$ (dist./undist.)	Single $\theta_s[deg]$	$h_{bk}[m]$	LC
208002	3.30/3.87	6.60	0.70	loaded
209002	4.20/4.89	7.64	0.70	loaded
322001	3.60/4.23	6.58	0.70	intermediate
323001	9.60/10.75	11.82	0.70	intermediate

Table A.5: Performed free floating irregular experiments with their respective parameters only beam waves with a 0.7 [m] bilge keel are included.

A.2. SCHUT EXPERIMENTS

The aim of the research done by Schut was: "to obtain a better understanding of the roll damping caused by FPSO bilge keels" [17]. To enable the use of a as large model as possible, as the equipment had weight restrictions, as well as minimizing influence of the hull geometry in the form of flow disturbance and water displacement a cylindrical model was used to approximate an FPSO. The hull pressures were measured using two sets of pressure sensors, the bilge keel normal force was measured using load cells and the radiated waves using wave probes. In Figure A.2 a render can be found of the model, including end plates to reduce end effects, resulting in a semi-2D situation.

A six-DoF frame was used (Hexamove) to perform the excitation and movements were captured using the Certus system which tracks four LEDs.

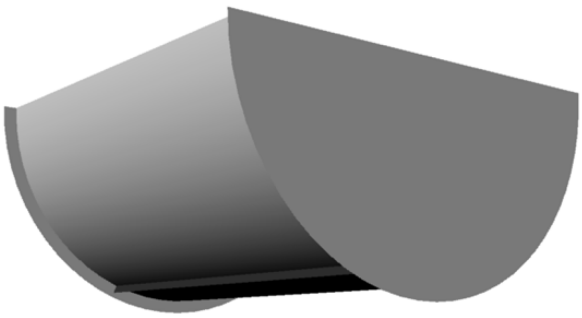

Figure A.2: 3D render of the 303 FPSO equivalent cylinder used in the experiments by Schut [17]

A.2.1. OVERVIEW

The model particulars can be found in Table A.6.

	Fully Loaded	Intermediate	Ballasted
Length [m]	1.218	1.218	1.218
Diameter [m]	1.461	1.461	1.461
Draft [m]	0.364	0.310	0.148
Water displacement [kg]	394	271	108

Table A.6: Schut model particulars

BILGE KEEL GEOMETRY

Various bilge keels were used in the experiments performed by Schut to allow the evaluation of complex bilge keel shape on bilge keel force and hull pressures, reference is made to Figure A.3 for an overview.

DRAFT

There are a few drafts available from experiments which correspond to the fully loaded, intermediate loaded and empty drafts of the full scale 303 FPSO. It should be noted that the draft of the 303 FPSO does not directly

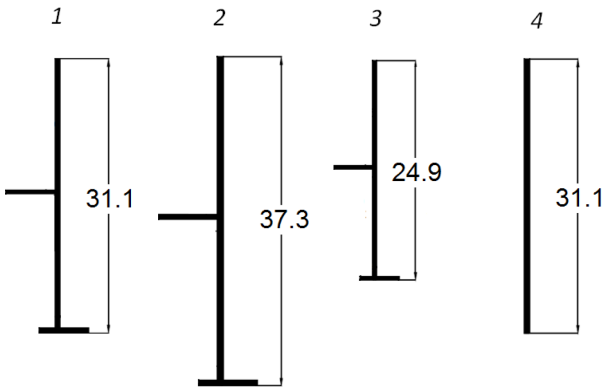

Figure A.3: Overview of various bilge keel geometries and dimensions [m]. From Schut [17]

translate to a draft for the experimental setup. The scaled draft of the 303 FPSO is wrapped along the experimental circular hull to determine an equivalent draft. Reference is made to Table A.7 for an overview of the various drafts.

Loading condition	303 FPSO draft [m]	Scaled 303 FPSO draft [m]	Experimental draft [m]
Fully Loaded	21.42	0.476	0.364
Intermediate	16.72	0.371	0.278
Ballasted	8.43	0.187	0.148

Table A.7: Various draft for full scale and model scale 303 FPSO as well as experimental drafts

FREQUENCY

Various frequencies are evaluated to determine impact on the various coefficients, i.e. C_D is usually assumed frequency independent. The frequencies evaluated were the natural frequency of 2.62 [rad/s] as well as frequencies 20% and 40% lower and higher: 2.10, 1.57, 3.14 and 3.67 [rad/s].

AMPLITUDE

A range of amplitudes were tested, ranging from zero to twelve degrees.

A.2.2. DISCUSSION

While the circular hull experiments done by Schut provide a basis for the validation of the CFD as all other effects should be small, it does not provide validation for other hull shapes. There is furthermore only a fictional hull pressure damping present as hull pressure do not generate a moment. This can be circumvented by interpolating the pressures to a real hull, emphasizing the pressures close to the keel with a large arm and depreciating pressures further from the hull with a small arm. The sensors used were of good quality, as well as the exciting system. Unfortunately some irregularities remain that have not been addressed, such as oscillations over all pressure sensors at certain points as well as 3D effects. It was furthermore noted that pressures and damping are most likely higher than measured which agrees with the CFD results.

B

LINEARIZATION OF DAMPING

While non-linear damping is applicable in the time domain, in the frequency domain non-linearities are not allowed. There are roughly two methods of linearization: the LMI method and through work performed. The methodology using work can be divided into two sub-methods: for regular waves and for irregular waves. For regular waves the linearization coefficient depends on motion or velocity amplitude, while for irregular waves it is tuned to the specific spectrum.

LINEARIZE, MATCH AND ITERATE

In the LMI method the probability of exceeding a certain roll amplitude is estimated to be a the fraction of the average number of upcrossings with this amplitude and the number of zero-upcrossings. To determine the number of upcrossings for this certain amplitude is simple for a Gaussian process but not as simple for a non-Gaussian process, for this the joint probability density function of roll and roll velocity are necessary. These can be obtained through the cross-moments of roll and roll velocity.

These cross moments are determined by first approximating the quadratic non-linearity with a cubic and linear damping (linearize). This equation is then used to construct a system of linear equations of size i that approximately maintain the $2i^{th}$ order moments of the cubic system (match). The retardation, or memory function, is included in the linear systems as well. This allows the moments to be calculated leading to the joint density of roll and roll velocity.

As the linearization step depends on the expected value of the roll velocity squared, iteration becomes possible, as the new density function allows to calculate a new expected value of the roll velocity squared (iteration).

While the LMI method seems very promising, yielding results in very good agreement with Monte Carlo simulations, it is best viewed as an improvement on normal linearization functions, as traditional linearization is required anyway. It furthermore relies on a constant quadratic damping coefficient, while in reality this varies, thus still requiring a representative value. Reference is made to Prevosto [35] and Minko [36].

STOCHASTIC LINEARIZATION

Stochastic linearization utilizes the fact that the RMS value can be deduced from a spectrum. It is based on the notion that the Gaussian seastate and the time-averaged least-square error between the linear and non-linear term [81]. This results in the average work performed by the non-linear term being equal to the average work performed by the equivalent linear term. While this technique is widely used its limits should be understood. Instead of assuming a correct damping for each waveheight a damping is chosen which is considered representative. This means the in the case of Equation B.1 the roll damping will be underestimated 28% of the time and overestimated 72% of the time, which results from the Rayleigh distribution which is assumed that velocity follows. Depending on the required results this might lead to significant underestimation of for example extreme loading prediction as the highest loads are underestimated. Wolfram [81] notes that in his opinion stochastic linearization based on work should only be performed when the desired outcome value proportionally depends on the time averaged work. For roll damping this seems to be valid as it depends on the RMS of the roll (the zeroth moment of the spectrum) which is equivalent to the work performed, as shown in the next Section. If this is not valid linearization should take place depending on another parameter that is proportional with the desired outcome value.

$$B_{lin} = \sqrt{8/\pi}\sigma_u B_q \tag{B.1}$$

THROUGH WORK DONE

This method is similar to the stochastic linearization method. The difference is that the linearization takes place a step earlier. Instead of linearizing a damping coefficient, a linearized damping coefficient is directly obtained from the work done by the relevant moment obtained from experiments or for example CFD. It furthermore depends on a regular wave/motion instead of a spectrum. A basic example is as follows, where a linear damping depending on roll velocity is assumed:

$$M = B\dot{x}_4, \tag{B.2}$$

$$W = \int B\dot{x}_4\dot{x}_4, \tag{B.3}$$

$$P = \frac{\int B\dot{x}_4\dot{x}_4 dt}{T}, \tag{B.4}$$

$$P = \frac{\sum B\dot{x}_4\dot{x}_4\Delta t}{n\Delta t}, \tag{B.5}$$

$$P = \frac{\sum B\dot{x}_4\dot{x}_4}{n}, \tag{B.6}$$

$$P = B\frac{\sum \dot{x}_4^2}{n}, \tag{B.7}$$

$$\frac{\sum \dot{x}_4^2}{n} = \sigma_{\dot{x}_4}^2, \tag{B.8}$$

$$\sigma_{\dot{x}_4} = \frac{1}{2}\sqrt{2}\dot{X}_4, \tag{B.9}$$

$$P = B\frac{1}{2}\dot{X}_4^2, \tag{B.10}$$

$$B = \frac{P(\omega, \dot{X}_4)}{{}^1/_2\dot{X}_4^2}. \tag{B.11}$$

Unfortunately this solution results in another problem which is similar to stochastic linearization, which is to be expected as they are both based around the time-averaged work. As this damping is linear with the velocity amplitude a maximum velocity is needed to select the correct damping, reference is made to Figures 4.9 and 4.10. As this velocity cannot be obtained from the spectrum explicitly for each cycle an equivalent value will be necessary such as used in stochastic linearization, reference is made to the previous Section. For stochastic linearization the time-averaged value is used, which is usable when the average value of for example the roll angle is desired. According to Wolfram if the extreme value is of interest the linearization should take place around that particular point [81].

C

HydroStar

Two models were created in HydroStar:

- a semi-2D model of the midship section which was simulated in CFD,
- a full 3D model of the scale model used in the MARIN tank for the experiments.

The second model is verified using an older model generated by Riaan van 't Veer and results were very similar for the fully loaded condition, other models were not available for validation.

While usually the RAOs are the output of interest, for this thesis they are not and thus the input parameters are limited to those in Table 3.1.

C.1. Meshes

The mesh geometry is constructed in CAD program Rhinoceros using the cross-section layout obtained from the small-scale body plan. This IGES file is then imported into Ezydro where a suitable mesh is generated in the hst format usable in HydroStar. The largest mesh element size is 5 centimeters and the entire mesh consist of respectively 6804 and 5108 panels for the loaded and intermediate loading condition. The results can be viewed in Figures C.1 and C.2.

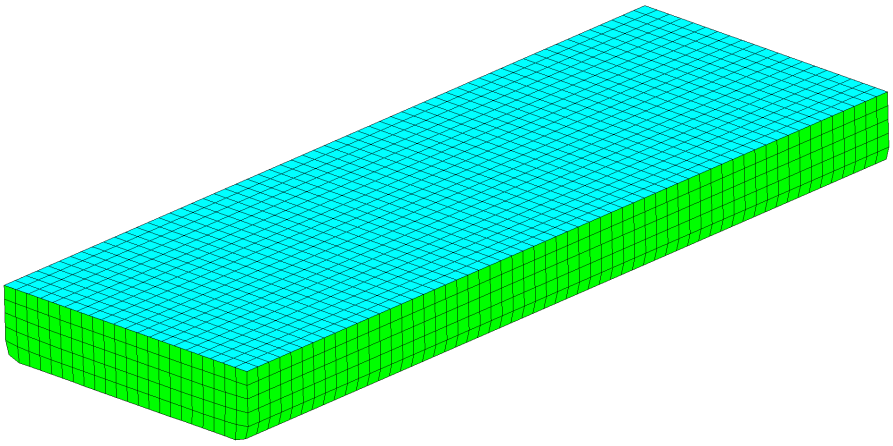

Figure C.1: Mesh of a semi-2D section of the Glas Dowr generated by Ezydro for use in HydroStar

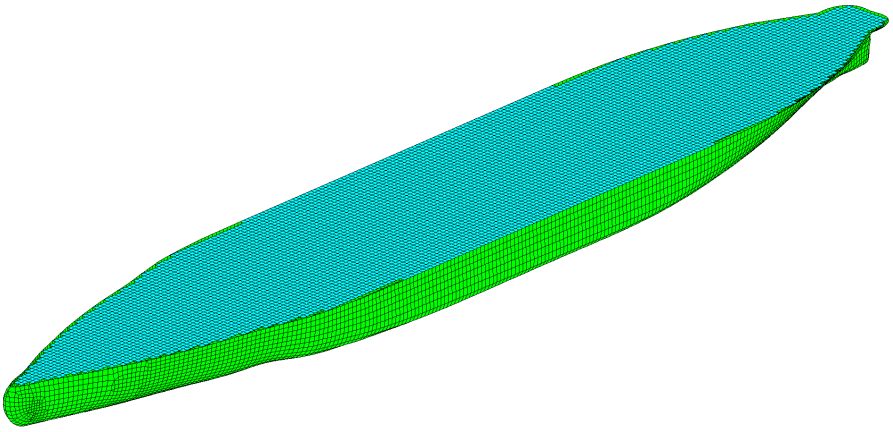

Figure C.2: Mesh of the Glas Dowr generated by Ezydro for use in HydroStar

C.2. INPUT PARAMETERS

It should be noted that the structural radius of gyration around the x-axis is slightly different than obtained from MARIN. During the preparation of the experiments the structural radius of gyration was determined using the following equation:

$$T = \frac{2\pi r_{xx,e}}{\sqrt{gGM_x}}. \tag{C.1}$$

Here is was assumed that the metacentric height GM, g and the natural period T were known. The effective radius of gyration was then obtained after which the calculated added mass was deducted to obtain the structural radius of gyration. As a correct natural period is essential to compare the simulations with the experiments and the added mass obtained from HydroStar was slightly higher the structural radius of gyration was adjusted downwards to compensate this change and allow for the correct natural period of 14.6 [s] instead of the computed 14.9 [s].

Parameters	Loaded	Intermediate
Mesh	See above	See above
r_{xx} [m]	0.3572	0.3875
r_{yy} [m]	1.409	1.4836
r_{zz} [m]	1.5155	1.5155
Mass [kg]	1845.3	1183.1
ρ $[kg/m^3]$	1000	1000
g	9.81	9.81
ω $[rad/s]$	0.1:0.1:15	0.1:0.1:15
CoG x,y,z [m]	0.14475 ,0 ,-0.040775	0.2197 ,0 ,0.0925
Bilge Keel Location x,y,z [m]	0.14475, ±0.523, -0.37	0.2197, ±0.523, -0.24625
Draft [m]	0.37125	0.2475

Table C.1: HydroStar input parameters

C.3. ADDITIONAL DAMPING

There is additional damping present besides the bilge keel due to friction and viscous damping from parts of the hull besides the 72 meter part where the bilge keel was located. The additional damping was obtained from HydroStar using the built-in ITH method which divides the ship into sections and calculates the damping coefficients. The damping caused by the mid-ship section where the bilge keel was attached is then deducted from the total.

C.4. RESULTS

A part of the results of the HydroStar calculations can be found in Table C.2 where they are compared to MARIN results for the intermediate load. For the fully loaded vessel an additional comparison is made with data obtained from simulations done by R. van 't Veer for SBM Offshore in 2012, results are very similar and can be found in Table C.3.

Parameters	HydroStar	MARIN
Added mass [kgm]	46	36.1 - 55.1
Damping [Nms/rad]	2	2.5
Hydrostatics [Nm/rad]	1392	1660
f	1.78	2 (experimental)
Displacement [m^3]	1.10	1.18

Table C.2: HydroStar output compared to MARIN results at the natural frequency for intermediate load.

Parameters	HydroStar	MARIN	van 't Veer
Added mass [kgm]	50.8	37.65 - 41.9	49.6
Damping [Nms/rad]	4.2	4.4	4.3
Hydrostatics [Nm/rad]	1675	1941	1670
f	-	2	-
Displacement [m^3]	1.72	1.85	1.72

Table C.3: HydroStar output compared to MARIN results at the natural frequency for full load.

D

SIGNAL ANALYSIS

D.1. THE TOOLBOX

The contents of 'the toolbox' used to analyze the signals is discussed in the following Sections.

D.1.1. FOURIER ANALYSIS

A Fourier analysis uses Fourier decomposition to reduce a signal to series of cosine and sine signals, or in phase and out of phase terms, with frequencies $n\omega$ with $n = 1...\infty$. The Equations used are integrals integrated over an integer amount of periods multiplied with two and divided by the length of the integral:

$$A_n = \frac{2}{T}\int^T F(t)cos(n\omega t)dt, \tag{D.1a}$$

$$B_n = \frac{2}{T}\int^T F(t)sin(n\omega t)dt. \tag{D.1b}$$

To apply the above Equation to a signal that has to be decomposed into a form where the first harmonic in phase component is quadratic the following corrections are used, obtained from the power expansion:

$$B_1' = \frac{3}{8\pi}B_1, \tag{D.2a}$$

$$B_3' = B_1 - \frac{1}{5}B_3, \tag{D.2b}$$

$$B_5' = B_5 - \frac{3}{105}B_1. \tag{D.2c}$$

The can then be used in an Equation of the form:

$$F(t) = B_1' sin(\omega t)|sin(\omega t)| + B'3sin(3\omega t) + B'5sin(5\omega t) + A_1 cos(\omega t) + A_3 cos(3\omega t) + A_5 cos(5\omega t) \tag{D.3}$$

The coefficients obtained from the Fourier analysis can be used as well to construct an approximation of the signal consisting of sines with a phase shift instead of sines and cosines. The sine will have amplitude C_n and phase ϕ_n:

$$C_n = \sqrt{A_n^2 + B_n^2}, \tag{D.4a}$$

$$\phi_n = atan\left(\frac{A_n}{B_n}\right). \tag{D.4b}$$

D.1.2. FILTERS

Most measured signals carry a certain amount of noise in them, especially high frequency noise. This noise disturbs the data that one would want to obtain from measurements. To remove this noise or other data not

of interest filters are used. As MATLAB is used during this thesis the filters used are limited to those available in MATLAB. A filter is easiest described as an operation that removes certain frequencies above or below a reference frequency from a signal. As the amplitudes that are obtained from the experiments are important, it is crucial that the frequencies that are not removed are not influenced a fourth order Buttersworth filter is designed. Phase shifts are corrected by using the *filtfilt* command.

D.1.3. LEAST-SQUARES FITTING

Another useful tool is least-squares fitting. Least-squares fitting can be used to minimize the sum of the squared errors between a timetrace and a certain function. Two forms are possible: linear and non-linear least-squares fitting. As there is an abundance of information on this subject reference is made to other readings for a more detailed explanation. While the least-squares method can yield good results and is used to fit for example the Morison Equation to signals it is only as reliable as the function being fitted.

D.2. HULL PRESSURE MOMENT

Measured pressures are corrected for hydrostatic pressure changes. The obtained pressures are then multiplied with the proper arm and integrated over the skin of the vessel. This results in a moment which is then corrected for the moments generated according to potential theory, namely the added mass and damping. As there is a difference between which side the vortex forms on Fourier analysis is less applicable. Instead a least-squares fitting is used for a positive and negative velocity half-period. The fitted formula is:

$$M(t) = B_h(sgn(U), U_a)U(t) + A_h(sgn(U), U_a)\dot{U}(t). \tag{D.5}$$

Here B_h and A_h are dependent on the sign of the relative local velocity over the bilge keel.

D.3. BILGE KEEL NORMAL FORCE

The bilge keel normal force is measured for both the Schut and Roll JIP experiments. To objective is to reliably obtain the coefficients to the Morison Equation in a regular motion:

$$F(t) = \frac{1}{2}\rho A C_D U(t)|U(t)| + \rho V C_m \dot{U}(t) + \Delta R. \tag{D.6}$$

Fourier analysis is a very suitable for this operation, but first the noisy signals are filtered using the Buttersworth filter, removing high frequency noise. The filter is designed as such that that pass-band edge is at least ten times as high as the highest exciting frequency. This ensures that the higher harmonics are properly captured. The Fourier method as described in Section D.1.1 is applied to obtain the relevant coefficients:

$$A_n = \frac{4}{\rho h w U_m^2 T}\int_T F(t) sin(n\omega t + \phi_u), \tag{D.7a}$$

$$B_n = \frac{4}{\rho h w U_m^2 T}\int_T F(t) cos(n\omega t + \phi_u), \tag{D.7b}$$

$$C_D = \frac{3}{8\pi}B_1, \tag{D.7c}$$

$$C_M = -\frac{KC}{\pi^2}A_1. \tag{D.7d}$$

E

TURBULENCE MODEL COMPARISON

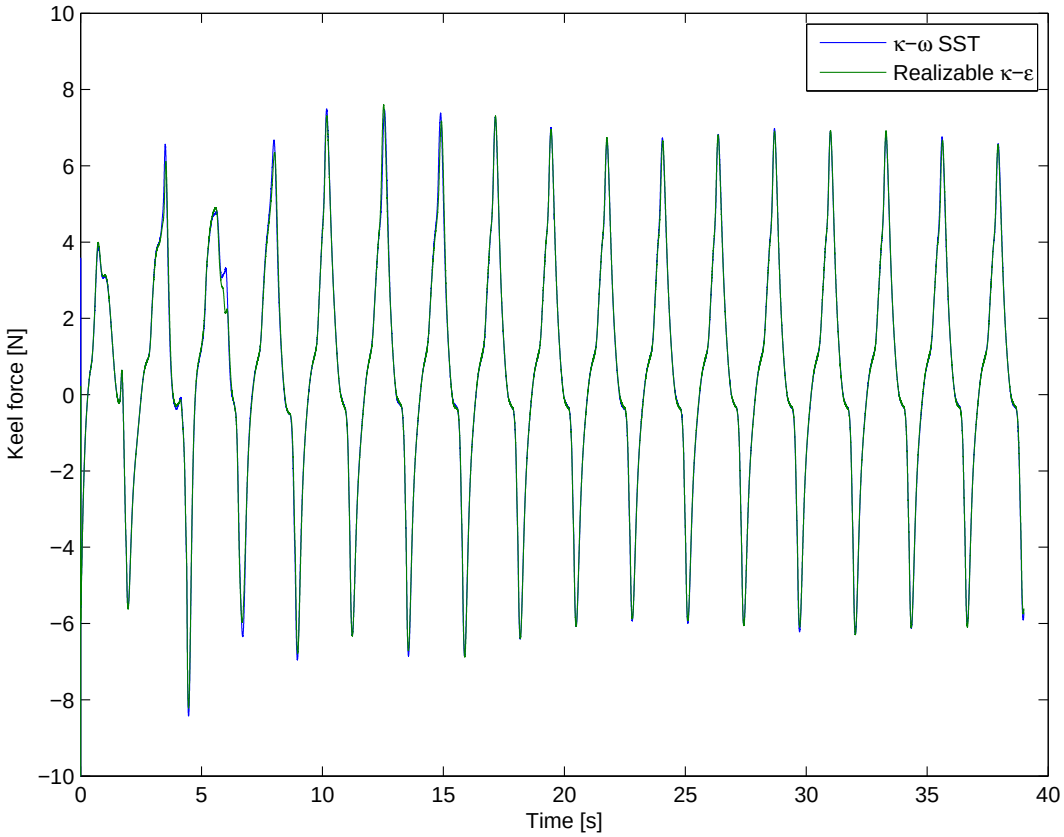

Figure E.1: Keel forces as predicted by an $\kappa - \omega$ SST turbulence model versus a Realizable $\kappa - \epsilon$ model.

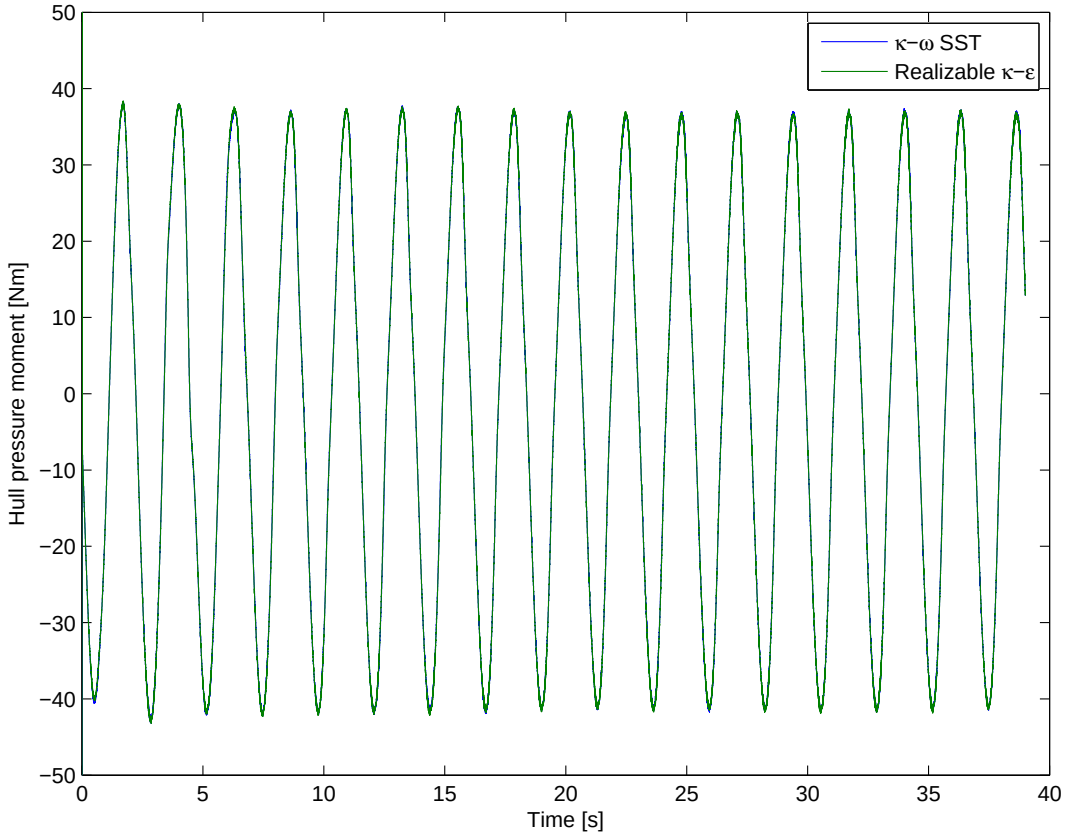

Figure E.2: Hull pressure generated moments as predicted by an $\kappa - \omega$ SST turbulence model versus a Realizable $\kappa - \epsilon$ model.

F

TIME DOMAIN VALIDATION

F.1. MOTION RAO RECONSTRUCTION VERIFICATION

The reconstructed RAO amplitudes and phases can be found in Figures F.1-F.6. The surge RAO is not exactly replicated as very fast and small motions are hard to capture without reducing the time-step to very small limits.

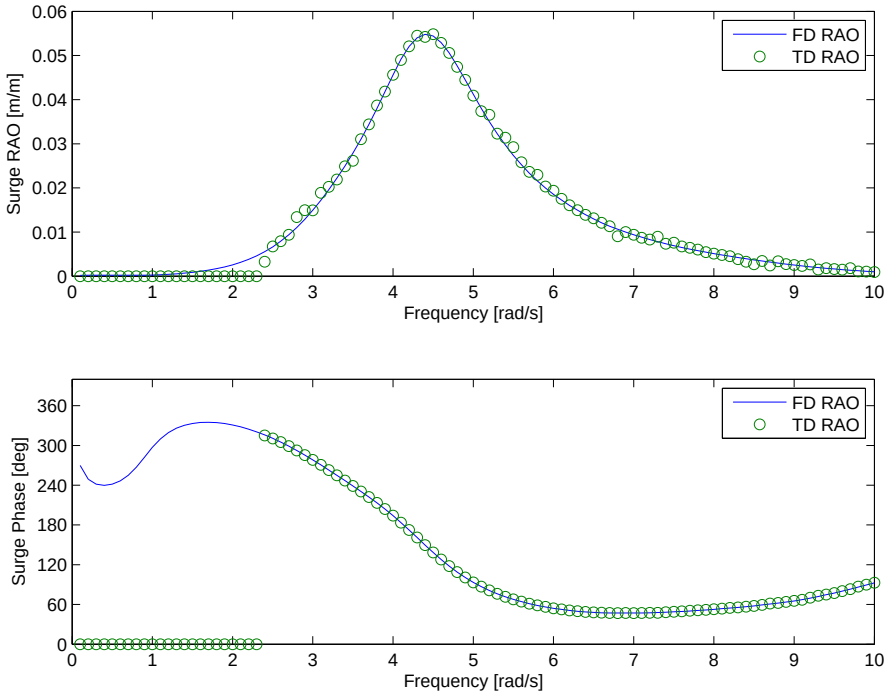

Figure F.1: Surge RAO reconstruction of the HydroStar results in the time domain.

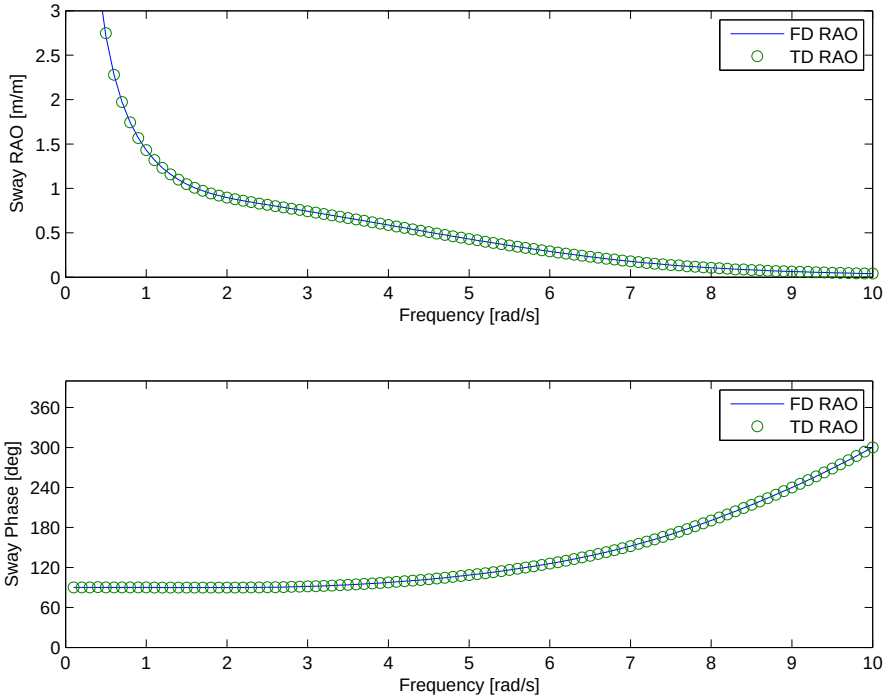

Figure F.2: Sway RAO reconstruction of the HydroStar results in the time domain.

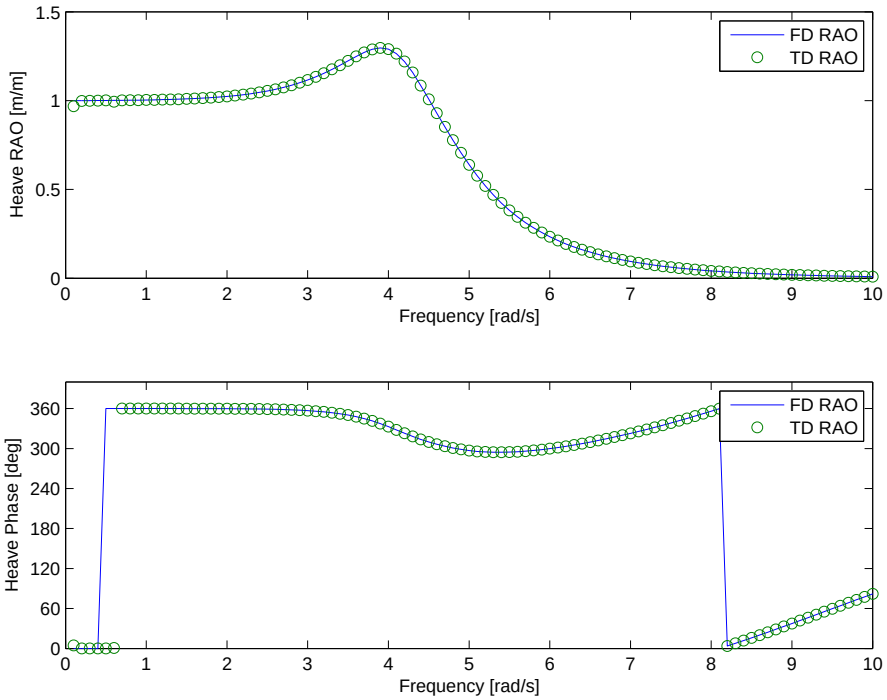

Figure F.3: Heave RAO reconstruction of the HydroStar results in the time domain.

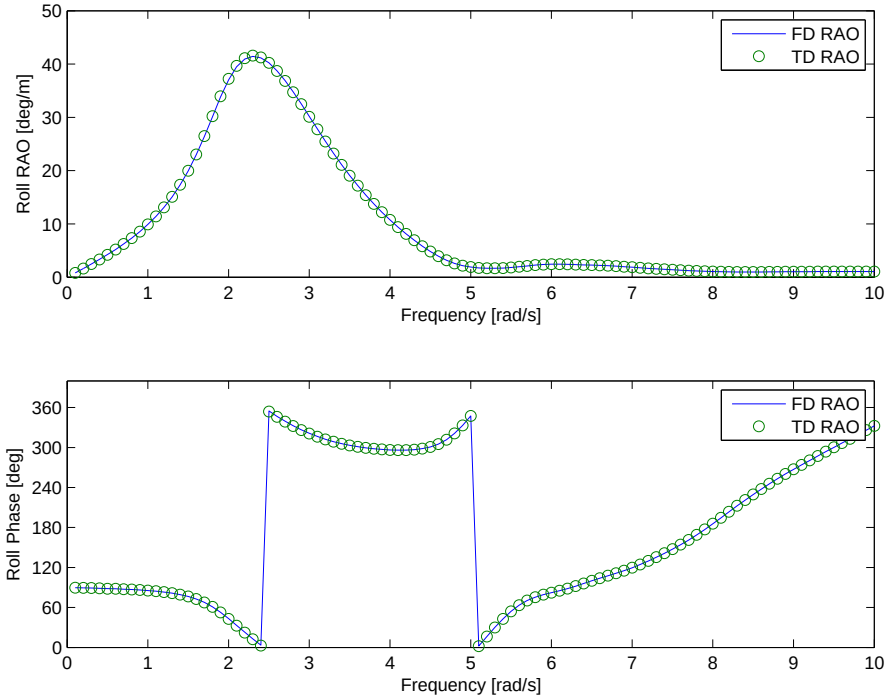

Figure F.4: Roll RAO reconstruction of the HydroStar results in the time domain.

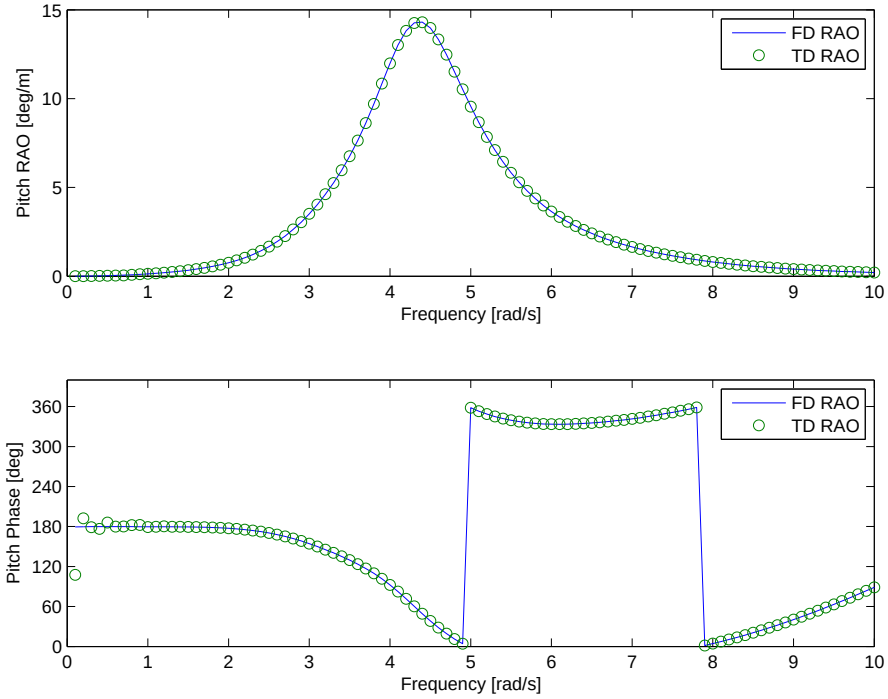

Figure F.5: Pitch RAO reconstruction of the HydroStar results in the time domain.

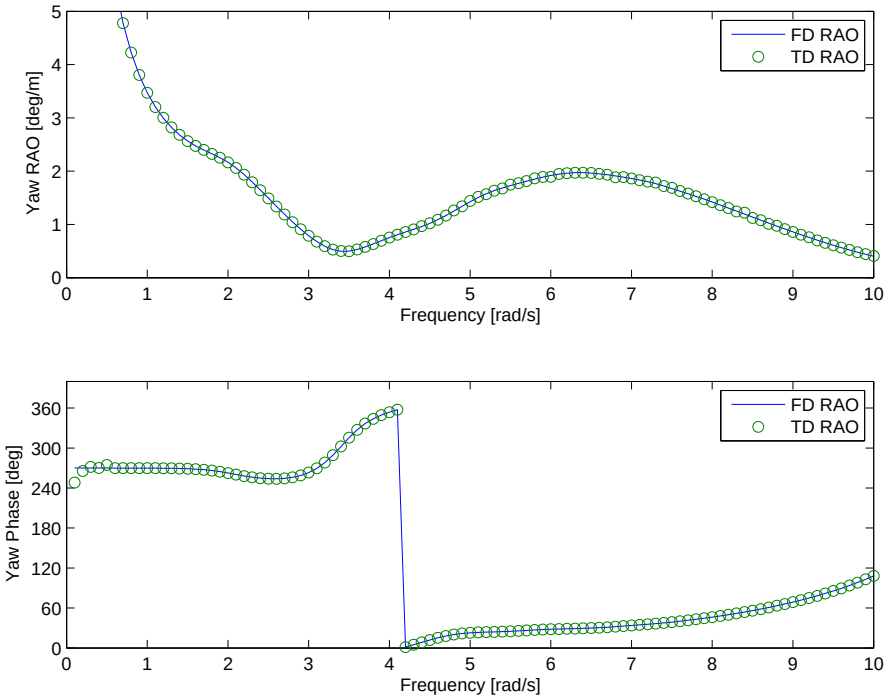

Figure F.6: Yaw RAO reconstruction of the HydroStar results in the time domain.

F.2. LOCAL VELOCITY RAO RECONSTRUCTION VERIFICATION

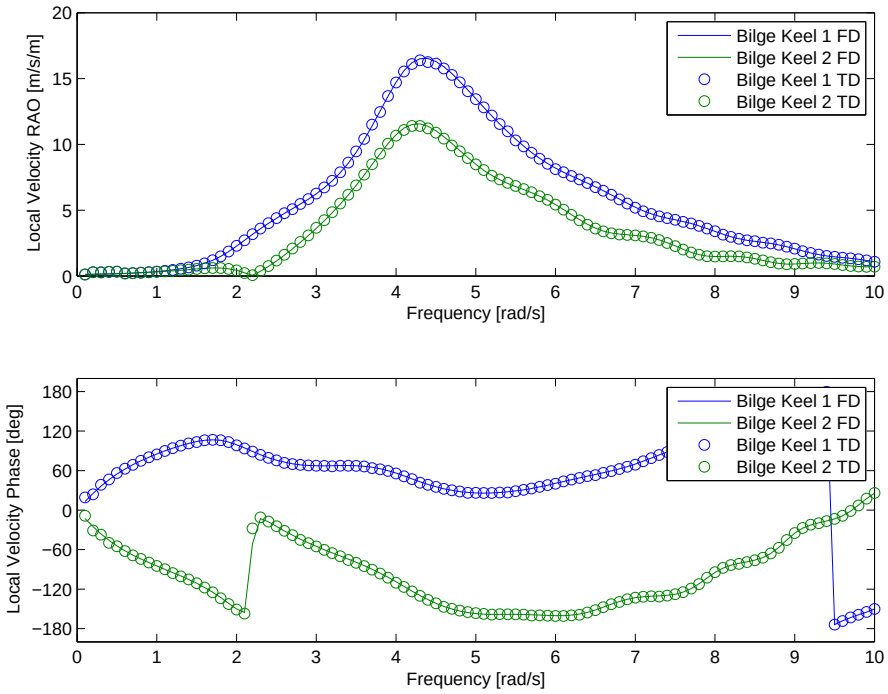

Figure F.7: Local velocity RAO reconstruction of the HydroStar results in the time domain.

F.3. RETARDATION VALIDATION

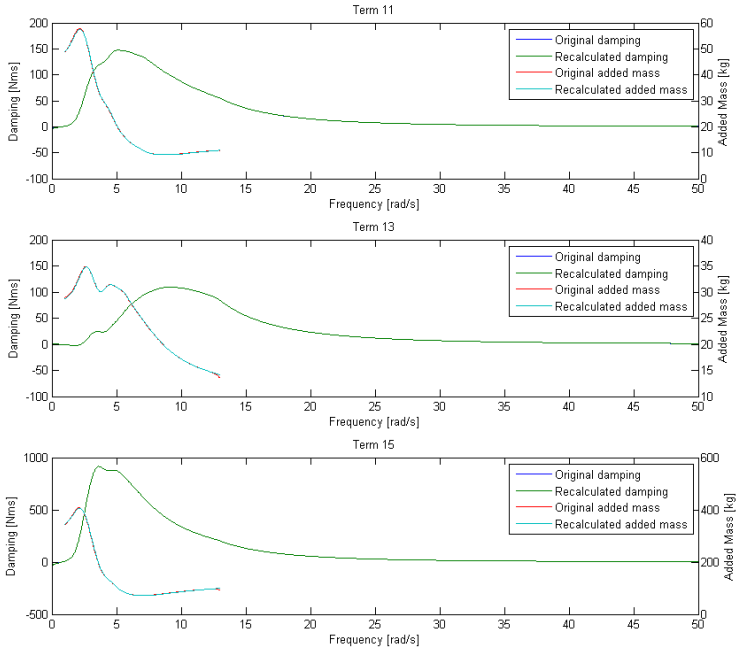

Figure F.8: Surge retardation functions

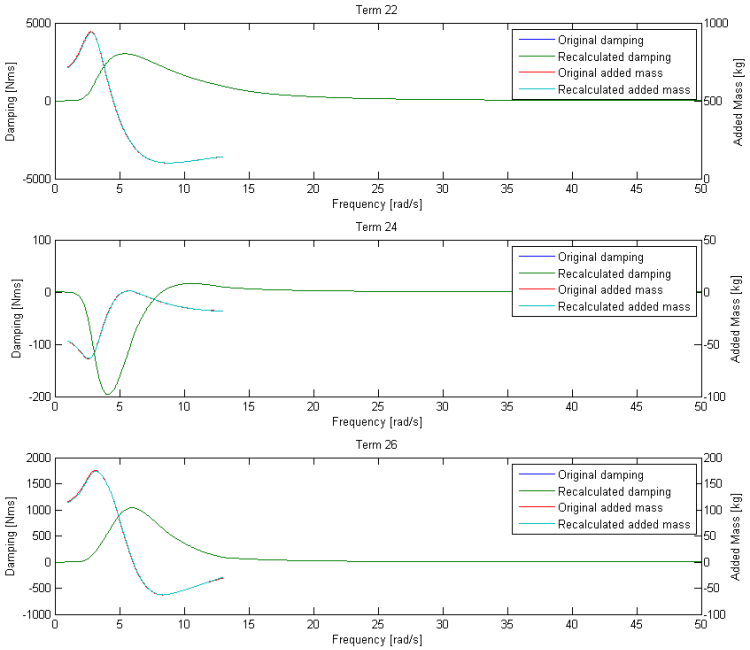

Figure F.9: Sway retardation functions

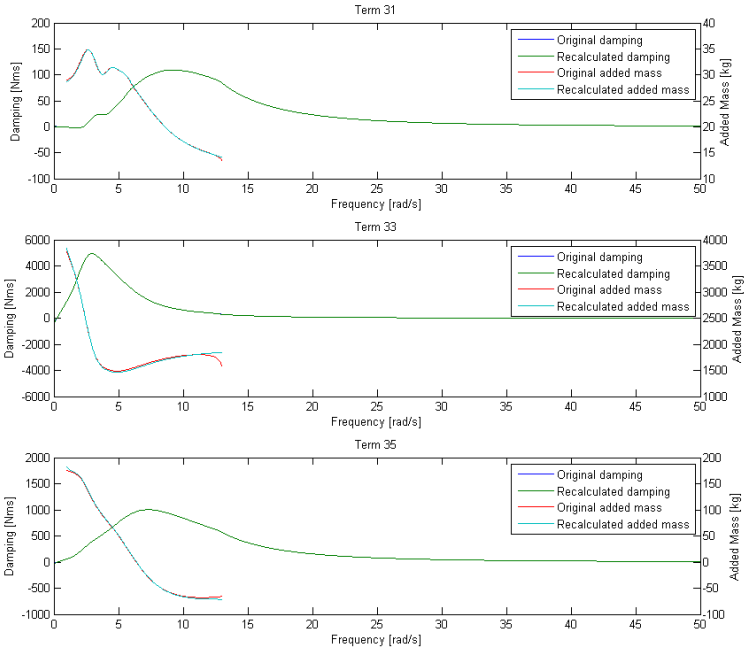

Figure F.10: Heave retardation functions

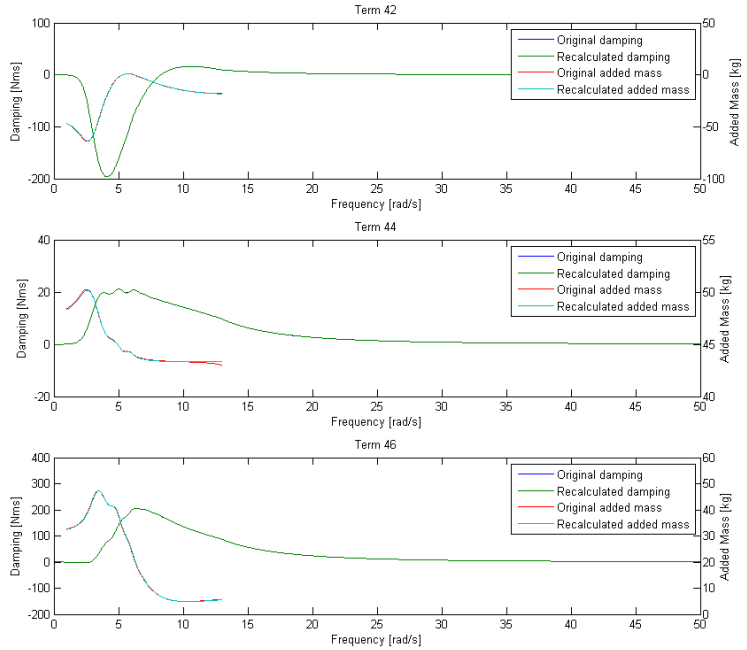

Figure F.11: Roll retardation functions

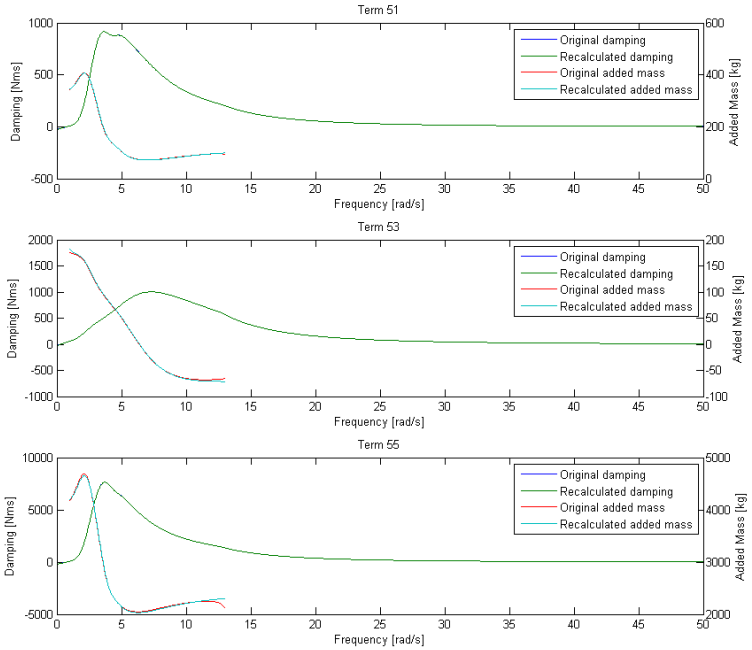

Figure F.12: Pitch retardation functions

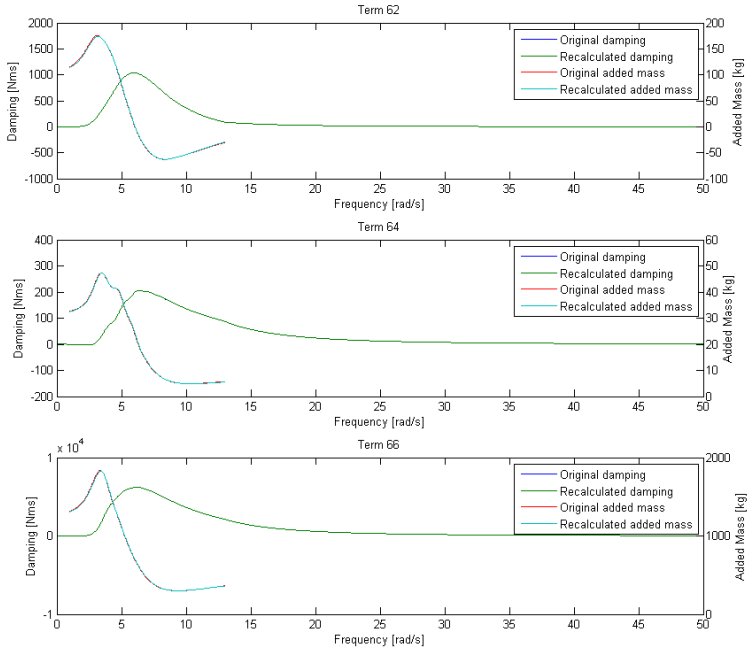

Figure F.13: Yaw retardation functions

G

Extended Abstract

Abstract

This thesis aims to provide a practical method to evaluate the roll damping and motions of an FPSO with aberrant bilge keels and/or riser balconies in waves. For this goal a literature review was performed after which it was concluded that the widely used ITH method could be modified to achieve this goal. The coefficients used in the ITH method are obtained from a forced roll oscillation 2D URANS SST CFD model, including the additional Out-Of-Phase (OOP) terms and using radiated wave velocities from linear potential theory instead of an empirical correction factor. The obtained coefficients are then used in conjunction with flow velocities obtained from linear potential flow theory, including radiated, diffracted and incoming wave velocities, to construct a time domain model. This model was compared to forced oscillation and regular wave experiments of the model scale Glas Dowr FPSO. Forced oscillations were reproduced satisfactory after a correction for additional heave and sway motions was applied. Regular wave results were compared to (a) measured roll angels, (b) simulations using damping coefficients obtained from experiments, (c) ITH method coefficients, (d) local velocity-based ITH method coefficients and (e) using the proposed methodology. Results were good when compared to simulations based on measured damping coefficients but inconclusive when compared directly to measured roll amplitudes. Reasonable agreement compared to simulations with damping coefficients obtained from experiments was obtained at low to medium wave amplitudes and an underestimation was obtained at high wave amplitudes. The underestimation at high amplitudes is faulted to the linear increasing hull pressure coefficient while it is more likely to become saturated at higher local velocities. It is concluded that the combination of CFD and local velocities yield promising results and is more flexible than the traditional ITH method. A more thorough validation should be performed against data at various frequencies, hulls, keels and wave amplitudes before application becomes feasible.

Introduction

Bilge keels are recognized as one of the most efficient measures to mitigate roll damping. Traditionally bilge keels dimensions were minimized to reduced drag for a vessel under power. With the advent of the Floating Production Storage and Offloading (FPSO) vessels larger bilge keels and riser balconies were introduced. The applicability of established methodologies became questionable in this application. In light of these developments the objective of this thesis is to:

"Develop a method to estimate roll motions/roll damping of an FPSO-like vessel in waves with aberrant bilge keels and/or riser balconies in a time-frame befitting a tender and design stage, i.e. two to four weeks. "

Conventional bilge keels and hull shapes allow their roll damping to be predicted by the method developed by Ikeda, Tanaka and Himeno around 1980. The semi-empirical method is based on a series of experiments on scaled cargo and fishing vessels. The Ikeda-Tanaka-Himeno Method (ITH method) for bilge keel damping is based on the notion that the relevant damping can be separated in seven components:

- friction damping,
- eddy damping,
- lift damping,
- wave damping,
- normal-force bilge keel damping,
- hull-pressure bilge keel damping, and
- wave-pressure bilge keel damping.

While the friction damping is quite small, lift damping is nonexistent in a vessel without forward speed the other components are all relevant. In the ITH method the normal-force damping is assumed to behave as a Morisonesque equation multiplied with an arm l while neglecting the inertial term:

$$M_{bk}(t) = l\frac{1}{2}\rho A_{bk} C_D U(t)|U(t)| \tag{G.1}$$

with l being the arm of the moment, ρ density, A_{bk} the surface area of the keel and U the relative water velocity at the bilge keel. A few assumptions are then made: from experiments C_D is assumed to have a correlation with the Keulegan-Carpenter number and U is assumed to be equal to the rigid body velocity times a correction factor f to account for free surface and geometry effects. Combined with a regular motion this results in the velocity being equal to

$$U(t) = f l X_4 \omega cos(\omega t) \tag{G.2}$$

with f being a correction factor, X_n the amplitude of the motion in the n-th direction and ω the oscillation frequency. The hull-pressure moment is treated in a similar manner with the pressure defined as:

$$P(t) = \frac{1}{2}\rho C_p U(t)|U(t)| \tag{G.3}$$

Rewriting and integrating over the hull surface equals to

$$M_{hp}(t) = \frac{1}{2}\rho \int_S C_P l_m dS U(t)|U(t)| \tag{G.4}$$

with l_m the moment lever and S the hull surface. Here C_P is again obtained from experiments lending the method its empirical nature. While the general foundations of the ITH method is sound there are some limitations that need to be grasped and where necessary addressed.

- Memory effects are not included.
- All moments are assumed to be in phase with the velocity and thus roll motion.
- Velocities are based on the rigid body roll motion, not actual local velocities due to waves or other motions.
- Free-surface effects are incorporated crudely.
- The semi-empirical nature in itself, limiting the range of application to certain selected scenarios.

Memory effects are a results of the history of the flow, i.e. a sudden change in amplitude will results in higher or lower moments than predicted in a steady state. Although memory effects are proven to be present the size of their contribution and the effort to implement them results in them often being neglected. The impact of the out-of-phase components on the damping is not directly evident, but as other velocities, for example due to other motions or waves, are introduced relevance for damping arises. This immediately leads to the second point. In the ITH method roll damping is assumed to be dependent on only the roll amplitude and frequency while the foundations are based on actual loca velocities the bilge keel experiences. While this is acceptable when the vessel is forcibly excited in only roll, as soon as other motions and wave velocities come into play this assumption is no longer valid, especially for more asymmetric configurations and aberrant shapes. These asymmetric configurations and aberrant shapes are furthermore not compatible with the current methodology due to its empirical and symmetric nature.

Methodology

From a literature review a path was formulated to potentially address the issues of predicting roll damping of vessels with aberrant bilge keels and/or riser balconies in waves. The basic premise is that the empirical coefficients used in the ITH method cannot be applied to a more general situation. It is furthermore recognized that especially the hull pressure cannot be properly described analytically and is furthermore hard to parameterize without requiring a stupendous amount of expensive and time-consuming experiments.

The proposed solution for this issue is the application of Computational Fluid Dynamics (CFD). CFD has the advantage of allowing any combination of bilge keel and hull shape to be simulated. One of the disadvantages of CFD is the old engineering dilemma of time versus accuracy. It is possible to simulate the motions of a vessel in all DoF and in 3D, including waves, using CFD, but this would result in a exceedingly complex simulation and impractical computational time-spans. This is why the problem is simplified in a manner similar to the strip theory. The problem is reduced to 2D slices of the vessel, where the relevant slices are simulated in one DoF undergoing forced oscillations in roll with a certain amplitude and frequency. This allows the desired coefficients to be obtained in a relatively short period of time as the simulation is quite simple.

The need to base a methodology around local velocities, incorporating waves as well as velocities due to other motions, is also recognized. Ir-rotational, non-viscous velocities in waves can be obtained using linear potential theory and superposition. The local velocities are divided into four separate components:

- rigid body velocities,
- radiated wave velocities,
- incoming wave velocities, and
- diffracted wave velocities.

Here the rigid and radiated velocities can be calculated depending on the six rigid body motions. The incoming and diffracted wave velocities are assumed to be independent of motion. The general assumption that is made here is that the velocities obtained from linear potential theory can be used to estimate the velocities 'felt' by the tip of the bilge keel. If the velocities are assumed to be known, the same applies to accelerations, allowing the use of the full Morison equation and pressure coefficients, resulting in the following equations:

$$M_{hp}(t) = B_{hp}U(t) + A_{hp}\dot{U}(t), \tag{G.5a}$$

$$M_{bk}(t) = \frac{1}{2}\rho A C_D U(t)|U(t)| + \rho V C_M \dot{U}(t). \tag{G.5b}$$

The basic differences between the ITH method and the proposed methodology are summarized in Table G.1.

Item	ITH method	Proposed method
Free surface influence	Velocity correction factor f	Radiated wave correction factor from potential theory
Wave velocities	Not included	Incoming and diffracted velocities
Other motions	Not included	Velocities from other motions included
OOP component	Not included	Full Morison equation and OOP hull pressure
Hull pressure	Determined semi-empirically	Coefficients w.r.t. local velocity and acceleration from CFD

Table G.1: Key differences between the ITH method and the proposed method

CFD Set-Up

A crucial part of the methodology is the design and reliability of the CFD model. The first consideration to be made here is the selection of an appropriate CFD approach. From literature it becomes apparent that methods such as Detached Eddy Simulation (DES) and Large Eddy Simulation (LES) are preferred, as they actually simulate the relevant eddies without resorting to modeling. Unfortunately computational efforts required by such methods are not economical in this particular situation. This leaves the well known Unsteady

Reynolds-Averaged Navier-Stokes (URANS) method with a turbulence model and Lagrangian methods such as the Direct Vortex Method (DVM).

While DVM seems very suited to this particular problem, with a clearly defined stagnation point, coupling with potential theory and the importance of vortices it has some disadvantages. Key disadvantages are the computational time depending on the amount of convected vortices, as it is in essence a n-body problem of complexity $O(N_p ln(N_p))$ (with the FMM). The DVM is furthermore less applied and generally not incorporated in commercial software, except for for example VorCat which only allows 3D applications, increasing computational demands.

The URANS model is widely used and more often applied on similar problems. Furthermore the sponsor of this thesis, SBM Offshore, has developed a general use interface for STAR-CCM+ for its engineers, relying on URANS with the SST turbulence model. From literature it is concluded that the SST and Realizable $\kappa-\epsilon$ model are best suited for this problem. The choice has thus been made to be pragmatic and employ the existing more general and widely accepted model in favor of the DVM. The model particulars can be found in Table G.2. For more information and theory on URANS and the various turbulence models, the DVM and other methods, as well as more basis for the decision made, reference is made to the literature review [1].

Item	Setting
Model	RANS
Turbulence	SST
Mesh	Automated adaptive meshing
Free-surface	VoF
Interface tracking	HRIC
Time discretization	Implicit 2^{nd} order
Space discretization	2^{nd} order
Solver type	Segregated
Timestep	Courant number < 0.5

Table G.2: Key CFD parameters

From the pressures and forces obtained from CFD the relevant coefficients need to be extracted. As the proposed methodology is seated on the premise of local velocities obtained from linear potential theory the local velocities used for determining the velocities are also derived from linear potential theory. When a forced oscillation in roll in calm water is considered the velocities as obtained from linear potential theory are:

$$U_{rig} = l\omega X_4 cos(\omega t), \tag{G.6a}$$

$$\begin{aligned} U_{rad} = {} & sin(\alpha_b k)\left|\frac{U_{rad,y}}{\omega X_4}\right|\omega X_4 cos(\omega t+\phi_Y) \\ & + cos(\alpha_b k)\left|\frac{U_{rad,z}}{\omega X_4}\right|\omega X_4 cos(\omega t+\phi_Z), \end{aligned} \tag{G.6b}$$

$$U = U_{rig} + U_{rad}, \tag{G.6c}$$

where $\left|\frac{X}{Y}\right|$ is the radiated velocity Response Amplitude Operator (RAO) and ϕ the phase difference w.r.t the rigid body velocity.

BILGE KEEL NORMAL FORCE COEFFICIENTS

The bilge keel force coefficients C_D and C_M coefficients for use in the Morison equation are obtained using Fourier analysis as described by Keulegan and Carpenter [69] based on the Morison equation including higher harmonics:

$$A_n = \frac{2}{T}\int_T \frac{2F(t)sin(n\omega t+\phi)}{\rho h w U_m^2} dt, \tag{G.7a}$$

$$B_n = \frac{2}{T}\int_T \frac{2F(t)cos(n\omega t+\phi)}{\rho h w U_m^2} dt, \tag{G.7b}$$

and

$$C_D = \frac{3\pi}{8} B_1, \tag{G.8a}$$

$$C_M = -\frac{KC}{\pi^2} A_1. \tag{G.8b}$$

Here F is the time trace of one or multiple oscillations of the keel force and T one or an integer number of periods.

Hull pressure coefficients

The hull pressure coefficients are obtained by fitting Equation G.5a using a linear least-squares method to the time-trace of the moment exerted by the hull pressures due to the presence of the bilge keel, which is:

$$M_{hp,m}(t) = \int_S p(t,S) l_m(S) dS - M_{rad}(t). \tag{G.9}$$

Here p are the pressures measured at position S on the hull and where B_h and A_h are the hull pressure coefficients. M_{rad} is the moment due to radiated waves from the hull.

Verification and validation

As a commercial code is used code verification is assumed to be unnecessary. The only verification that was performed for this thesis was a mesh convergence study for which the results were considered satisfactory. The validation is performed using experiments done by X. Schut for SBM Offshore. The experiments constituted of the one DoF forced oscillations in roll of a long cylinder with end plates in calm water at various amplitudes, frequencies, bilge keels and drafts. Due to the length of the cylinder and end plates a semi-2D situation is created. Furthermore by choosing a cylinder shape, radiated wave velocities are zero, eliminating the possibility of errors in the potential theory. Validation is performed through the comparison of C_D, C_M and hull pressure coefficients. The C_D and C_M coefficients are well predicted as expected. The hull pressure coefficients are slightly overestimated which was expected due to errors in the measurements. The hull pressure coefficients were obtained by projecting the results of the circular hull onto a rectangular hull to generate a virtual moment. This is done to emphasize the importance of pressures at the bilge compared to pressures further from the bilge which have a shorter moment lever and thus less relevance.

Implementation

The implementation of the proposed methodology can be done in a variety of manners where a distinction is made between the frequency domain and time domain, forced oscillations, regular waves and irregular waves. Three methods will be discussed, in the time domain forced oscillations and regular waves, as well as irregular waves in time domain and irregular waves in the frequency domain. The focus is on the time-domain simulations due to the non-linear nature of the system.

The basic governing equation for a harmonic motion is a second order Ordinary Differential Equation (ODE) in the form of

$$(\boldsymbol{M} + \boldsymbol{A}(\omega))\ddot{\vec{x}}(t) + \boldsymbol{B}(\omega)\dot{\vec{x}}(t) + \boldsymbol{C}\vec{x}(t) = \vec{F}_e(t,\omega), \tag{G.10}$$

where M, A, B and C are the 6x6 matrices of the mass, added mass, damping and hydrostatic coefficients obtained from Bureau Veritas (BV) software HydroStar which is based on linear potential theory. x and $F_e(t)$ are both six element vectors where x are the rigid body motions and F_e the exciting forces. A change is made in the fourth DoF, where the roll motion ODE becomes

$$(M + A(\omega))\ddot{x}_4(t) + B(\omega)\dot{x}_4(t) + Cx_4(t) = F_4(t,\omega) - M_{bk}(t,\omega) - M_{hp}(t,\omega) \tag{G.11}$$

with M_{bk} and M_{hp} as defined in equations G.5a and G.5b. The leaves the issue of selecting the appropriate coefficients and velocities. Global velocities are obtained using rigid body motions, coefficients from radiation and diffraction calculations and the undisturbed wave velocities, reference is made to the Appendix for detailed descriptions. The coefficient database is obtained from the CFD and the correct coefficients are selected from the determined velocity and period. In regular waves the velocity period and amplitude is readily obtained, in irregular wave half-periods are utilized which are defined as twice the time between two zero-crossings with the amplitude as the absolute maximum between two zero-crossings.

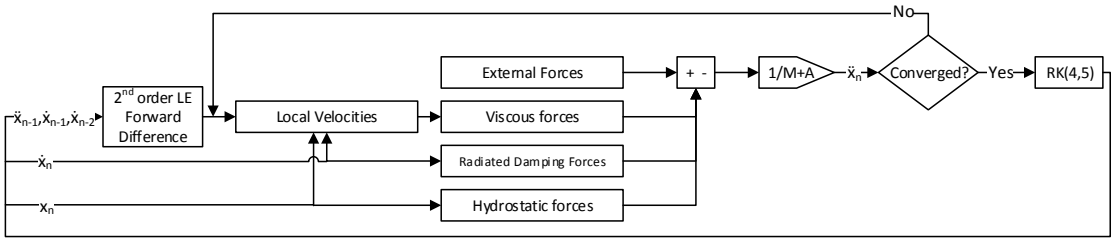

Figure G.1: Diagram of the implemented differential equation.

FORCED OSCILLATIONS AND REGULAR WAVES

As harmonic excitation results in a response at the same frequency, the frequency of the system is known in forced oscillation and regular wave oscillation, allowing direct use of coefficients obtained from linear potential theory and allowing no compromises to be made for local velocity amplitudes and periods. A MATLAB code is written using a slightly modified ODE45 solver, based on the Runge-Kutta(4,5) algorithm. The second order ODE is simplified to two first order ODEs as

$$y_1 = x_n, \tag{G.12a}$$
$$y_2 = \dot{x}_n, \tag{G.12b}$$
$$dy_1 = y_2, \tag{G.12c}$$
$$dy_2 = f(x_n, \dot{x}_n, \dot{x}_{n-1}, \dot{x}_{n-2}, \ddot{x}_{n-1}, t_n, t_{n-1}, t_{n-2}). \tag{G.12d}$$

A schematic overview of the implementation can be found in Figure G.1. Besides the internal loop in the RK(4,5) solver for each time-step and the loop for the accelerations in each time-step, another loop is present over the entire system to allow the selection of the proper hull pressure and keel force coefficients based on the local velocity amplitude and frequency. The convergence criteria is the Keulegan-Carpenter number, i.e. local velocity amplitude and period for each keel.

IRREGULAR WAVES

In irregular waves three problems arise: the determination of the local velocity amplitude and period, the implementation of the coefficients obtained from the potential theory and the relevance of higher harmonics. The local velocity amplitude and period can be determined using three methods:

- using the maximum velocity and time between to consecutive zero-crossings [15];
- using FFTs to select the dominant frequency and amplitude in the velocity time trace [71]; and
- using an a-posteriori approach where a representative amplitude and period are chosen after one run has been completed and thus assuming that impact of a constant KC-number is small during a simulation.

The first method is preferred as it is the most representative, but it does require an additional loop over each zero-crossing, resulting in a substantial amount of iterations. The second option is computationally intensive and is incapable of handling fast changes of the amplitude and period as a time-delay is introduced, but is robust and does not require an iterative procedure. The last option is quite fast, but rest upon an assumption of which the impact is not evaluated.

The radiated velocity and force coefficients are frequency dependent and are thus represented in the time domain as convolution integrals as described by Cummins [19] and Ogilvie [70]. These integrals can also be approximated by higher derivatives and thus a state-space model.

In irregular waves higher harmonics can play a role in damping, their influence is evaluated by evaluating the energy removed which is a measure for damping as follows:

$$P = \int \frac{M\dot{x}_4}{T} dt \tag{G.13}$$

and filling in a harmonic motion and moment

$$\frac{\omega}{2\pi}\int_0^{\frac{2\pi}{\omega}} \underbrace{Bsin(\Omega t+\phi)}_{\text{Moment}}\underbrace{X_4(\omega)\omega sin(\omega t)}_{\text{Roll velocity}}\,dt = BX_4(\omega)\frac{\omega^2\left(sin(\phi(\omega))-sin(2\pi\frac{\Omega}{\omega}+\phi)\right)}{(\omega-\Omega)(\omega+\Omega)}. \tag{G.14}$$

with P being the power, or energy removed, M the moment, B a measure of the damping and Ω the frequency of the moment. Equation G.14 is evaluated numerically using Wolfram Alpha. Integrating the above equation over dω would results in the total energy removed. Examination shows that there is a normalized envelope, independent of phase, present of

$$\pm\frac{\omega^3}{\pi}\frac{sin\left(\pi\frac{\Omega}{\omega}\right)}{(\omega+\Omega)(\omega-\Omega)}. \tag{G.15}$$

Considering this envelope, the small size of B for higher harmonics, the relatively small motions at frequencies other than the natural frequencies and a narrow banded excitation spectrum it is assumed that higher harmonics can be neglected when calculating ship motions.

Frequency Domain

As a practical engineering solution the frequency domain is often preferred for ship motions over the time domain due to the speed for which responses can be calculated for various sea-states and fast estimation of design parameters such as the MPM roll motion. To apply the proposed methodology to the frequency domain various issues have to be addressed. The non-linearity in the proposed methodology cannot be evaluated in the frequency domain and as such linearization using methodologies such as stochastic linearization [81] and the Linearize, Match and Iterate (LMI) method [36]. Another issue is how to obtain proper damping and added mass coefficients, as the methodology relies on local velocities, thus introducing phase differences and non-constant coefficients. To address these issues careful study of irregular wave time-domain simulations is recommended. This is outside the scope of this thesis.

Results

Three types of results are presented:

- the hull pressure and keel force coefficients as obtained from the CFD simulations as used for implementation in the time domain simulations;
- the roll amplitudes as obtained from time domain simulations using the proposed methodology for forced oscillations of a vessel in calm water, compared to roll amplitudes as measured during experiments; and
- the roll amplitudes as obtained from time domain simulations using the proposed methodology for regular wave excitation (including wave-induced velocities) of a vessel, compared to roll amplitudes as measured during experiments, as simulated using damping coefficients obtained from the experiments, as simulated using the ITH method but including actual local velocities and as simulated using the traditional ITH method based on global motions.

Irregular wave simulations and frequency domain simulations are not performed. The experimental results to which the simulated results are compared to are obtained from the Roll JIP as performed by MARIN in 2006.

CFD

The results from the CFD in the form of the coefficients as used in the time domain simulations can be viewed in Figures G.2, G.3 and G.4. In Figure G.2 the keel force coefficients are presented. The results are as expected and quite close to the Ikeda formulation with expected deviations as observed by van 't Veer [25]. The C_M values show a slight sensitivity to frequency which is in line with performed experiments. In Figures G.3 and G.4 the hull pressure coefficients in-phase and out-of-phase with the local velocities are presented for positive and negative velocities past the keel. It should be noted that as the CFD results started to show unwanted oscillations at higher frequencies due to the sliding interface, as such the simulations were limited a maximum amplitude of ten degrees. Thus a similar linear dependency as observed at lower amplitudes was assumed for higher amplitudes allowing for extrapolation.

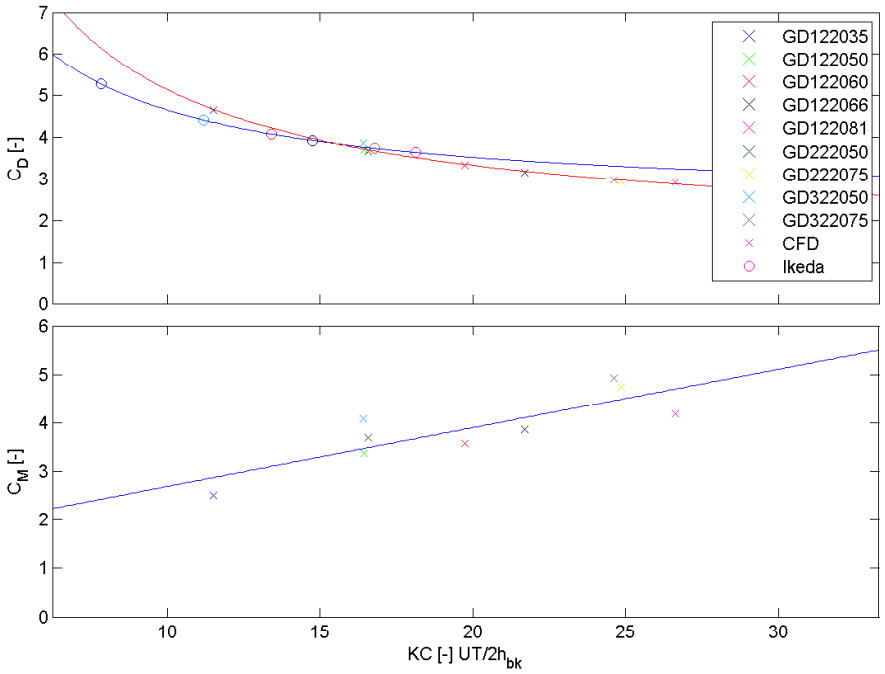

Figure G.2: C_D and C_M coefficients as obtained from CFD including fitted lines.

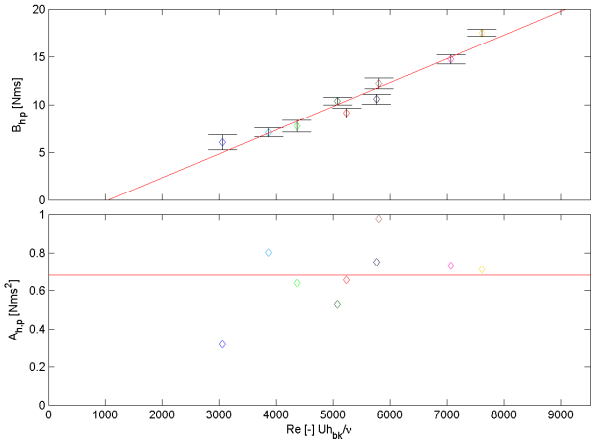

Figure G.3: Positive hull pressure coefficients as obtained from CFD including fitted lines, the legend is the same as Figure G.2.

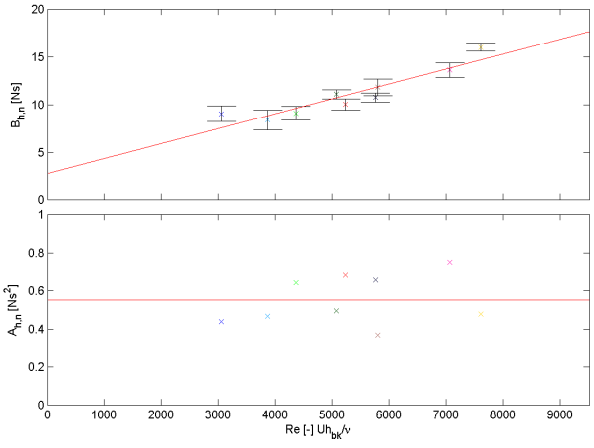

Figure G.4: Negative hull pressure coefficients as obtained from CFD including fitting lines, the legend is the same as Figure G.2.

Forced Oscillation Simulations

Forced oscillation time domain simulation results are corrected to account for a ten percent velocity increase due to the measured sway and heave motions being larger than the simulated motions. This has an impact on the local velocities and thus damping. Results are presented in Table G.3. Good agreement is observed for small to reasonably large amplitudes. A discrepancy is noted at higher amplitudes. This is most likely due to extrapolation from the CFD results as these are most likely not valid anymore for these amplitudes as the hull pressure moment becomes saturated at higher velocities.

Measured [°]	Simulated [°]	Error [%]	KC [-]
4.4	4.8	9	13.4
6.6	6.8	3	18.9
8.1	8.4	4	22.6
11.7	11.9	2	33.2
13.5	13.3	-1	37.1
17.4	15.8	-9	44.0
19.0	17.1	-10	47.7

Table G.3: Results from forced oscillations

Regular Waves

As the regular wave experiments were performed at only one frequency, and a frequency close to the natural frequency but not at the natural frequency correct comparison is hard. Furthermore an unexpectedly large discrepancy is observed between measured and simulated values. To counter this unexpected results the response is reconstructed using the damping coefficients obtained from the experiments and then compared to the proposed methodology, the ITH method and the ITH method based on local velocities. Reference is made to Figure G.5 for plotted results and Table G.4 for predicted peak amplitudes, measured values are not peak amplitudes but at 0.43 [rad/s]. In Figure G.6 a comparison of bilge keel loads as measured, as simulated using the CFD coefficients and local velocities and as predicted by the traditional ITH method. The forcing moment in the roll DoF is adjusted to allow for the same roll angle as measured without compromising the other motions which were predicted correctly. The agreement is quite good considering that the higher harmonics and 3D effects are neglected.

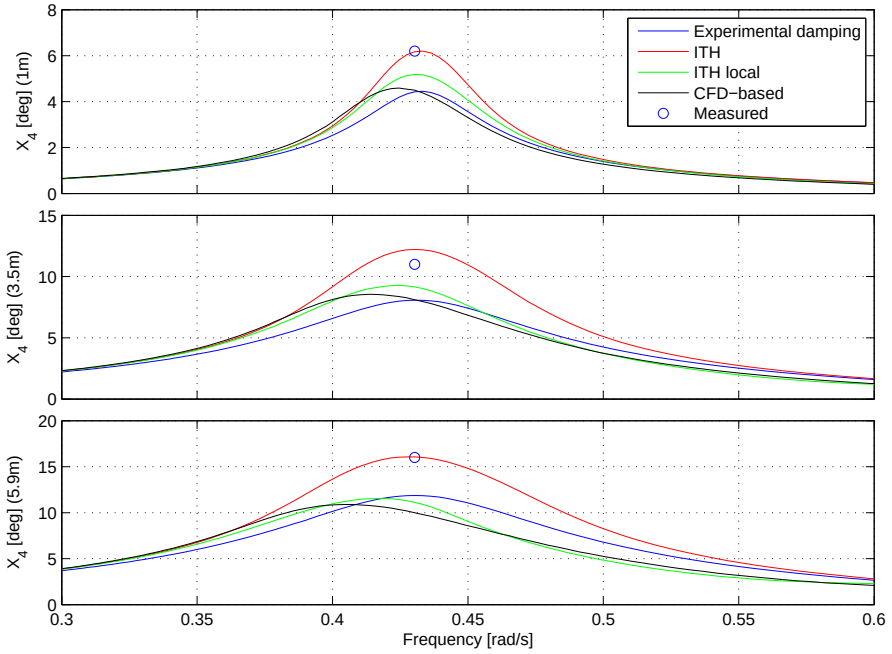

Figure G.5: Various amplitude plots for a 1, 3.5 and 5.9 meter amplitude incoming wave.

Wave amplitude [m]	Measured [°]	Experiment-based [°]	CFD-based [°]	ITH local [°]	ITH global [°]
1.0	6.2	4.5	4.6	5.2	6.2
3.5	11.0	8.1	8.5	9.3	12.2
5.9	16.0	11.9	10.8	11.5	16.1

Table G.4: Maximum roll amplitude in waves.

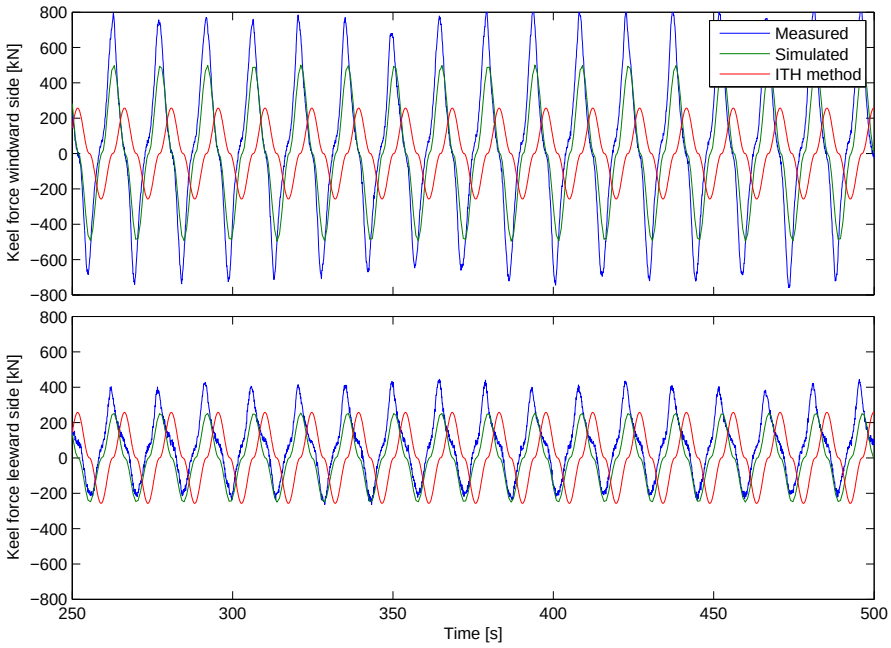

Figure G.6: Predicted bilge keel loads in waves with adjusted forcing moment in roll.

DISCUSSION

While the forced oscillations are reasonably well predicted except at higher amplitudes, the regular wave simulation do not predict the measured experimental results well. A large underestimation of the roll amplitude is present. When simulating with the roll damping coefficients obtained from the experiments a similar underestimation compared to the actual measured amplitude is found.

The source for this is not clear. As the time domain code is validated two possible sources remain: the HydroStar input/output or in the reporting/results of the experiments. HydroStar is a widely used package and is considered verified and validated. Linear potential theory is also widely used and wave forces are assumed to be properly predicted. Especially as other motions such as heave are correctly predicted. The input to HydroStar, i.e. the mesh, water-depth, water density and gravity are all checked and compared to independently created input by R. van 't Veer and results are found to be within less than 1% of each other. Model test and reporting errors are hard to quantify ten years after the tests and the model tests were furthermore performed by professionals with a great deal of experience. Thus the source of this error is not yet found.

If the simulations with the experimentally obtained damping are used as a reference the various methods perform as expected. The traditional ITH method produced by HydroStar shows a severe underestimation of the damping and as such a very conservative estimate. This is expected due to the neglect of local velocities. The ITH method based on local velocities performs much better which makes sense as damping is increased due to the additional incorporated velocities. The CFD-based methodology seems to perform even better with peak amplitudes close to the predicted value and an expected shift of the peak response. Performance in the highest wave degrades for the CFD-based method, as well as the ITH method based on local velocities. KC numbers will run well into a range over fifty and up to ninety. This explains the better estimate by the modified ITH method method as the C_P value drops at high KC numbers, reference is made to Figure G.7. This while the results from the CFD are proportional to the local and thus local velocity amplitude. It does

not reach the same 'barrier' as the C_P. As the ITH method is not based on these high KC number such as these it also enters a range of uncertainty. The results are thus in line with what was expected from the forced oscillations.

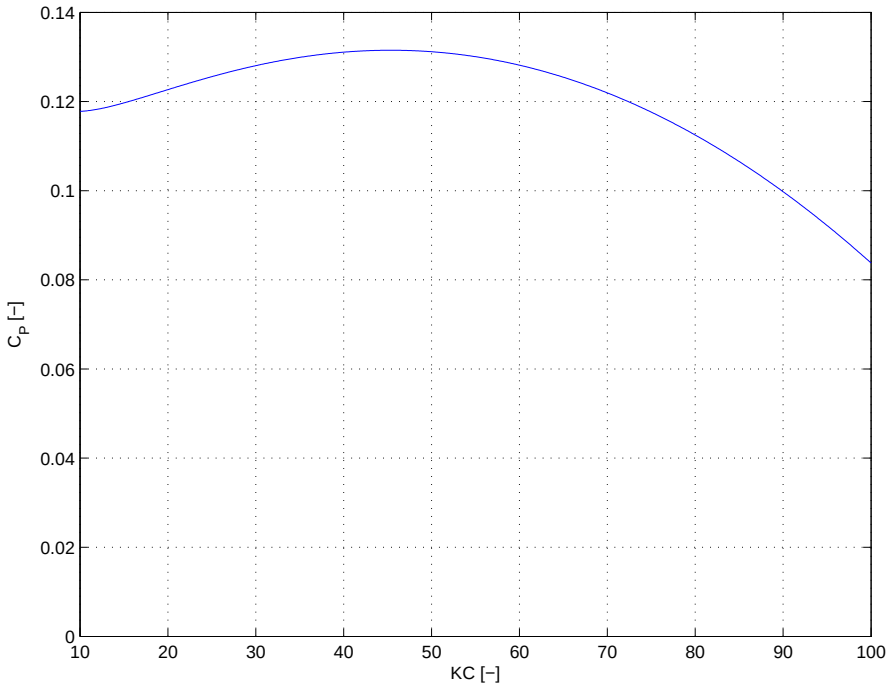

Figure G.7: The C_P coefficients as by the ITH method of the Glas Dowr FPSO plotted versus the KC number.

Conclusion and Recommendations

The proposed methodology utilizes combination similar to the well-known section theory, the ITH method of separating bilge keel damping components and CFD. From 2D forced roll oscillation CFD simulations hull pressure and bilge keel normal force coefficients with respect to local velocities are obtained. These are then utilized in time-domain simulations, including water velocities due to the rigid body motions, radiated, diffracted and incoming waves. The results are then compared to forced oscillations and regular wave experiments performed during the Roll JIP in 2006.

From the results it can be concluded that the proposed methodology based on local velocities seems a viable approach. It shows a more realistic physical interpretation than current methods and should allow more flexibility when the CFD-based coefficients are used. It allows for simulations without any up front knowledge in the form of experiments, while still allowing results to be obtained within a time-frame of one to two weeks. It shows good agreement with simulations using damping coefficients obtained from experiments. While this seems promising it is strongly emphasized that the validation foundations are not very solid. The model underestimates the actual roll angle as measured by a large margin. The source of this error is not fully understood, as simulations with damping coefficients from experiments show a similar underestimation. There are furthermore only three data points available for comparison in waves, i.e. three wave amplitudes but only one frequency. A sensitivity study shows large sensitivity to local velocities, which was expected, and in a lesser extent to hull pressure coefficients. These coefficients are obtained from the CFD and thus sensitive to the quality of the CFD results.

It is recommended that further validation is performed in irregular waves and for other vessels and bilge keels to gain confidence in such a methodology. It is furthermore recommended to evaluate the hull pressure coefficients at higher velocities to gain an insight into possible saturation. Use of an overset mesh is recommended to avoid errors at the sliding interface. While there is still a lot of work to be done a foundation is built which can be used for further testing.

ACKNOWLEDGMENTS

This thesis was sponsored by SBM Offshore and supported by the TU Delft. The author would like to show great appreciation to Riaan van 't Veer for support throughout the project, Xavier Schut for mental support and discussion and Jean-Luc Pelerin for his CFD model and patient support in further CFD development. Further gratitude is extended to the committee chair Prof.Dr.Ir. R.H.M. Huijsmans and committee members Dr.Ir. I. Akkermans and Dr. A. Romeijn for their valuable insight and evaluation. Another thanks goes out to P. Dahlin from CD-Adapco for allowing me to use a free license for their extensive CFD package STAR-CCM+.

APPENDIX A: VELOCITIES

Rigid body velocities in the global coordinate system are obtained using Equations G.16 and G.18 where x_{bk}, y_{bk} and z_{bk} are the coordinates of the tip of the bilge keel and A and B are the in- and out-of-phase terms of the radiated velocities obtained from HydroStar after transformation. The total relative velocities are obtained through Equation G.19 where diffracted and incoming velocities are readily obtained. The bilge keel normal vector is obtained and corrected for rotations in Equation G.17 after which the magnitude of the total normal vector can readily be obtained. The R_n matrices in Equations G.20a-c are the standard right-hand-rule rotational matrices for use in a Cartesian coordinate system. Accelerations are determined in a similar manner, taking the derivative off all velocity terms. In case of the radiated velocities this results in dependence on the physical less relevant and suspicable to numerical noise term jerk, $\dddot{x}$. A is then reduces to $A_{red} = -A\omega^2$ which reduces the dependence to the first order derivative, velocity.

$$\begin{bmatrix} U_{rig,x} \\ U_{rig,y} \\ U_{rig,z} \end{bmatrix} = \begin{bmatrix} 1 & 0 & 0 & 0 & z_{bk}sin(x_5) & -y_{bk}sin(x_6) \\ 0 & 1 & 0 & -z_{bk}sin(x_4+a) & 0 & x_{bk}cos(x_6) \\ 0 & 0 & 1 & y_{bk}cos(x_4+a) & -x_{bk}cos(x_5) & 0 \end{bmatrix} \begin{bmatrix} \dot{x}_1 \\ \dot{x}_2 \\ \dot{x}_3 \\ \dot{x}_4 \\ \dot{x}_5 \\ \dot{x}_6 \end{bmatrix} \tag{G.16}$$

$$U_{rig} = \begin{bmatrix} 0 & -sin(\alpha_{bk}) & cos(\alpha_{bk}) \end{bmatrix} R_x(x_4)R_y(x_5)R_z(x_6) \begin{bmatrix} U_{rig,x} \\ U_{rig,y} \\ U_{rig,z} \end{bmatrix} \tag{G.17}$$

$$\begin{bmatrix} U_{rad,x} \\ U_{rad,y} \\ U_{rad,z} \end{bmatrix} = \sum_{n=2,3,4} \begin{bmatrix} B_{x,n} & A_{x,n} \\ B_{y,n} & A_{y,n} \\ B_{z,n} & A_{z,n} \end{bmatrix} \begin{bmatrix} \dot{x}_n \\ \ddot{x}_n \end{bmatrix} \tag{G.18}$$

$$U = \begin{bmatrix} 0 & -sin(\alpha_{bk}) & cos(\alpha_{bk}) \end{bmatrix} \begin{bmatrix} U_{rad,x} + U_{diff,x} + U_{inc,x} \\ U_{rad,y} + U_{diff,y} + U_{inc,y} \\ U_{rad,z} + U_{diff,z} + U_{inc,z} \end{bmatrix} + U_{rig} \tag{G.19}$$

$$R_x(x_4) = \begin{bmatrix} 1 & 0 & 0 \\ 0 & cos(x_4) & -sin(x_4) \\ 0 & sin(x_4) & cos(x_4) \end{bmatrix}, \tag{G.20a}$$

$$R_y(x_5) = \begin{bmatrix} cos(x_5) & 0 & sin(x_5) \\ 0 & 1 & 0 \\ -sin(x_5) & 0 & cos(x_5) \end{bmatrix}, \tag{G.20b}$$

$$R_z(x_6) = \begin{bmatrix} cos(x_6) & -sin(x_6) & 0 \\ sin(x_6) & cos(x_6) & 0 \\ 0 & 0 & 1 \end{bmatrix}. \tag{G.20c}$$

BIBLIOGRAPHY

[1] M. van Kampen, *Bilge-keel induced roll damping: Hull pressure - literature review,* (2014).

[2] J. Journée and W. Massie, *Offshore Hydromechanics* (Delft Univerisity of Technology).

[3] Y. Himeno, *Prediction of Ship Roll Damping - State of the Art*, Tech. Rep. (University of Michigan).

[4] Delft University of Technology, *Guide for literature search process,* .

[5] A. van Boeijen and D. U. of Technology Faculty of Industrial Design Engineering, *Delft design guide* (TU Delft, Delft, 2013) p. 165 blz., (NL-LeOCL) 350306427 Studiecollectie 2013-2014.

[6] Y. Ikeda, Y. Himeno, and N. Tanaka, *Ship roll damping - frictional component and normal pressure on bilge keel,* Journal of The Kansai Society of Naval Architects **161** (1976).

[7] Y. Ikeda, K. Komatsu, Y. Himeno, and N. Tanaka, *On roll damping force of ship - effect of hull surface pressure created by bilge keels,* Journal of The Kansai Society of Naval Architects **165** (1977).

[8] R. Seah, F. Bigot, and N. T. D. Roddier, *A comparison of time domain methods for asymmetric roll prediction,* in *33rd International Conference on Ocean, Offshore and Arctic Engineering* (2014).

[9] F. Bigot, R. Seah, and N. T. D. Roddier, *Prediction of asymmetric fpso roll using a frequency domain method,* in *33rd International Conference on Ocean, Offshore and Arctic Engineering* (2014).

[10] T. Katayama, Y. Yoshioka, T. Kakinoki, and Y. Ikeda, *Some topics for estimation of bilge-keel component of roll damping,* in *Proceedings of the* 11^{th} *International Ship Stability Workshop* (2010).

[11] Y. Ikeda, K. Osa, and N. Tanaka, *Viscous forces acting on irrgularly oscillating cicrular cylinders and flat plates,* in *Transactions of the International Symposium on Ocean, Offshore and Arctic Engineering*, Vol. 110 (1988).

[12] A. C. de Oliveira and A. C. Fernandes, *The nonlinear roll damping of a FPSO hull,* Journal of Offshore Mechanics and Arctic Engineering **136** (2014).

[13] R. R. van Dijk, *Comparison of full-scale measurements with calculated motion characteristics of a West of Africa FPSO,* in *Proceedings of OMEA03 22ND International Conference on Offshore Mechanics and Arctic Engineering* (2003).

[14] R. Korpus and J. Falzarano, *Prediction of viscous ship roll damping by unsteady navier-stokes techniques,* Journal of Offshore Mechanics and Arctic Engineering **119**, 108 (1997).

[15] R. van 't Veer, X. Schut, and R. Huijsmans, *Bilge keel loads and hull pressures created by bilge keels fitted to a rotating cylinder,* Applied Ocean Research (2014 (submitted)).

[16] R. van 't Veer and F. Fath, *On the roll damping of an FPSO fitted with bilge keels and riser balcony,* International Journal of Maritime Engineering **153** (2011).

[17] X. Schut, *Contribution of hull pressures created by bilge keels on the roll damping of FPSOs,* Master's thesis, Delft University of Technology (2013).

[18] T. Katayama, J. Umeda, H. Hashimoto, and B. Yildiz, *A study on roll damping estimation for non periodic motion,* in *Proceedings of the* 13^{th} *International Ship Stability Workshop* (2013).

[19] Cummins and D. W. T. M. Basin, *The Impulse Response Function and Ship Motions*, Report (David W. Taylor Model Basin) (Navy Department, David Taylor Model Basin, 1962).

[20] R. Ibrahim and I. Grace, *Modeling of ship roll dynamics and its coupling with heave and pitch,* Mathematical Problems in Engineering **2010**, 32 (2010).

[21] J. Orozco, C. Raposo, and Š Malenica, *A practival procedure for the evaluation of the roll motions of FPSO's including the non potential damping,* in *Offshore Technology Conference* (2002).

[22] K. H. Jung, K.-A. Chang, and E. T. Huang, *Two-dimensional flow characteristics of wave interactions with a free-rolling rectangular structure,* Ocean Engineering **32**, 1 (2005).

[23] K. H. Jung, K.-A. Chang, and H. J. Jo, *Viscous effect on the roll motion of a rectangular structure,* Journal of Engineering Mechanics **132**, 190 (2006).

[24] R. van 't Veer, F. Fathi, and J. Kherian, *On roll hydrodynamics of FPSO's fitted with riser balcony and bilge keels,* in *International Conference on Ocean, Offshore and Arctic Engineering* (2011).

[25] R. van 't Veer, A. Pistidda, and A. Koop, *Forces on bilge keels in regular and irregular oscillating flow,* in *Proceedings of the Twenty-second (2012) International Offshore and Polar Engineering Conference* (2012).

[26] R. van 't Veer, *Time varying force on FPSO bilge keels,* in *Proceedings of the ASME 2013 32nd International Conference on Ocean, Offshore and Arctic Engineering* (2013).

[27] D. Brown and M. Patel, *A theory for vortex shedding from the keels of marine vehicles,* Journal of Engineering Mathematics **19** (1985).

[28] M. Downie, *Effect of vortex shedding on the coupled roll response of bodies in waves,* in *Journal of Fluid Mechanics*, Vol. 189 (1988).

[29] M. Hajiarab, J. M. R. Graham, and M. Downie, *Prediction of roll damping in the frequency domain using the discrete vortex method,* in *Proceedings of the ASME 2010 19th International Conference on Ocean, Offshore and Arctic Engineering* (2010).

[30] M. Hajiarab, M. Downie, and J. M. R. Graham, *A study on the viscous roll damping of a box-shaped vessel in the frequency domain using the discrete vortex method,* Transaction of the Royal Institution of Naval Architects. Part A: International Journal of Maritime Engineering **153** (2011).

[31] M. Hajiarab, *Roll Damping Prediction of a Free Floating Barge,* Ph.D. thesis, Newcastle University School of Maritime Science and Technology (2013).

[32] D. Brown, R. E. Taylor, and M. Patel, *Barge motions in random seas - a comparison of theory and experiment,* Journal of Fluid Mechanics **129**, 385 (1983).

[33] Y. Drobyshevski and J. Whelan, *An approximate method for stochastic linearization of viscous roll damping,* in *Proceedings of the ASME* 29^{th} *International Conference on Offshore Mechanics and Arctic Engineering* (2010).

[34] A. Leloux, B. Molin, C. de Jouette, and T. Coudray, *FPSO roll damping prediction from CFD and 2D and 3D model tests investigations,* in *Proceedings of The Fourteenth (2004) International Offshore and Polar Engineering Conference* (2004).

[35] M. Prevosto, *Distribution of maxima of non-linear barge rolling with medium damping,* in *Proceedings of the Eleventh Internation Offshore and Polar Engineering Conference* (2001).

[36] I. D. M. Minko, M. Prevosto, and M. L. Boulluec, *Distribution of maxima of non-linear rolling in case of coupled sway and roll motions of a floating body in waves,* in *Proceedings of the ASME* 27^{th} *International Conference on Offshore Mechanics and Arctic Engineering* (2008).

[37] M. Gachet and J.-G. Kherian, *Impact of linearization of bilge keel damping on the early assesment of vessel operability,* in *Proceedings of the ASME 27th International Conference on Offshore Mechanics and Arctic Engineering* (2008).

[38] Y. R. Choi, J. H. Kim, M. J. Song, and Y. S. Kim, *An experimental and numerical study of roll motions for a barge-type LNG FPSO,* in *Proceedings of The Fourteenth (2004) International Offshore and Polar Engineering Conference* (2004).

[39] R. van 't Veer, *Application of linearized morison load in pipe lay stinger design,* in *Proceedings of the ASME* 27^{th} *International Conference of Offshore Mechanics and Arctic Engineering* (2008).

[40] T. Sarpkaya and J. O'Keefe, *Oscillating flow about two and three-dimensional bilge keels,* Journal of Offshore Mechanics and Arctic Engineering **118** (1996).

[41] R. Yeung, C. Cermelli, and S.-W. Liao, *Vorticity fields due to rolling bodies in a free surface - experiment and theory,* in *Twenty-First Symposium on Naval Hydrodynamics* (1997).

[42] K. Klaka, J. Penrose, R. Horsley, and M. Renilson, *Hydrodynamic tests on a plate in forced oscillation,* Ocean Engineering **34** (2007).

[43] G. Aloisio and F. D. Felice, *PIV analysis around the Bilge Keel of a Ship Model in Free Roll Decay*, Tech. Rep. (INSEAN).

[44] A. C. de Oliveira, A. C. Fernandes, and H. B. G. aes, *Comparison of full-scale measurements with calculated motion characteristics of a West of Africa FPSO,* in *Proceedings of OMEA03 22ND International Conference on Offshore Mechanics and Arctic Engineering* (2003).

[45] G. O. Avalos, J. B. Wanderley, A. C. Fernandes, and A. C. Oliveira, *Roll damping decay of a FPSO with bilge keel,* Ocean Engineering **87**, 111 (2014).

[46] L. Bernal and J. Kwon, *Vortex ring dynamics at a free surface,* Physics of Fluids A: Fluid Dynamics **1** (1989).

[47] S. Ohring and H. J. Lugt, *Interaction of a viscous vortex pair with a free surface,* Journal of Fluid Mechanics **227**, 47 (1997).

[48] E. Rood, *Interpreting vortex interactions with a free surface,* Journal of Fluid Engineering **116**, 91 (1994).

[49] K. H. Jung, K.-A. Chang, H.-C. Chen, and E. T. Huang, *Experimental study on wave interactions with a fixed rectangular barge in a beam sea,* in *Proceedings of The Twelfth (2002) International Offshore and Polar Engineering Conference* (2002).

[50] K. H. Jung, K.-A. Chang, and E. T. Huang, *Two-dimensional flow characteristics of wave interactions with a fixed rectangular structure,* Ocean Engineering **31**, 975 (2004).

[51] P. Oshkai and D. Rockwell, *Free surface wave interaction with a horizontal cylinder,* Journal of Fluids and Structures **13**, 935 (1999).

[52] H.-C. Chen, T. Liu, and K.-A. Chang, *Time-domain simulation of barge capsizing by a chimera domain decomposition approach,* in *Proceedings of The Twelfth (2002) International Offshore and Polar Engineering Conference* (2002).

[53] H.-C. Chen, T. Liu, and K.-A. Chang, *Time-domain simulation of large amplitude ship roll motions by a chimera RANS method,* in *Proceedings of The Eleventh (2001) International Offshore and Polar Engineering Conference* (2001).

[54] P. L. Davis, A. T. Rinehimer, and M.Uddin, *A Comparison of RANS-based Turbulence Modeling for Flow over a Wall-Mounted Square Cylinder*, Tech. Rep. (University of North Carolina Charlotte N.C. Motorsports and Automotive Research Center).

[55] T. Miyake and Y. Ikeda, *A study on roll damping of bilge keels for new non-ballast ship with rounder cross section,* in *Proceedings of the* 13^{th} *International Ship Stability Workshop* (2013).

[56] Z. Khatir, *A boundary element method for the numerical investigation of near-wall fluid flow with vortex method simulation,* Engineering Analyis with Boundary Elements **28**, 1405 (2004).

[57] R. W. Yeung, *Fluid dynamics of finned bodies - from VIV to FPSO,* in *Proceedings of The Twelfth (2002) International Offshore and Polar Engineering Conference* (2002).

[58] S. A. Kinnas, Y.-H. Yu, H. Lee, and K. Kakar, *Modeling of oscillating flow past a vertical plate,* in *Proceedings of the Thirteenth (2003) International Offshore and Polar Engineering Conference* (2003).

[59] S. A. Kinnas, Y.-H. Yu, B. Kacham, and H. Lee, *A model of the flow around bilge keels of FPSO hull sections subject to roll motions,* in *Proceedings of the 12th Offshore Symposium* (2003).

[60] S. A. Kinnas, Y.-H. Yu, and V. Vinayan, *Prediction of flows around FPSO hull sections in roll using an unsteady Navier-Stokes solver,* in *Proceedings of the Sixteenth (2006) International Offshore and Polar Engineering Conference* (2006).

[61] Y.-H. Yu and S. A. Kinnas, *Roll response of various hull sectional shapes using a Navier-Stokes solver,* International Journal of Offshore and Polar Engineering **19**, 46 (2009).

[62] R. Seah and R. W. Yeung, *Sway and roll hydrodynamics of cylindrical sections,* International Journal of Offshore and Polar Engineering **13** (2003).

[63] J. M. R. Graham, *The application of Lagrangian vortex methods to the prediction of hydrodynamics damping of floating bodies,* in *II International Conference on Particle-based Methods - Fundamentals and Applications* (2011).

[64] R. Huijsmans and J. Borleteau, *The flow around FPSO's in steep regular waves,* in *Proceedings of The Thirteenth (2003) International Offshore and Polar Engineering Conference* (2003).

[65] I. Taylor and M. Vezza, *Prediction of unsteady flow around square and rectangular section cylinders using a discrete vortex method,* Journal of Wind Engineering and Industrial Aerodynamics **82**, 247 (1999).

[66] J. Graham and P. Cozens, *Vortex shedding from edges including viscous effects,* Fluid Dynamics Research **3**, 111 (1988).

[67] J. Na, W. Lee, S. Shin, and I. Park, *A design of bilge keels for harsh environment FPSOs,* in *Proceedings of the 12th International Offshore and Polar Engineering Conference,* Vol. 1 (2002) pp. 114 – 1117.

[68] W. Lian, *A numerical study of two-dimensional seperated flow past bluff bodies at moderate KC-numbers,* Applied Ocean Research **10** (1988).

[69] G. Keulegan and L. Caperenter, *Forces on cylinders and plates in an oscillating fluid,* J. Research of the National Bureau of Standards **60** (1958).

[70] T. Ogilvie, *Recent progress towards the understanding and prediciton of ship motions,* in *Fifth Symposium on Naval Hydrodynamics* (1964).

[71] D. S. Greeley and B. J. Petersen, *Efficient time-domain computation of bilge keel forces,* in *Twenty-eight Symposium on Naval Hydrodynamics* (2010).

[72] R. Sobey, *The distribution of zero-crossing wave heights and periods in a stationary sea state,* Ocean Engineering **19**, 101 (1992).

[73] M. Longuet-Higgins, *On the joint distribution of wave periods and amplitudes in a random wave field,* in *Proceedings of the Royal Society of London. Series A, Mathematical and Physical Sciences* (1983).

[74] P. Stansell, J. Wolfram, and B. Linfoot, *Improved join probability distribution for ocean wave heights and periods,* Journal of Fluid Mechanics **503**, 273 (2004).

[75] V. K. Rohatgi and A. M. E. Saleh, *An Introduction to Probability and Statistics, 2nd editions,* Wiley Series in Probability and Statistics (Wiley, 2011).

[76] L. Eça and M. Hoekstra, *An evaluation of verification procedures for CFD applications,* in 24^{th} *Symposium on Naval Hydrodynamics* (2002).

[77] L. Eça and M. Hoekstra, *Verification and validation of marine applications of CFD,* in 29^{th} *Symposium on Naval Hydrodynamics* (2012).

[78] L. Eça and M. Hoekstra, *A procedure for the estimation of the numerical uncertainty of CFD calculations based on grid refinement studies,* Journal of Computational Physics **262**, 104 (2014).

[79] Y. Ikeda, T. Fujiwara, and T. Katayama, *Roll damping of a sharp-cornered barge and roll control by a new-type stabilizer,* in *Proceedings of the Third (1993) International Offshore and Polar Engineering Conference* (1993).

[80] Y. Ikeda, B. Ali, and H. Yoshida, *A roll damping prediction model for a fpso with steady drift motion,* in *Proceedings of the Fourteenth (2004) International Offshore and Polar Engineering Conference* (2004).

[81] J. Wolfram, *On alternative approaches on linearization and morison's equation for wave forces,* in *Proceedings of the Royal Society of London*, Vol. 455 (1999) pp. 2957 – 2974.